INPUT-DEPENDENT NEURONAL REPRESENTATIONS OF VIRTUAL ENVIRONMENTS IN THE HIPPOCAMPUS

OLIVIA V. HAAS

Graduate School of
Systemic Neurosciences
LMU Munich

Dissertation der Graduate School of Systemic Neurosciences der Ludwig-Maximilians-Universität München

11th April, 2017

Olivia V. Haas: *Input-Dependent Neuronal Representations of Virtual Environments in the Hippocampus*

Supervisor: Prof. Dr. Christian Leibold
2nd reviewer: Prof. Dr. Mark Hübener
3rd reviewer: PD Dr. Tobias Meilinger

Defence date: 2nd August, 2017

To the two peas in their pod.

CONTENTS

LIST OF FIGURES

LIST OF TABLES

LIST OF ABBREVIATIONS

CA	**C**ornu **A**mmonis
CS	**C**onditioned **S**timulus
DG	**D**entate **G**yrus
EC	**E**ntorhinal **C**ortex
EEG	**E**lectro**e**ncephalo**g**ram
EIB	**E**lectrode **I**nterface **B**oard
EPSP	**E**xcitatory **P**ostsynaptic **P**otential
FFT	**F**ast **F**ourier **T**ransform
HF	**H**ippocampal textbfFormation
LEC	**L**ateral **E**ntorhinal **C**ortex
LFP	**L**ocal **F**ield **P**otentials
LIA	**L**arge **I**rregular **A**ctivity
LTD	**L**ong-**T**erm-**D**epression
LTP	**L**ong-**T**erm-**P**otentiation
MEC	**M**ateral **E**ntorhinal **C**ortex
NMDA	**N**-**M**ethyl-**D**-**A**spartate
PaS	**Pa**ra**s**ubiculum
PER	**Per**i**r**hinal cortex
POR	**Po**st**r**hinal cortex
PrS	**Pr**e**s**ubiculum
REM	**R**apid **E**ye **M**ovement
RSA	**R**hythmic **S**low **A**ctivity
SPW	**S**har**p** **W**ave
SPWR	**S**har**p** **W**ave-**R**ipple
STDP	**S**pike-**T**iming-**D**ependent **P**lasticity
Sub	**Sub**iculum
SWS	**S**low **W**ave **S**leep

US	**U**nconditioned **S**timulus
V1	Primary **V**isual Cortex
VR	**V**irtual **R**eality

ABSTRACT

Animals live in highly complex sensory environments that are represented across multiple sensory-modalities. These multi-sensory neural representations allow animals to successfully navigate in space and to form relevant associative memories critical to survival. The remembered location of a plentiful food source or a predator could mean the difference between life and death.

To form survival relevant associative memories across multiple sensory modalities animals must be able to sense, encode, and integrate information from their immediate environment. The Information gathered across multiple sensory systems must therefore be temporally correlated and converge within the brain.

The mammalian hippocampus is one such structure where sensory information converges. Hippocampal place cells are known to fire at a particular location within an animal's environment (place field). As the animal moves through a place field action potentials proceed in phase with respect to hippocampal theta oscillations (phase precession).
Place fields encode specific positions in the animal's environment, and therefore provide a suitable substrate for the integration of diverse sensory inputs with spatial information. Such association would position sensory landmarks within the environment and would thus be crucial for successful spatial orientation and navigation.

To better understand how multi-sensory information is integrated for the formation of a neuronal place map, I performed in-vivo extracellular recordings in the hippocampus of behaving Mongolian gerbils (*Meriones unguiculatus*). Specifically, I sought to understand the relative contribution of visual and locomotor inputs to place cell activity.
Recordings were performed in a virtual reality behavioural setup in

which animals ran along a virtual linear corridor. Animal locomotion was determined via a tracking-ball treadmill. By altering the gain factor between the movement of the ball and the speed of the visual projection on a single trial basis I could decouple visually perceived movement from the animal's locomotion.

Through these experiments I showed that place cells in Cornu Ammonis area 3 (CA3) responded differentially to closed loop manipulation. One subset of place cells formed its place field based on visual information within the virtual environment, independent of the distance travelled by the animal. Such visually driven place fields predominantly occurred at visual texture changes within the virtual corridor. A second subset of place cells relied predominantly on locomotor inputs, as place fields remained at the same running distance on a single trial basis. This was also confirmed in dark trials during which the projection was switched off. This meant that animals had to rely on internal cues such as path-integration and proprioceptive/motor efference information. A third subset of cells exhibited two place fields, with each field being driven by one of the two different inputs.

As a population both types of place fields formed input-specific maps that were simultaneously represented in the hippocampus. This notion is corroborated by the fact that place field firing was adjusted on a single trial basis without adaptive processes required.
Furthermore, I investigated whether overlapping input-specific place maps are integrated in a common processing frame. To this end I analysed phase precession of overlapping place fields, which is thought to be crucial for encoding time ordered events that are compressed within a theta cycle.
I found that theta-scale timing correlations shift with gain changes, which argues against mechanisms based exclusively on recurrent CA3 connections for memory formation.

My results therefore indicate that the hippocampus preserves information from distinct processing streams to form coexisting space representations. These coexisting input-specific maps could then be associated on a population level in order to form multimodal memories. Such association is likely to be formed from sensory information, fed-

forward via the hippocampus, rather than via recurrent hippocampal connections.
Thus, the hippocampus provides animals with several maps of their environment, each specified for a specific sensory-input. Animals could therefore rely on the most appropriate map such that locomotor information would be more precise than visual information when the animal is navigating in darkness.

1

INTRODUCTION

Brains create a neural representation of the world we live in, reflecting external and internal information available to an animal. In order to secure survival, animals must be able to interact with their surrounding environment to e.g. perceive and locate potential predators or food sources. To accomplish such a representation in the brain in the form of neural activity patterns, all senses have to sample the environment and report internal states such as hunger or anxiety to further processing areas (Moser et al., 2014). In order to evaluate the importance and significance of sensory information, the nervous system has to reflect upon learned versus innate responses and needs to be able to adapt decision making and the resulting behaviour upon changes in the internal or external state. Adequate behaviour upon a sequence of events embedded in the context of memories or environmental influences is of high importance to the animal. Understanding how neural correlates are formed and linked has therefore become one of the goals of contemporary neuroscience.

Neural correlates for specific sensory inputs, such as a visual scene, have been studied from low hierarchical levels (sensory receptors) up to high hierarchical, cortical levels (Moser et al., 2014). Albeit the fact that much is known about how sensory stimuli are processed individually, it is still unclear how these representations are associated with one another.

In order to perform learning of associative, cross-modal information, the nervous system must thus possess an area where all sensory and internal state information converges. In mammals a good candidate for such a structure is the hippocampus, which is known to be crucial e.g. for relational processing and the formation of spatio-temporal context representation within the brain (Andersen et al., 2007). Both of these functions are important for the encoding and retrieval of

memory and will be referred to in later subsections (see subsection 1.1.1 and 1.1.2).

1.1 THE ROLE OF THE MAMMALIAN HIPPOCAMPUS

The hippocampus is located in the medial temporal lobe and is part of the limbic system of the brain (Kandel et al., 2013). It is known to be involved in many processes of the nervous system, but in the last 25 years two main hypothesis of its function dominated, 1. its role within the formation and consolidation of different types of memory, and 2., its crucial function for spatial navigation and the implementation of a cognitive map within the brain (Andersen et al., 2007).
Historically the hippocampus was thought to be primarily involved in olfactory processing as its anatomical size seemed to correlate with the significance of olfactory information for the species. Potential roots for this hypothesis become apparent when comparing the macroscopic size of the hippocampus in macrosmatic animals such as rodents with the human hippocampus. The rodent which is known for its strong dependence on olfactory stimuli seemed to have an especially large hippocampus. After the 1930s this idea lost momentum and was later disproven, as the ratio of hippocampus to olfactory bulb is largest in humans (Brodal, 1947).
Instead the theory of the hippocampus as the primary substrate for emotional processing started to take over (Papez, 1937). Temporal lobe lesions lead to loss of fear in the monkey and were thought to underpin the hypothesis from Papez. It was, however, later confirmed that this observation was rather due to amygdala damage (Weiskrantz, 1956).
In 1900, bilateral softening of the hippocampus and adjacent cortical structures was found to lead to memory deficits (Bechterew, 1900). This first hint for the role of the mammalian hippocampus in memory formation was confirmed in 1953 via bilateral hippocampal ablation of severely epileptic patient Henry Gustav Molaison (H.M.). After surgery he suffered of severe anterograde amnesia, or the inability to form new memories, and partial retrograde amnesia in the time just before the surgery.

1.1.1 *Learning and memory*

The inability to form new memories after hippocampal removal from patient H.M. revealed that the hippocampus is a crucial structure for the formation and retrieval of memory (Scoville and Milner, 2000). According to Kandel, Schwartz, Jessell, Siegelbaum and Hudspeth (2013), 'memory is the process by which [...] knowledge [about the world] is encoded, stored, and later retrieved' (p. 1441). Knowledge about the world on the other hand is acquired via learning.
Memory is thus not one discrete function, but rather needs to be split up into three different stages. The first stage, memory formation, is achieved via receiving sensory information and processing and combining this information. Second, memory storage can be described as the formation of a long-lasting engram or trace of the encoded information. Third, retrieval of stored memory can be defined as the process of recalling stored information from the past upon e.g. conscious effort or a stimulus which is part of the stored information.
The way memories are accessed or retrieved subcategorises memory into declarative (explicit) and nondeclarative (implicit) memory (Bird and Burgess, 2008). Declarative memories are known to be accessed via conscious recollection and can be e.g. episodic when remembering events or semantic when remembering facts (Bird and Burgess, 2008). Nondeclarative memories on the other hand mainly address procedural memories (Squire, 1986; Bird and Burgess, 2008). These are either associative or non-associative and can be e.g. memories concerning skills, behavioural procedures or emotional associations (Squire, 1986). A non-associative memory is formed when an animal is e.g. repeatedly presented with the same sound stimulus and therefore learns to not associate any action with that sound and finally decreases its response (habituation) (Hawkins et al., 2006). A second example would be sensitization, where an animal increases its response to a stimulus due to a previous experience, e.g. a loud noise (Hawkins et al., 2006).
Associative memories are formed when an animal learns that several stimuli or behaviours belong to one event in a certain order. Such memories can be formed via e.g. classical and operant conditioning (Maia, 2009). The russian physiologist Ivan Petrovich Pavlov is primarily known for his work on classical conditioning, by pairing an unconditioned stimulus (US), e.g. meat, which evokes the response of

salvation in dogs with a conditioned stimulus (CS), e.g. a bell, which by itself does not evoke such a response (Pavlov, 1927). Pairing these stimuli with the bell predicting the arrival of meat within a short time window (in the order of half a second), the dog would salivate when hearing the bell, no matter whether the meat is presented or not. The delay between the CS and US can also be up to several hours, to develop e.g. taste aversion upon an unconditioned response such as nausea (Best and Orr, 1973). In operant conditioning the animal learns to associate a behaviour with e.g. a reward or punishment and will therefore repeat or suppress that behaviour. Operant conditioning is therefore a useful and widespread tool in teaching animals experimental paradigms (Thorndike, 1901).

The second dimension under which memories can be classified is the time course of memory storage. Memories are stored as short-term and long-term memories, for which different neural mechanisms and brain areas are of importance (Bird and Burgess, 2008). Short-term memories are known to last for seconds to hours whereas long-term memories are recallable for days up to years after initial storage (Squire, 1986; Bird and Burgess, 2008). Long-term memories are formed directly or from short-term memories via a process referred to as memory consolidation (Squire et al., 1975).
Patient H.M. had intact long-term memories from events before the bilateral ablation of his hippocampal formation, amygdala and parts of the multimodal association area of the temporal cortex. He was also able to remember events for seconds or minutes after surgery. However, he was not able to perform memory consolidation in order to transfer information after the surgery into long-term memory (Scoville and Milner, 2000). In patient R.B. lesions in hippocampal area cornu ammonis 1 (CA1) led to almost no loss of retrograde memory but severe dysfunction of anterograde memory (Zola-Morgan et al., 1986). The hippocampus is therefore known to play a crucial role in the formation of new memories and memory consolidation in order to enable long-term memory formation. This however only holds true for declarative memories, as patient H.M. was able to learn and recall nondeclarative memories formed after the surgery. Examples for such nondeclarative memories were of procedural nature such as drawing an object and also included all types of associative and non-associative learning described earlier.

Thus, for memories which do depend on concious recall (declarative memories) the hippocampus is a key component, whereas memories which do not depend on concious recall (nondeclarative memories) or have been already consolidated and stored as long-term memories or are still in the immediate or working memory process are rather hippocampus independent (Andersen et al., 2007).

Knowing that the hippocampus is crucial for the formation and consolidation of several types of declarative memories, the question arises how learning and storage of knowledge in memories is implemented on a single cell or network level.
The Canadian psychologist Donald Olding Hebb focussed on this question. A key component of his theory is often summarised as 'neurons wire together if they fire together' (e.g. Löwel and Singer, 1992). Such 'wiring' or strengthening of synaptic transmission at e.g. hippocampal synapses is achieved when a presynaptic neuron is active and a postsynaptic neuron is strongly activated at the same time (Hebb, 1949). This strengthening and therefore validation of a particular synapse is called long-term-potentiation (LTP) (Bliss and Lømo, 1973; Malenka, 2003). Strengthening also occurs when the postsynaptic neuron is activated immediately after the presynaptic neuron fires an action potential, which is referred to as spike-timing-dependent plasticity (STDP) (Taylor, 1973; Levy and Steward, 1983).
For LTP to occur, N-methyl-D-aspartate (NMDA) receptors serve as detectors for simultaneous activity or when neurons 'fire together' (Coan and Collingridge, 1987; Lynch, 2004). The release of glutamate from the presynaptic neuron and simultaneous depolarization (activation) of the postsynaptic membrane leads to displacement of the magnesium (Mg^{2+}) block from the postsynaptic NMDA receptor. This Mg^{2+} displacement allows calcium (CA^{2+}) to flow through, into the postsynaptic dendrite and causes further depolarization (Lynch, 2004). A direct consequence is the insertion of new glutamate AMPA receptors into the postsynaptic membrane which enhances synaptic transmission. As a result, the excitatory postsynaptic potential (EPSP) will stay potentiated or enhanced for a long time (Lynch, 2004).
In contrast to that, synapses whose pre- and postsynaptic activity does not correlate are weakened, which is referred to as long-term-depression (LTD) (Collingridge et al., 2010). Such attenuation is due to less NMDA receptor activation as a response to less coinciding activ-

ity of pre- and postsynaptic partners, which results in loss of AMPA receptors and therefore a reduction in postsynaptic EPSP size (Collingridge et al., 2010).

LTP and LTD are core phenomena of synaptic plasticity and allow chemical synapses to increase (LTP) or decrease (LTD) their strength, dependent on the synchronous activity of the pre- and postsynaptic neurons. In a neural circuit, learning and memory formation is thought to be implemented via the modification of synaptic strength of neuronal partners within that circuit.

1.1.2 *The hippocampal cognitive map*

The importance of LTP for memory formation has been substantiated through many different experimental approaches. Many of those show interference of LTP disruption with the formation of spatial memory (Morris, 1989; Davis et al., 1992; Riedel, 1999; Nakazawa et al., 2004).
Spatial memory can be defined as memories formed on spatial information, describing the layout and structure of the nonegocentric environment (Tolman, 1948; Nakazawa et al., 2004). Spatial memories are often referred to as forming the foundation for a 'cognitive map' within the brain. Tolman (1948) first coined the term 'cognitive map' as a mental representation or field map of the animal's environment. Such an allocentric map allows for a broader, comprehensive or conceptual understanding of the environmental layout and gives an animal the option to take a novel shortcut to reach a goal location.
The involvement of the hippocampus in spatial memory or cognitive map formation has been studied e.g. using the Morris water maze and comparing healthy animals with bilateral hippocampal damaged animals (Scoville and Milner, 1957; Morris, 1981; Morris et al., 1982). In the experimental paradigm of the 'Morris water maze' rats have to find an invisible platform in a swimming pool filled with milky water. Normal rats quickly learn to swim directly to the platform, located just under the surface of the water. Animals with bilateral hippocampal lesion however do not learn the spatial location of the hidden

platform and swim around randomly until the platform is located. Additionally animals fail remembering the location of the platform when NMDA receptors are blocked via injection of a pharmacological antagonist into the hippocampus (Morris, 1989). This suggests that LTP in the hippocampus is involved in spatial learning and therefore in the formation of spatial memory (O'Keefe and Nadel, 1978).

1.1.3 *Hippocampal modes*

When analysing the hippocampus as a substrate for memory formation, one can study single neuron activity or the activity of large neuronal populations.
The techniques used to measure activity depends on the scale of neuronal ensembles. For single neurons, or the microscopic scale, one can record single action potentials with e.g. patch electrodes where signals are in the range of single milliseconds. Activity from local networks, part of the mesoscopic scale, are described as local field potentials (LFP). Large scale networks on the other hand are part of the marcoscopic scale and can be recorded from the superficial layers of the cortex, using the electroencephalogram (EEG) (Buzsáki et al., 2012; Ros et al., 2014).
EEG is primarily used as diagnostic method, for e.g. epilepsy diagnosis and monitoring, or for research purposes, to e.g. study sleep.
LFPs on the other hand are the measured extracellular field potential from a smaller volume of brain tissue (about 100-1000 neurons) in respect to a reference potential. This field potential is created by superimposed currents which mostly originate from slow events, such as synaptic currents and calcium spikes (Buzsáki et al., 2012).
When the LFP is recorded from hippocampal tissue, the measured electrical activity can be categorised into two different modes, rhythmic slow activity (RSA) and large irregular activity (LIA) (O'Keefe and Nadel, 1978).
In all mammals, including humans hippocampal RSA is characteristic for strong rhytmic oscillations in the theta-alpha band with a frequency range of about 4-12 Hz (Arnolds et al., 1980; Kahana et al.,

1999; Tesche and Karhu, 2000; Bódizs et al., 2001). In contrast to that, the LIA mode is dominated by large voltage deflections lasting for 30-120 ms, which are randomly timed. Such deflections are referred to as sharp waves (SPWs) (Buzsaki, 1986).

Theta oscillations

Theta oscillations are in the frequency band of about 4-12 Hz and depend on the animals behaviour. They are most reliably present during rapid eye movement (REM) sleep (Jouvet, 1969) and different types of locomotion (Vanderwolf, 1969).
Besides the hippocampus, field oscillations in the theta band have been observed in several structures with parallel arranged neurons, where extracellular potentials can sum in order to create a strong oscillatory signal. Such structures include for example cortical structures (e.g. the entorhinal cortex) and the amygdala (Steriade, 2000; Paré and Collins, 2000). These oscillations seem to be however not coherent with hippocampal theta and occur during different behavioural states (Kahana et al., 1999; Raghavachari et al., 2001).
Within the hippocampus, theta oscillations are known to vary in amplitude and coherence dependent on dorso-vental depth, whereas theta phase shifts monotonically along the septotemporal axis. The largest theta amplitude and most regular activity can be found in the stratum lacunosum-moleculare within the hippocampus (Buzsaki et al., 1986; Bullock et al., 1990; Bragin et al., 1995; Lubenov and Siapas, 2009; Patel et al., 2012).
The 'pacemaker' or main source for hippocampal theta has been identified to be the medial septum (Petsche et al., 1962; Hangya et al., 2009; Brandon et al., 2014). Upon injection of a GABA receptor agonist (muscimol) in the medial septum, the injection site region is inactivated and hippocampal LFP power is reduced dramatically (e.g. Brandon et al., 2011).
The 4-12 Hz rhythm within the hippocampus is thought to be crucial for several phenomena. First, for temporal coding, as hippocampal pyramidal neurons tend to discharge on the negative phase of the theta cycle (Csicsvari et al., 1999; Buzsáki, 2002). Second for the modification of synaptic weights, which is critical for mnemonic pro-

cesses (Raghavachari et al., 2001; Buzsáki, 2002). Theta phase shifts along the septotemporal axis result in an activity delay of about half a theta cycle (~70 ms) between the septal and temporal poles (Patel et al., 2012). This may prevent associations of signals from the poles and rather suggest the intermediate hippocampus as a substrate for associative mnemonic processes.
According to Kramis et al. (1975) theta oscillations observed during behavioural states such as locomotion and REM sleep can be categorised as type 1 theta and is pharmacologically identifiable as being atropine sulphate resistant but on the other hand abolished during ether or urethane induced anaesthesia. Type 1 theta usually covers a frequency range of 7–12 Hz whereas type 2 theta has a typical frequency of 4-7 Hz and appears during immobility and anaesthesia and is considered as atropine sensitive.
Type 2 theta however can rarely be observed in behaving rodents as it occurs during brief preparatory behaviour prior to movement or during predator induced freezing (Sainsbury et al., 1987).
Thus, when addressing theta activity in this thesis, it will generally refer to type 1 theta, which correlates with voluntary movements of the animal.

Sharp waves

The hippocampal LIA mode is dominated by randomly occurring sharp waves (SPWs) which occur during awake immobility, grooming, eating and during deep sleep, referred to as slow wave sleep (SWS) (Buzsaki, 1986). SPWs are associated with high frequency field oscillations (ripples) in the range of about 140-220 Hz and are known to be among the most synchronous patterns in the mammalian brain (Sullivan et al., 2011; Jouvet et al., 1959), named sharp wave-ripple (SPWR) complexes. These SPWR complexes are known to co-occur with activity replay of hippocampal principal neurons. Ordered activity replay within the short time window of a SPW, which lasts for about 30-120 ms, compresses previous waking activity in a temporal manner. Such reoccurence of firing patterns within a short time window enables synaptic plasticity to take place via LTP and is therefore thought to be crucial for memory consolidation (Buzsáki, 2005; Gir-

ardeau and Zugaro, 2011).
During SWS lower levels of acetylcholine in the hippocampus allow extensive endogenous neuronal activation, which enhances recurrent hippocampal connectivity and is therefore the basis for SPW generation (Buzsaki, 1986; Hasselmo, 1999) and the cellular and molecular foundation for off-line memory consolidation (Buzsaki, 1989). In this brain state SPWs are triggered by synchronous population bursts of upstream CA3 cells, which cause strong depolarisation of apical CA1 dendrites resulting in such large voltage deflections (Buzsaki, 1986; Csicsvari et al., 2000). As recurrent connectivity is enhanced, CA1 interneurons are also firing with a high population frequency, similar to the ripple band of 140-220 Hz. Such oscillating inhibition, together with excitation from CA3 is thought to cause ripple oscillations (Buzsaki et al., 1992; Ylinen et al., 1995).

1.2 FUNCTIONAL ANATOMY OF RODENT HIPPOCAMPAL AND PARAHIPPOCAMPAL AREAS

Knowledge about the anatomy and therefore structuring of a brain region is the basis for understanding a neuronal circuitry and its function. As mentioned in the previous chapter (see subsection 1.1.3), the distal input from hippocampal area CA3 to CA1 is of great importance for the formation of SPWR complexes. Both areas are part of the trisynaptic loop, connecting the hippocampus with the entorhinal cortex (EC).

1.2.1 *The trisynaptic loop*

The trisynaptic loop (Fig. 1.1) describes the anatomical connections and information flow from the EC, as the cortical information source to the hippocampal CA1 region via three synapses, from where information is passed back to the EC to close the loop (Andersen et al., 1966a; Andersen et al., 1966b). Such serial information flow via unidirectional organization of the circuit has been derived after the

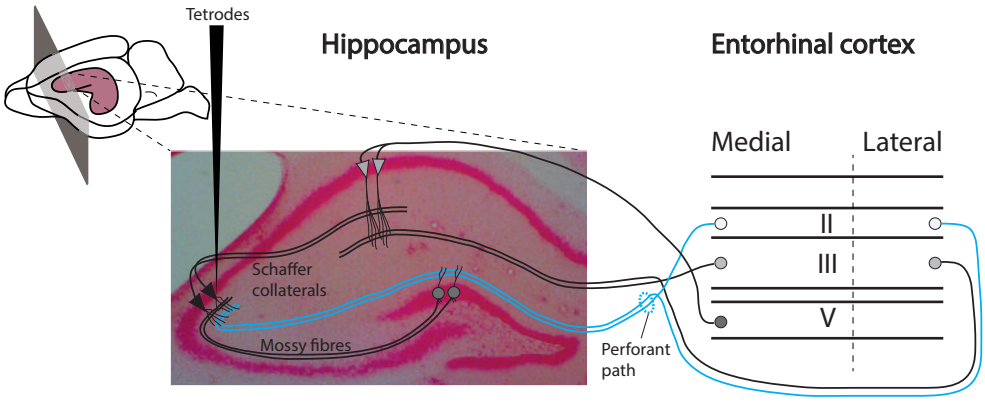

Figure 1.1: The trisynaptic loop. Polymodal sensory information reaches the DG from lateral and medial layer II of the EC via the perforant path (blue). Information is then transferred to apical dendrites of CA3 pyramidal neurons, which project to CA1 pyramidal neurons via Schaffer collaterals.

initial description of the trisynaptic loop by the neuroanatomist Santiago Ramón y Cajal in 1911 (Andersen et al., 1971; Hjorth-Simonsen, 1973; Andersen, 1975).
The three synapses of the loop are the following. First, the EC connects to granule cells in the dentate gyrus (DG) within the hippocampal formation via the perforant path. The second synapse is formed between the DG and CA3 via mossy fibres. Third, Schaffer collaterals connect CA3 pyramidal neurons with CA1 pyramidal neurons in the hippocampus (Neves et al., 2008; Cappaert et al., 2015).
It is important to note, however, that besides the described serial information processing concept, the entorhinal-hippocampal circuitry has also parallel pathways coexisting with the trisynaptic loop. The EC e.g. forms parallel projections with all fields within the hippocampal formation (HF), with EC Layer III neurons projecting to CA1 and the subiculum (Sub), whereas EC layer II neurons terminate in DG and CA3 (Witter et al., 2000).

1.2.2 *Major inputs to the entorhinal cortex*

Major inputs to the entorhinal cortex originate from the presubiculum (PrS), parasubiculum (PaS), postrhinal cortex (POR) and perirhinal cortex (PER).
The PER mainly projects to the lateral entorhinal cortex (LEC) and is known to process non-spatial information, as lesions of the PER cause deficits in object recognition memory (Winters and Bussey, 2005; Deshmukh et al., 2012).
The PrS, PaS and POR on the other hand provide substantial inputs to the medial entorhinal cortex (MEC). Damage of POR neurons is known to impair learning about position and context (Eacott and Gaffan, 2005). Not only POR neurons show postitional firing (Burwell and Hafeman, 2003), but also PrS and PaS are involved in the brains navigational system (Taube, 2007; Boccara et al., 2010), with e.g. the septal PrS containing head-direction cells (Taube et al., 1990).
Such clear functional separation of cortical inputs to anatomical distinct entorhinal regions LEC and MEC point towards the assumption that two parallel and different networks exist to streamline information from the neocortex and via the parahippocampal region, including PER and POR as well as the entorhinal cortex (Witter et al., 2000; Eichenbaum et al., 2012; Ranganath and Ritchey, 2012).

1.2.3 *The entorhinal cortex*

The entorhinal cortex (EC) can be subdivided on one hand into subareas, such as the LEC and MEC (Brodmann, 1909). On the other hand the EC can organised into its laminar structure. This organisation is formed via the subdivision into six different layers (Ramón y Cajal, 1909). Four layers are considered as cellular layers (layer II, III, V and VI) and two are rather acellular layers (layer I and IV).
EC layer II provides the main source to the perforant path of the trisynaptic loop (see subsection 1.2.1), projecting to the HF. Layer II contains pyramidal neurons and pyramidal-like cells, such as MEC stellate cells and LEC fan and multiform cells (Lorente de Nó, 1933; Klink

and Alonso, 1997; Dugladze et al., 2001; Canto and Witter, 2012). The EC is most famous for its MEC layer II neurons, which show i.a. spatially modulated, hexagonal grid-like firing pattern and are therefore referred to as grid cells (see subsection 1.3.2).
The axonal fibre tract connecting the parahipocampal region with the hippocampal formation is called the 'angular bundle' and is formed by neurons from all EC layers, through which e.g. layer III pyramidal cells travel to connect to neurons in CA1 and the Sub.
Layer V and VI contain three and two different classes of principle neurons respectively (Hamam et al., 2000; Gloveli et al., 2001; Haeften et al., 2003). Their axons also project to the angular bundle with layer V providing strong input to EC layers II and III and layer VI connecting to the subiculum (Haeften et al., 2003; Kloosterman et al., 2003; Dugladze et al., 2001).

1.2.4 *The dentate gyrus*

Via the perforant path, the EC directly connects to the 'U-shaped' structure, the dentate gyrus (DG) (see subsection 1.2.1). The DG can be subcategorised into three major layers.
First, the molecular or cell-free layer, which is closest to the hippocampal fissure and mainly hosts dendrites from other DG layers (Cappaert et al., 2015).
Second, the principal or granule cell layer, which consists mainly of tightly packed granule cells (Gaarskjaer, 1978), forming the terminal point of the perforant path. These first two layers constitute to the DG 'U-shaped' structure by forming two substructures, the enclosed blade (adjacent to the hippocampal fissure) and the free blade. Their contact point is called crest (Cappaert et al., 2015).
The third and last layer of the DG is the hilus or polymorph layer, host of mainly mossy and fusiform cells (Amaral, 1978).

1.2.5 *Hippocampus proper and subiculum*

The hippocampus proper was divided by Lorente de Nó (1934) into three fields (CA1, CA2 and CA3) which have similar laminar organisation.
The stratum oriens is a cell free layer, directly adjacent to the stratum pyramidale or pyramidal layer which comprises the main cellular layer of all three fields. On the other side of the pyramidal layer, the acellular stratum lucidum is present in CA3 but not in CA1 and CA2. The stratum radiatum on the other hand is present in all three fields and hosts associational CA3-CA3 connections as well as Schaffer collaterals, connecting CA3 to CA1. The last layer of the hippocampus proper is the stratum lacnosum-moleculare, where fibres from the perforant path terminate.
The only projection from the DG to the hippocampus proper is via the mossy fibre pathway, from granule cells to the border of CA2 and CA3 hippocampal subfields. The mossy fiber pathway can be split into three major bundles, the infrapyramidal, intrapyramidal and suprapyramidal bundle. These bundles travel through the deep pyramidal layer, within and superficial (in the stratum lucidum) to the pyramidal layer respectively (Cappaert et al., 2015).
Each CA3 pyramidal cell receives information from about 50 DG granule cells (Acsády et al., 1998). The dominant transmitter used by mossy fibers for that synapse is thought to be glutamate (Storm-Mathisen and Fonnum, 1972).
CA1 and CA2 do not receive direct input from the DG and CA1 pyramidal cells differ additionally by hosting smaller pyramidal cell bodies. The hippocampal CA2 region is very narrow with about 250 µm and is wedged between CA1 and CA3. Additionally CA2 is thought to show connective and functional differences to the other fields of the hippocampus proper (Jones and McHugh, 2011; Piskorowski and Chevaleyre, 2012).
In all three subfields, pyramidal cells are the dominant cell type of the pyramidal layer. Their basal dendritic tree reaches into the neighbouring stratum oriens, whereas their apical dendritic tree reaches through all other layers to the hippocampal fissure (Cappaert et al., 2015).
More than 20 different subtypes of nonpyramidal interneurons are

located in HF layers (Klausberger and Somogyi, 2008; Somogyi, 2010) and provide GABAergic input onto pyramidal cell dendrites (Ribak et al., 1978). Examples for subtypes which can have their cell bodies also within the pyramidal cell layer are basket cells and bistratified cells (Somogyi, 2010).

CA3 pyramidal neurons mainly target CA1 via Schaffer collaterals in a highly ordered fashion but also terminate within CA2 (Li et al., 1994; Ishizuka et al., 1995; Chevaleyre and Siegelbaum, 2010). CA2 cells give rise to sparse projections to CA1, from where information is propagated primarily via the stratum oriens to the subiculum (Sub). This CA1-to-Sub projection is known to be ordered in a columnar fashion of three parts, such that projections from the proximal third of CA1 terminate in the distal third of the Sub and vice versa. Accordingly, neurons from the middle CA1 section terminate preferentially within the middle Sub section (Tamamaki et al., 1987; Amaral et al., 1991). The proximal Sub hosts predominantly regular-spiking neurons whereas the distal Sub shows rather bursting activity (Kim and Spruston, 2012). Such columnar difference in spiking behaviour might encounter for a functional segregation of pathways leading to the medial or lateral EC.
Whether CA1 projections occur indirectly via the Sub or directly to the EC, they are point-to-point reciprocal with projections from the EC to CA1 (Naber et al., 2001). Proximal CA1 neurons project to the MEC, whereas distal CA1 pyramidal cells terminate preferentially in the LEC (Tamamaki and Nojyo, 1995; Witter et al., 2000; Naber et al., 2001).

1.3 Spatial representation in the rodent brain

According to the philosopher Immanuel Kant (1781) space does not form a property of things in themselves and should be considered as *a priori*. If on the other hand geometrical knowledge is considered as empirical, an animal's perception of space would also be empirical and depend on the appearance of objects, which constitute the animals surrounding environment, and their placement with respect to

each other. According to this theory, everything we perceive would be represented spatially, such as being somewhere in space and taking up space.
The first confirmation that spatial structure has a direct neural correlate was delivered by John O'Keefe (1971), who received the nobel prize in physiology or medicine in 2014 for his work on hippocampal place cells (see subsection 1.3.1) together with the discoverers of entorhinal grid cells, Edvard Moser and May-Britt Moser (2004) (see subsection 1.3.3).

1.3.1 *Hippocampal place cells*

Besides many other important memories or facts encoded by the hippocampus (see section 1.1), the position of an animal in its environment is thought to be a fundamental one in order to guide its navigation via the creation of a 'cognitive map' (see subsection 1.1.2).
O'Keefe and Dostrovsky (1971) discovered complex-spiking neurons in the hippocampus proper, which showed activity whenever the rat moved across a certain area within its environment, referred to as 'place field'. These pyramidal cells where thus named 'place cells' and have been suggested to play an important role in spatial memory (O'Keefe, 1978). Together with other place cells, which have their place fields at different positions, the population can tile the entire environment of an animal with its activity (O'Keefe, 1976; Wilson and McNaughton, 1993).
Such representation was however found to be flexible, such that upon either radical changes of the environment (e.g. changing the color of the room walls) or exploration of a novel environment, place cells would rearrange and encode a different position with their place field. Such phenomenon is referred to as global remapping (O'Keefe and Conway, 1978; Muller and Kubie, 1987; Jeffery and Anderson, 2003; Leutgeb et al., 2005a). A second form of remapping is rate remapping, where place cells keep their stable firing field but change their firing rate within the place field (Leutgeb et al., 2005b).
Two basic properties of place fields are their shape and size. The average field size was found to correlate with the recording site, where

field sizes increase from the dorsal to the ventral hippocampus (Jung et al., 1994; Maurer et al., 2005).
Another property is that place cells do not map space in a topographical manner, as has been observed for sensory maps in the neocortex. Place cells which are close to each other anatomically do therefore not necessarily have their place fields located next to each other (O'Keefe et al., 1998). A tendency for spatial clustering of fields has been observed to appear around crucial spatial positions such as choice points or reward/goal zones (O'Keefe, 1976; Olton et al., 1978; McNaughton et al., 1983; Hollup et al., 2001).
A very well known feature of place cells is that directionality of their activity is environment dependent. In open fields, such as a two dimensional arena, place field firing is non-directional (Muller et al., 1994). In more restricted environments, such as linear tracks or more complicated radial arm mazes, place cell activity depends on the running direction of the animal (McNaughton et al., 1983; O'Keefe and Recce, 1993; Muller et al., 1994; Markus et al., 1995; Gothard et al., 1996; Battaglia et al., 2004).

1.3.2 *Hippocampal phase precession*

Place cell activity is accompanied by theta oscillations (see section 1.1.3), and it has been observed that when entering the place field, place cells start firing in the late theta cycle. Additionally place cells show a slightly faster oscillatory activity than the local field potential such that firing advances to the early theta cycle whilst the animal passes through the place field. This phenomenon of place cells to fire at progressively earlier phases of the hippocampal theta rythm is called phase precession (Fig. 1.2) (O'Keefe and Recce, 1993; Hopfield, 1995; Skaggs et al., 1996).
Place cells display a rate code by firing different amounts of action potentials depending on their position within the place field (O'Keefe and Dostrovsky, 1971; Wilson and McNaughton, 1993). Contrastingly, phase precession constitutes a temporal code (Singer, 1993) in the rodent hippocampus, where spike timing within the theta cycle provides

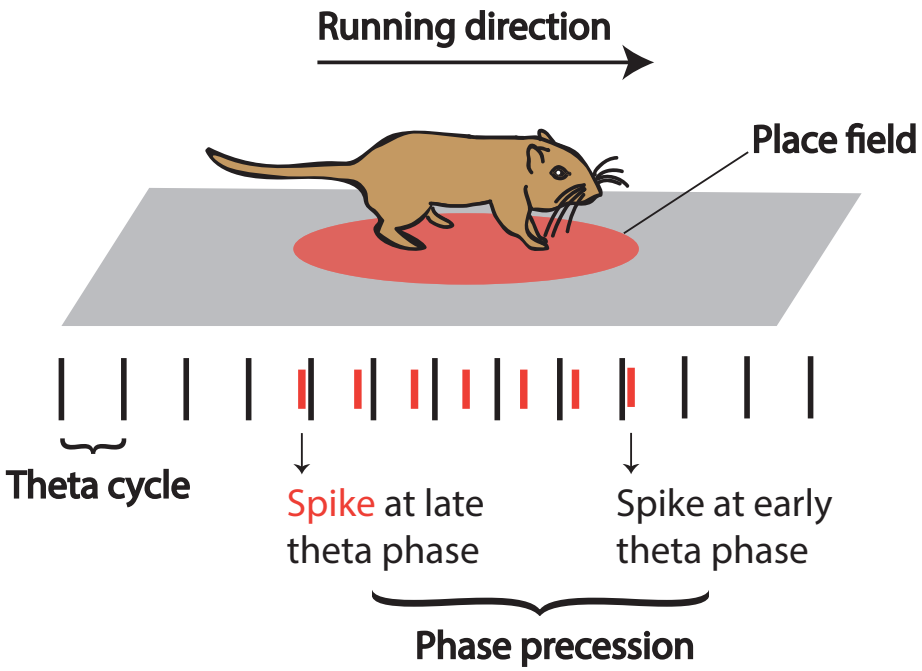

Figure 1.2: Hippocampal phase precession. When an animal enters a place field, place cell action potentials start firing at a late theta phase. Spikes move to earlier theta phases whilst the animal moves through the place field (phase precession), such that spikes occur at early theta phases when the animal exits the place field.

more precise spatial information (O'Keefe and Recce, 1993; Skaggs et al., 1996). Mehta et al. (2002) proposed that both, rate and temporal code are directly linked such that when the firing rate increases, the correlated theta phase decreases. From place field entry to exit, the spike phase can precess through an entire 360 degree cycle (Mehta et al., 2002).

When an animal passes through a sequence of overlapping place fields, newly entered fields will always correlate to spikes at late theta phases whereas when the end of a field is reached correlating spikes will coincide with early theta phases. When the end of a field A overlaps with the beginning of field B, spikes of both fields will appear in the same theta cycle, but at early and late phases respectively. The firing sequence of both place cells will therefore be replicated in a compressed manner within an individual theta cycle of about 120

ms (Skaggs et al., 1996; Tsodyks et al., 1996; Jensen and Lisman, 1996; Dragoi and Buzsáki, 2006). As the animal traverses the overlapping fields A and B, several theta cycles occur such that the compressed replication of place field sequences is repeated several times. Such repetition is thought to be the basis of sequence learning using STDP (see subsection 1.1.1) (Dan and Poo, 2004).

1.3.3 *Entorhinal grid cells*

Spatial modulation of firing behaviour was shown not only in the hippocampus proper (see subsection 1.3.1) but also in MEC layers II and III which project to the hippocampus via the perforant path (see subsection 1.2.1). A fraction of these MEC neurons each display a hexagonal grid like firing pattern with multipeaked place fields and are therefore called grid cells (Fyhn et al., 2004; Hafting et al., 2005; Giocomo et al., 2011). Grid cells coexist in the EC with head direction and border cells, which show more specific firing properties.
Each grid cell forms a hexagonal grid of firing positions and is characterised by several parameters. First, by its spacing which describes the distance between its firing fields. Second, by the size of the firing fields. Third, the orientation or tilt of the grid in respect to the external reference frame and fourth, its phase which describes the xy-displacement in the two dimensional plane of the external reference frame (Hafting et al., 2005).
Along the dorso-ventral axis of the MEC, grid spacing is known to increase in discrete steps in synchrony with the field size, which is together often referred to as grid scale (Brun et al., 2008; Stensola et al., 2012; Moser and Moser, 2013). The grid scale therefore shows topographic distribution, in contrast to the grid phase which displays no large scale topographic organisation (Hafting et al., 2005; Brun et al., 2008; Stensola et al., 2012). Because of these different properties of grid cells, each place in an environment is uniquely represented by the single field overlap of active cells.
When prominent features of the environment (e.g. visual cues) are changed, hippocampal place cells remap in a random fashion (see subsection 1.3.1). In contrast, grid cells retain their firing pattern and

their firing relationships to other grid cells (Hafting et al., 2005; Fyhn et al., 2007). Such rigid firing properties, independent of contextual details suggest that grid cells could be substantially driven by self-motion cues (Parron and Save, 2004; Kim et al., 2013).
These differences between place and grid cells propose that there are two complementary maps of space in the hippocampus and EC.

1.4 MULTISENSORY PROCESSING OF SPACE

Animals can use information from all senses to help them orient within an environment. The hippocampus is known to be a crucial structure for memory consolidation, linking elements from multiple sensory modalities in order to form complex memories such as episodic or spatial memories (Squire, 1987). Information from all sensory modalities is thought to reach the hippocampus in a highly processed manner (e.g. Wiebe and Stäubli, 1999), making it difficult to isolate the contribution of a single sensory modality.

1.4.1 *Path integration*

A well known navigation strategy is path integration (Barlow, 1964; Mittelstaedt and Mittelstaedt, 1980), which is used by ants (Müller and Wehner, 1988; Wittlinger et al., 2006), bees (Frisch, 1967), spiders (Moller and Görner, 1994), birds (Saint Paul, 1982), crabs (Zeil, 1988) rodents (Mittelstaedt and Mittelstaedt, 1980; Kautzky and Thurley, 2016) and humans (Mittelstaedt and Glasauer, 1991). Path integration is thought to be the navigation strategy of dead reckoning or estimation of the current position by integrating linear and angular self-motion from previously defined positions. Underlying sensory information for path integration is mainly based on vestibular input for the steering direction and self motion cues (e.g. proprioceptive cues) in order to form a running estimate (home vector) (Wittlinger et al., 2006). This home vector then provides an estimate of the distance between the animal itself and its start or home location (Vickerstaff

and Cheung, 2010). When for example the stride lengths of ants is manipulated by altering the length of their legs, the travelled distance is misjudged by the animals (Wittlinger et al., 2006).

1.4.2 *Visual representation of space*

Travelled distance which can be estimated by path integration occurs within a stable space or environment. Such a reference frame can be provided using visual information of landmarks such as edges and different wall surfaces (Gibson, 1954). Thus one would expect that the rotation of distal cues, which provide a reference frame, would also rotate the resulting place field map. This was indeed found by O'Keefe and Conway (1978) and Muller and Kubie (1987). Additionally they revealed that rotation of the proximal environment did not have the effect of reference frame rotation. Similar to these results, O'Keefe and Burgess (1996) showed that not only rotation but also stretching of the reference frame is able to take the anchored place fields with it, such that they stretch accordingly. These results confirm that distal visual landmarks provide a framework to define place cell firing locations and seem to be sufficient for navigation (Cushman et al., 2013).
Visual information reaches the hippocampus from the visual cortex and activity from the primary visual cortex (V1) has been found to lead hippocampal place cell activity spatially and temporally, suggesting a functional coupling between the two brain regions and the direction of information flow from V1 to the hippocampus (Haggerty and Ji, 2015).

In order to guide movement and to explore the environment which is most salient to the animal, it is known that other senses such as e.g. the olfactory or auditory sense is used. When e.g. a relevant odour or sound is located via an odour gradient or inter-aural and spectral cues respectively, the animal is able to orient its gaze to the direction of interest to switch to an eye-centred representation used by the visual system for further exploration of the novel walking direction (Maier and Groh, 2009).
Therefore all senses contribute to multiple encoding modes in the

hippocampus to create a plastic map of spatial memories (Wiebe and Stäubli, 1999).

1.4.3 *Spatial representation in virtual reality*

As different sensory modalities have been shown to impact spatial representation and learning in rodents, the question arose whether one sensory modality alone would be sufficient for navigation and place field formation. In physical environments one sensory modality can not easily be isolated without means of brain lesions. In order to study the influence of visual cues separately from other sensory cues without lesions, closed loop virtual realities have been used for rodents since 2005 (Holscher et al., 2005; Lee et al., 2007). It was confirmed that head-fixed rodents are able to learn how to navigate in virtual reality (VR) to reach goal locations using solely visual cues (Youngstrom and Strowbridge, 2012). Allowing rotational vestibular cues from the semicircular canals by providing the animal with the freedom of rotation around its vertical body axis is however crucial in 2D virtual environments for place cell activity to appear normally (Ravassard et al., 2013; Aronov and Tank, 2014; Aghajan et al., 2015).
Thus, VR studies showed that place cell activity is comparable with real world results and therefore provides the unique possibility of having a controlled environment to study sensory influence to place field formation (Thurley and Ayaz, 2017). This can be achieved by conflicting information of the animal's own-movement and movement of the visual scene by introducing a gain factor between the two (Chen et al., 2013; Saleem et al., 2013; Kautzky and Thurley, 2016). Chen et al. (2013) used such manipulation to separate visual and non-visual contributions to place cell coding and found a broad spectrum of dependence on the combination of both types of inputs. Underpinning the importance of multisensory contributions to higher order brain activity, Saleem et al. (2013) found that under VR gain manipulations, both the animal's running speed as well as the speed of the visual scene modulates neuronal responses in V1.

1.5 THE MONGOLIAN GERBIL AS A MODEL ORGANISM

The Mongolian gerbil, *Meriones unguiculatus* has been a laboratory animal since the late 1980s and has been used predominantly in auditory (Kraus et al., 1987; Stuermer and Scheich, 2000) and learning research (Ohl et al., 1999). Its importance for auditory research derives from the hearing sensitivity of gerbils at low frequencies, which is similar to humans, while rats and mice have much higher hearing thresholds (Grothe and Pecka, 2014).
Most laboratory gerbils descend from 20 wild pairs which were caught in Mongolia in 1935. Specimens of the first offspring were transferred from Japan to New York in 1954 from where 5 females and 4 males were used to breed laboratory gerbils as we know them today (Stuermer et al., 2003). As known from the domestication process of e.g. rats and mice, laboratory animals show docility, smaller brain sizes, change in fur color and larger litter sizes (Stuermer et al., 2003). Additionally to these attributes, laboratory gerbils show susceptibility to epileptiform seizures (Kaplan and Miezejeski, 1972), which have never been reported from wild gerbils (Stuermer et al., 2003).
In contrast to other rodents gerbils are rather diurnal (Pietrewicz et al., 1982; Stuermer, 2003). Their activity increases however around and after dusk and is additionally modulated by temperature (Surjosukotjo et al., 1999). Ingle (1981) described the gerbil as more visually alert than other rodents, having rather the multiple visual system bauplann of the monkey without the association cortex.
Gerbils are also known to show complex behavioural strategies, which are between the 'reflexive' tendencies of the frog and 'cognitive' abilities of monkeys and apes (Ingle, 1981).
Behaviourally gerbils show a stronger exploration drive compared to other rodents, by not moving along walls in unfamiliar environments (thigmotaxis). Gerbils rather move across open fields without any sign of anxiousness (Stuermer, 2003).

Due to their particularly well developed visual system with unique receptor configuration (Govardovskii et al., 1992; Garbers et al., 2015) and behavioural abilities, gerbils proved to be an ideal model organism to study challenging visual tasks in virtual reality (Thurley et al., 2014; Garbers et al., 2015; Kautzky and Thurley, 2016).

Navigation requires the brain to interpret input from all sensory modalities to determine the current location and to make predictions and decisions about the future location.
In the present thesis I aim to investigate the impact of visual and locomotor cues on place field formation. Achieving this aim requires to decouple visual from other sensory information as well as to update visual cues online. Such requirements can be fulfilled using a VR setup, which minimises sensory input via other modalities.

The approach I chose can be broken down to three parts:

1. Training of animals to VR linear track and extracellular recordings from CA hippocampal regions on real and VR linear track, in order to ensure VR place cell quality.

2. Online alternation of the relation between self-motion and vision on a single run basis, by changing the gain of the mapping between track ball and projection. This forms the main body of experimental work and allows me to test whether place cells form their field based on visual or locomotor information or a combination of the two.

3. Analysis of gain change impact on LFP and theta phase precession.

2

MATERIALS AND METHODS

2.1 MONGOLIAN GERBILS

Experiments were conducted with three female and one male adult Mongolian gerbil (*Meriones unguiculatus*) from a wild-type colony at the local animal house. Gerbils were housed together with a sibling before surgery and alone after, in a 71x46x31 cm^3 box, containing wooden chipping as bedding and a sleeping house (Fig. 2.1 A). They were kept under constant laboratory conditions, i.e., 12 hour light/dark cycle, 23°C and 55 % humidity. Animals had unrestricted water access but received a diet designed to maintain them at about 85-95 % of their free feeding weight (usually 60 - 70 g), in order to allow reward conditioning. During training or experiments, gerbils received chocolate or banana flavoured pellets as reward (20 mg Purified Rodent Tablet, TestDiet, Sandown Scientific, UK), whereas they were given normal dry food otherwise (ssniff Gerbil; ssniff Spezialdiäten GmbH; Soest, Germany).
Adult gerbils of at least four months required no training for real linear track sessions (Fig. 2.1 B), whereas virtual reality (VR) training was performed for 5 days, followed by a 2 day break. All behavioural training and recording sessions were performed in the light phase of the cycle. All experiments were approved according to national and European guidelines on animal welfare (Reg. von Oberbayern, AZ 55.2-1-54-2532-10-11).

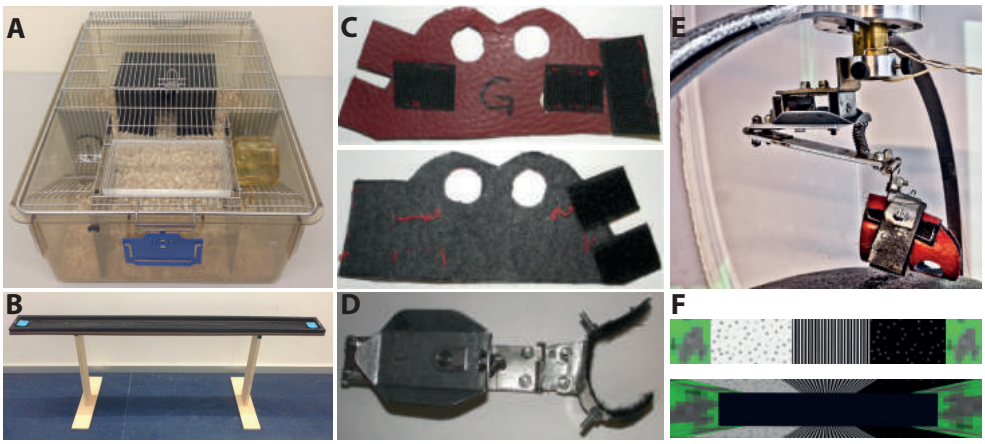

Figure 2.1: Animal cage, setup attachment and virtual texture. (A) Gerbil cage with wooden chipping, water bottle and house. (B) Linear track of 150 cm length and 12 cm width, with blue reward bowls at both ends. The track has barriers around the plane area and 50 cm high legs, to prevent the gerbil from falling or jumping off. (C) Harness design with Velcro closure, from the outside (top) and with a soft inside (bottom). (D) Velcro connector. (E) Full design of the animal fixation in the setup. (F) Linear track pattern, from the side (top) and above (bottom).

2.2 BEHAVIOURAL PARADIGM AND TRAINING

For real linear track sessions gerbils had to shuffle between blue bowls (Fig. 2.1 B), where they received a flavoured pellet as reward. This paradigm did not require training before microdrive implantation (see subsection 2.4.2).

Behavioural training for VR sessions was subdivided into two phases (similar to Thurley et al., 2014). First, gerbils were adapted to the experimenter and harness (Fig. 2.1 C). Animals were handled, i.e. petted and allowed to run over the experimenters hands, for approximately 3 days. After, gerbils were guided to run through the harness, which was closed loosely when they got familiar with its smell and appearance. They were then placed into a separate cage to move around wearing the harness, where they were rewarded with flavoured pellets. This procedure took 5 to 10 days and took place in the VR lab for the second half.

The second phase was comprised of the adaptation to the VR setup. For that, gerbils were put tightly into the harness and rewarded with flavoured pellets in a separate cage in the VR lab. Next, the animal was attached to a Velcro connector (Fig. 2.1 D and D), which was used to manually hold the gerbil on top of the Styrofoam ball within the setup to allow first contact. If it did not appear too stressed, the Velcro connector was attached to the magnetic mount point of the setup (Fig. 2.1 E). At this point, the projection screen was only closed to 270°, such that it was possible to intervene at any time. The projection of a linear maze onto the screen enabled training of the animal to the behavioural paradigm of shuttling back and forth between the two ends of the virtual linear track (Fig. 2.1 F). Reward was given manually (using a tea spoon) typically for the first 5-7 days. Later, reward was delivered automatically via the feeder.
The virtual linear track was 200 cm long and 30 cm wide (virtual coordinates) and its walls were covered with different stripe and dot textures (Fig. 2.1 F). A reward was delivered when the animal reached one of the two green ends of the track at the end of a full run. Naive animals were acclimatized to the VR setup in gain 1.0, i.e. with congruent visual and locomotor information, for about five sessions and then trained for roughly another ten sessions to run along the track (Thurley et al., 2014). When performance reached sufficient levels (at least 40 runs within 20 min), animals were implanted. After surgery it took one to two weeks to reach the CA3 subfield. During that time animals were trained in the gain change paradigm, for which the gain of a single run changed randomly to either 0.5 or 1.5 whenever the animal entered a reward zone. An experimental session typically lasted between 15 and 30 min in which animals performed 40 to 80 runs. One or two sessions were conducted per day.

Experiments were conducted on a virtual reality (VR) setup (as described in Thurley et al., 2014) for rodents (Fig. 2.2) similar to (Holscher et al., 2005; Harvey et al., 2009). The setup consisted of a styrofoam sphere with a diameter of 50 cm that was suspended by air from below and thereby acted as a treadmill (Fig. 2.2 A). On top of the sphere an animal was fixated (see section 2.2) such that its head and legs were freely movable and rotation around the animals vertical body axis was possible. Rotations of the sphere were induced when the animal moved its legs, whilst the animal itself stayed in place (Fig. 2.2 A and C). Treadmill rotations around the vertical axis were reduced by two small directional wheels (Fig. 2.2 A), which were placed on the north and west pole of the aluminium bowl.
To produce a realistic feeling of acceleration, the moment of inertia of the Styrofoam ball was designed to approximately match the mass of the animal (150% of the animal's average mass).
The ball moved in an aluminium bowl with a diameter of 50.4 cm, leaving 2 mm gaps on each side of the treadmill. Pressured air was connected to an 8 cm hole at the bottom of the bowl. In order to dampen pressure waves, turbulence and air flow noise, the tube connecting bowl and air supply was filled with cotton wool and a layer of sound dampening foam.
The treadmill movements were detected by two infrared sensors (optical mice), whose sampling rate had to provide sufficient sampling points during high speed of the animal, which was enhanced during gain 1.5 runs. Optical mice supported a throughput of 16 bit per axis (x and y axis) and therefore tracked 2^{16} pixels between successive USB messages. USB signals were fed into a computer with a rate of at least 1000 Hz, which generated and updated a visual virtual scene every 0.05 seconds (20 Hz). To synchronize the electrophysiological data arriving at a separate computer, it received a TTL-pulse every 0.05 seconds from the VR computer.
The virtual scene was displayed via a projector (Sanyo PCL-ET30L) onto a toroidal screen that fully surrounded the treadmill and was held in place by 16 spokes (Fig. 2.2 A). This was achieved via projection to a plane mirror (LINOS Photonics) onto a aspherical mirror (www.kugler-precision.com) to create a 360° image. The curvature of

the aspherical mirror was adjusted to produce a linear relationship between the distance of the projected image center from the projector and the height of the image on the screen. The required surface profile of the aspherical mirror was calculated according to Chahl and Srinivasan (1997, p. 8277-8278) using Snell's law of reflection and an angular magnification of $\alpha = 11$.
Real-time rendering, for VR scene creation was done with Vizard Virtual Reality Toolkit (v5, WorldViz), whereas the maze was designed in Blender (v2.49b). Animals were rewarded with one automatically delivered food pellet, which was controlled by the VR software. When an animal entered a reward zone, Vizard activated the stepper motor of the reward delivery system, fixed above the screen next to the projector. Such activation would trigger one reward pellet to fall out of the feeder, which was guided through a connected tube into a 3D-printed spoon. Tube and spoon were fixed in place, such that the reward was always delivered adjacent to the northern metal spoke, in order to be equidistant from both reward zones.

2.4 ELECTROPHYSIOLOGICAL RECORDINGS

2.4.1 *Electrodes and microdrives*

I chronically implanted microdrives (Axona Ltd., St. Albans, UK) with 4 or 8 tetrodes (Fig. 2.3). Drives allowed for movement of all tetrodes together via the screw head (Fig. 2.3 A). Each tetrode was comprised of four twisted platinum-iridium wires (California Fine Wire Co., inset of Fig. 2.3 C) with a wire diameter of 17 µm. To produce one tetrode, a 23 cm long platinum-iridium wire was formed to a loop and then twisted about 90 times, such that the lower two-thirds formed a bundle and the upper third was comprised of four separate wires. The bundle was then heated (230-240°) such that wires stuck together. After trimming the wire bundle, the insulation at the tip of the separate wires was burned off. This step was crucial in order to connect each wire to one pin of the microdrive, after having slid it through its guide tube (Fig. 2.3 C inset).

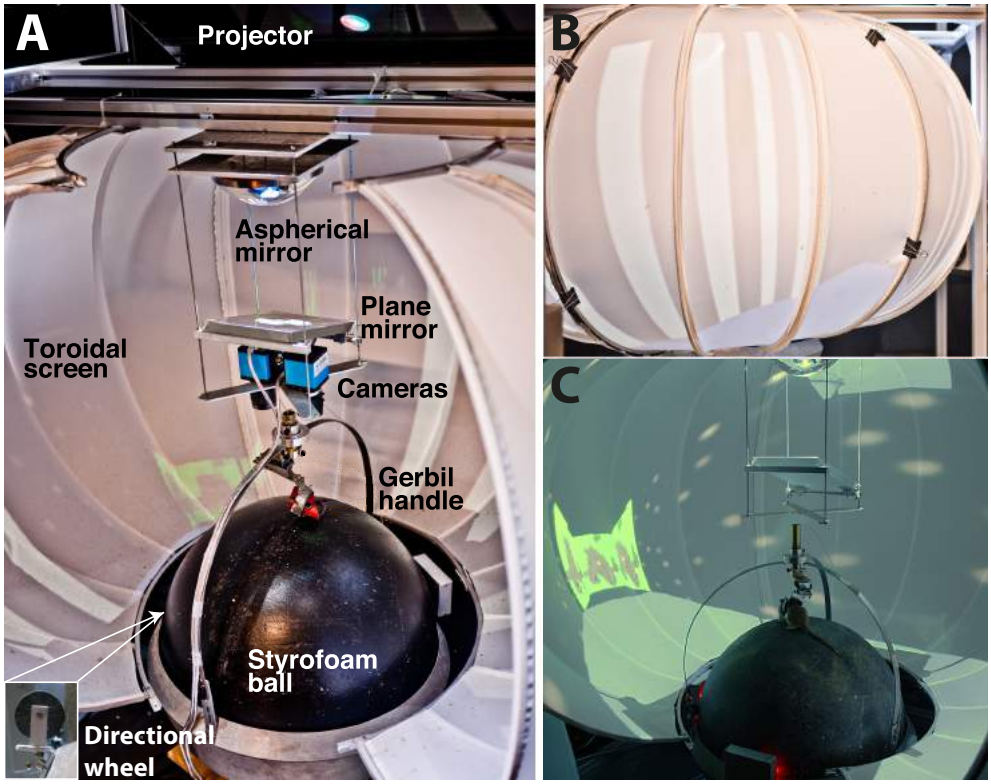

Figure 2.2: VR setup (adapted from Thurley et al., 2014, with permission). (A) Overview of the VR setup. (B) Closed VR setup with full 360° screen. (C) Example training session with linear track projection.

When all tetrodes were inserted, pins and wire tips were covered in silver paint to assure their connection. Tetrodes were then glued to the guide tube entry to fix them in place. To prevent damage and to provide insulation, pins and wires were then coved with nail polish (Fig. 2.3 C, blue box).
As a last step, tetrode tips had to be cut such that no insulation would cover the electrodes and then gold-plated to reduce their resistance to 150-250 kΩ (measured in saline).

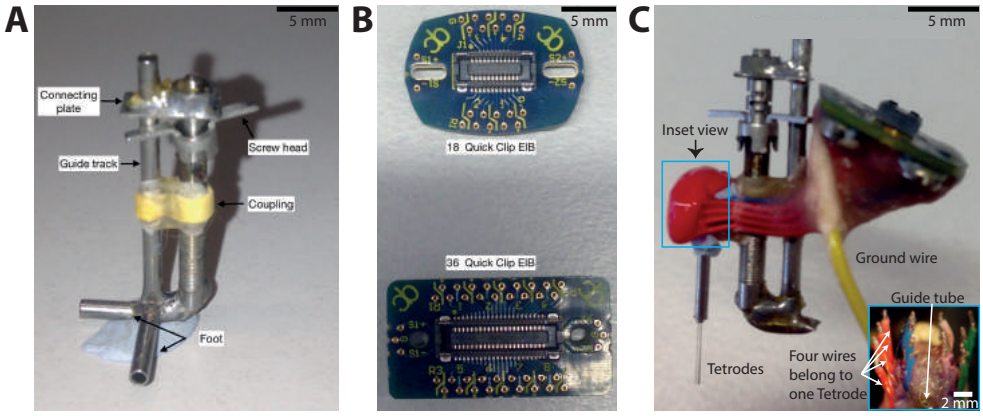

Figure 2.3: Axona microdrive components. (A) Bare bone. The foot was placed on the animals' skull and one turn of the screw head moved tetrodes 50 µm dorso-ventrally. (B) Quick clip electrode interface board (EIB) for 4 tetrodes (top) with 18 channels (16 tetrode wires, 2 references) and for 8 tetrodes (bottom) with 36 channels (32 tetrode wires, 4 references) (C) Side view of assembled microdrive. Inset (blue) shows an example for a 4 tetrode drive, with 4 pins of one color connecting to 4 wires (one tetrode). That tetrode was then guided through a tube (inset bottom), such that all tetrodes enter the brain as a bundle.

2.4.2 *Surgery*

Animals were anaesthetised with an initial dose of medetomidine-midazolam-fentanyl (0.15 mg/kg, 7.5 mg/kg, 0.03 mg/kg, s.c.) and placed in a stereotactic unit (Stoelting Co.). To maintain surgical anaesthesia during the operation, I gave 2/3 doses every 2h. The animal was placed on a heating pad to keep body temperature at 37°C. A hole was drilled above the right dorsal hippocampus, 2.5 mm anterior-posterior (AP) and 2.5 mm medial-lateral (ML) from the bregma, the point where sutura coronalis and saggitalis meet (Fig. 2.4 A).
Anchor screw holes to hold the microdrive were drilled in the frontal, parietal and occipital bone, respectively, into which small jewelers' screws were inserted (Fig. 2.4 A). One of the screws served as electrical ground and was placed above the cerebellum. Electrical currents are therefore least correlated with the recorded signals but receive similar noise which was subtracted from the recorded signal.

The microdrive was fixed to the stereotaxic frame (Fig. 2.4 B) and carefully lowered such that tetrodes could enter the cortex within a small area inside the screw hole, where the thick membrane between brain and skull (dura) was removed using forceps (Fig. 2.4 C). From the point where tetrodes touched brain tissue, they where moved 0.8 mm into the cortex on the dorso-ventral (DV) axis. The foot of the microdrive (Fig. 2.4 B) would then almost touch the skull.
To protect the exposed part of the brain (Fig. 2.4 C, dotted circle), I used alginate (0.5% sodium alginate and 10% calcium chloride, Sigma-Aldrich) which was carefully applied using a syringe. Tetrodes were protected by an outer cannula (Fig. 2.4 B), which was pulled down over the tetrodes until it touched the alginate protection. The microdrive was further shielded and anchored to skull and screws by dental acrylic (iBond Etch, Heraeus Kulzer GmbH, Germany; Simplex Rapid, Kemdent, UK). At the end of the surgery, anaesthesia was antagonized with atipamezole-flumazenil-naloxone (0.4 mg/kg, 0.4 mg/kg, 0.5 mg/kg, s.c.).
During surgery and for three post-surgical days analgesia was done with meloxicam (0.2 mg/kg, s.c.). In addition, antibiotics (enrofloxacin, 10 mg/kg, s.c.) were given for five to seven post-surgical days. Animals were allowed to recover for two days after surgery before recordings started.

2.4.3 *Recording procedures*

For recording, the microdrive was connected to a 16 or 32 channel head-mounted preamplifier (for 4 or 8 tetrodes respectively). Signals were passed into a digital data acquisition system connected to a personal computer (Neuralynx Inc.). I recorded both, extracellular action potentials of single units and local field potentials (LFPs). Unit activity was amplified, band-pass filtered at 600 Hz to 6 kHz and recorded at a sampling rate of 32 kHz. LFPs were recorded from one channel of each tetrode at a rate of 2 kHz and band-pass filtered between 1 to 500 Hz. Each tetrode could be recorded differentially, being referenced by

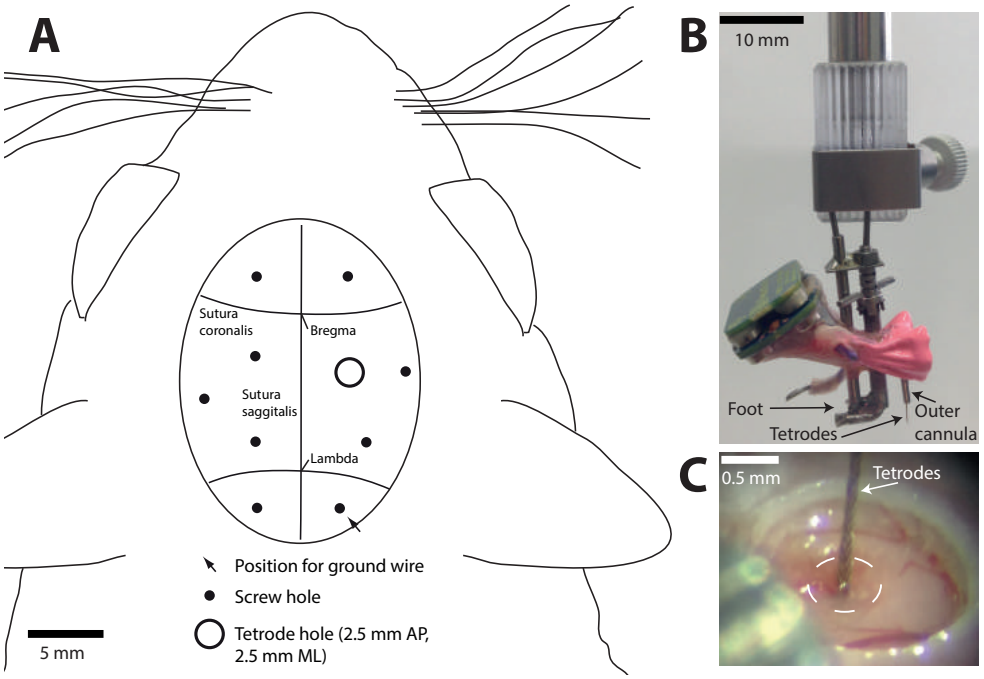

Figure 2.4: Surgery. (A) Gerbil head with exposed skull (oval area) and positions for ground wire, screws and tetrodes. (B) Microdrive fixation in stereotaxic frame for tetrode insertion. (C) Tetrodes placed in the brain. Large circle shows tetrode screw hole depicted in (A). The dura was removed within the dashed white circle, such that tetrodes were able to enter, whereas the rest of the exposed area stayed protected.

one electrode of another tetrode or the ground connected to one of the jewelers' screws (Fig. 2.3 C and Fig. 2.4 A).
With the help of the microdrive's screw (Fig. 2.3 A), I adjusted the tetrode position during the course of the recording period to get stable recordings in the hippocampal CA3 subfield. To reach that area, I lowered the tetrodes 100 µm per day. Arrival in the subfield was determined electrophysiologically from the presence of spatially selective principal cells. For the period of days in which I recorded, tetrodes were only finely adjusted to optimize recording quality (25-50 µm per day). Tetrode adjustments where performed every day after recording sessions (1-2 sessions per day), such that data from new cells could be collected the following day.

2.4.4 *Histology and tetrode position reconstruction*

Tetrode location was verified by postmortem histological visualisation. Animals received an overdose of sodium pentobarbital, depending on their weight (intraperitoneal, 400-800 mg/kg). They were perfused intracardially with 4% paraformaldehyde (Fig. 2.5 A). Brains were extracted and stored over night in paraformaldehyde, placed on a shaker inside a cold room.
On the next day, brains were washed 3 times in 0.02 M PBS for 10-15 minutes each time, using a shaker. After that, brains were trimmed, such that the cerebellum was removed with a cut, perpendicular to the brain midline. Further, about half of the left hemisphere was removed, in order to identify the right hemisphere, were recordings where obtained from (Fig. 2.5 B). The area from which the cerebellum was removed served as glue surface and was attached to a metal plate (using super glue, see Fig. 2.5 C), which was placed on the bottom of the vibratome bath chamber. The bath chamber was filled with 0.02 M PBS.
Coronal slices of 80 µm thickness were obtained using the vibratome (Fig. 2.5 D). Slices were collected with a brush and pulled onto gelatin covered microscope slides. Slides were then placed under a laboratory hood over night.
The next day, slices were stained with Neutralred (according to Tab. 7.1) which stains all lysosomes red and therefore marks all cell bodies (Winckler, 1973). Stained slices were embedded and coverslipped using depex.
Recordings were included in the data analysis if the tetrodes' deepest position was in the CA3 pyramidal cell layer (Fig. 2.6).

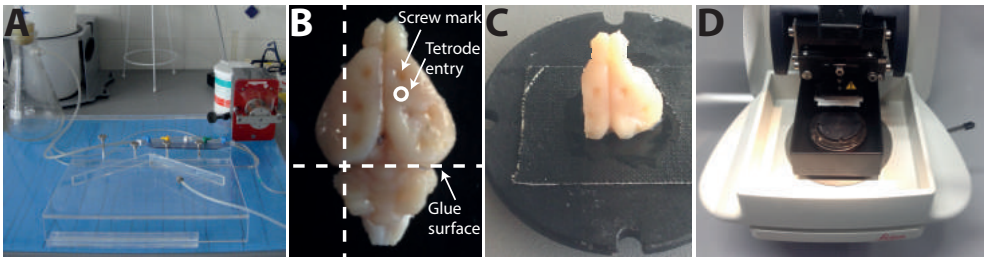

Figure 2.5: Perfusion and histology. (A) Perfusion setup, with animal support plate. (B) Brain trimming for slicing (dashed lines). (C) Trimmed brain attached for slicing. (D) Vibratome used for slicing with bath chamber containing the metal place shown in (C) and razor blade.

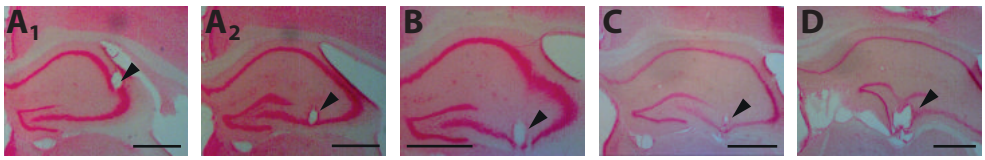

Figure 2.6: Stained slices from animals used for recordings. (A) Example sections with two different recordings sites in CA3 in one animal (A_1 and A_2). Lesions from the tetrodes are marked by black arrow heads. Scale bars correspond to 1 mm. (B-D) Sections from the other three animals, showing CA3 recording sites.

2.5 DATA ANALYSIS

Data analysis was done with Python 2.7 using the packages Matplotlib 1.4, Numpy 1.12, Scikit-learn 0.16, Scipy 0.17, Seaborn 0.5 and Statsmodels 0.6.

2.5.1 *Spike sorting*

Spike sorting was done offline and in two steps. First, data was automatically pre-clustered using klustakwik (v1.6). Afterwards clustering was improved manually in 2D projections of the multidimensional parameter space (consisting of waveform amplitudes, i.e. peak and valley, the difference between peak and trough of the waveform, and waveform energies) with SpikeSort 3D (v2.5.2, Neuralynx Inc., see Fig. 2.7 A). Putative excitatory cells were distinguished from putative interneurons by spike width and average rate. Only putative excitatory cells were included in the analysis.
Spike sorting quality was determined via isolation distance and L-ratio calculated using two spike features, the peak and the valley of the waveform for each cell (Schmitzer-Torbert et al., 2005; Maurer et al., 2006). Comparison of cells with one field and two fields gave similar results (Fig. 2.7 B), ensuring that cells with two place fields were not due to spike sorting errors.

2.5.2 *Spatial firing rate maps*

Units were included in the place-field analysis if they had a peak firing rate of at least 3 Hz in one gain and at least 2 Hz in the other gain, a place field width between 10 and 160 cm, and if they fired a minimum of 100 spikes. Spike and position information was only used when the animal's running speed was $\geqslant$ 10 cm/s. Rate maps were constructed by dividing the total number of spikes that occurred in a given location bin along the track (bin size of 3 cm) by the amount

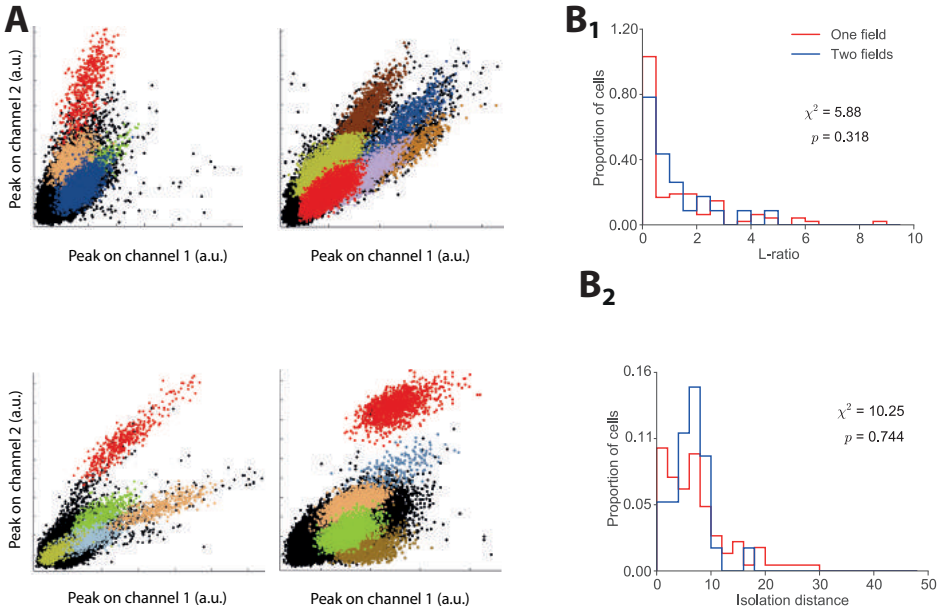

Figure 2.7: Spike clustering and cluster quality verification. (A) Example clusters of CA3 pyramidal cells. Clustered spikes from the same unit are coloured, unclustered spikes are displayed as black dots. Only two projections are shown for each example. (B) Place cells with two fields are not due to insufficient cluster separation. Distributions of L-ratio (B_1) and isolation distance (B_2) scores for spike waveform clusters from neurons with a single place field (red) and neurons with two place fields (blue). Isolation quality of the spikes from cells with two fields is similar to that for cells with one field (χ^2 test of homogeneity between both distributions, n = 93 single field cells, n = 18 double field cells)

of time that the animal spent in that location. Finally, the rate map was smoothed with a Gaussian window of 9 cm width. The extent of the place field was determined as the connected region where the firing rate of the cell was above 10% of the peak rate.

2.5.3 *Spatial information*

Spatial information content was calculated in bits from the binned data using the following formula (Skaggs et al., 1993; Skaggs et al., 1996; Ravassard et al., 2013):

$$I = \sum_i P_i \frac{\lambda_i}{\bar{\lambda}} \log_2 \frac{\lambda_i}{\bar{\lambda}} \text{ , with } P_i = \frac{o_i}{\sum_j o_j} \text{ , and } \bar{\lambda} = \sum_i P_i \lambda_i \qquad (2.1)$$

where P_i is the occupancy probability in bin i, o_i the occupancy within bin i, $\sum_j o_j$ the mean occupancy for all bins, and λ_i the mean firing rate in bin i.

2.5.4 *Comparison of place fields for small and large gains*

We characterized place fields with respect to either virtual or real (i.e treadmill) coordinates. Treadmill coordinates r were calculated from virtual coordinates v by dividing by the gain at a particular trial, i.e. $r_l = v_l/0.5$ for low gain or $r_h = v_h/1.5$ for high gain.

For each of the two gains, we extracted the location of a firing field in virtual coordinates v_l and v_h, respectively. When field locations for each gain are compared, place fields that are purely driven by visual inputs would be on the bisecting line, i.e. $v_l = v_h$.

Purely locomotion-sensitive fields such a comparison would be located at $r_l = r_h$, i.e., the line were the virtual positions are normalized by its respective gain

$$\frac{v_l}{0.5} = \frac{v_h}{1.5} \quad \Leftrightarrow \quad v_h = 3\, v_l \ .$$

2.5.5 *Modelling cells with two place fields using two Gaussians*

Cells with two firing fields in one running direction were determined by fitting a mixture of two Gaussian functions to the spatial firing rate

profiles. The linear combination of two gaussians comprised six parameters: the mean values μ_1 and μ_2, the widths σ_1 and σ_2, and the amplitudes A_1 and A_2. Fitting was performed in two steps. First, we estimated approximate values for all parameters by fitting a Gaussian mixture model. The parameters from this procedure were then used as initial guesses for a non-linear least-squares fit of the double-Gaussian. For the least-squares fit the parameters were bound to $A_1, A_2 \in [0, \infty)$, μ_1, μ_2 inside the track, and $\sigma_1, \sigma_2 \in [0, \text{track width}/3]$. Gaussian mixtures were fit with scikit-learn and non-linear least-squares was performed with scipy (Fig. 2.8 A_2 left and A_3 left).
Fit quality was confirmed by comparing place field center, firing rate maximum and place field width of place cells firing rate profile with fitted gaussians. Ideally fits should yield the same values as recordings. Therefore, data points for their comparison should lie on the bisecting line. Figure 2.8 B confirms that fits succeed to represent data very well.

2.5.6 *Surrogate data test*

For testing if the firing rate profile included one or two peaks, we performed a surrogate test. The firing rate profile of a particular cell was shuffled across the extend of the entire track and then fitted with the two linearly combined gaussians as described above. This procedure was repeated 1000 times for every place cell. Fitting theoretically gave two peaks with a valley in between. From each shuffled and fitted sample, we calculated a test statistic (M-value) as the difference ΔFR of smaller peak and minimum of the modulus of the derivative (typically the valley) between the two gaussians (note that if the derivative is unequal to zero, ΔFR could also be negative). The difference ΔFR was normalized by the average firing rate $\overline{FR}$ connected to the smaller peak (Fig. 2.8 A_1)

$$M = \frac{\Delta FR}{\overline{FR}} \qquad \text{with} \qquad \overline{FR} = \frac{1}{n} \sum_{i=1}^{n} FR(x_i) \; . \tag{2.2}$$

If the M-value of the actual data corresponded to a probability above 95% and the smaller place field had a peak firing rate of at least 3

Hz, the cell was counted as having two place fields; otherwise the cell only had one place field (Fig. 2.8 A_2 and A_3). Firing rate profiles were tested for single or double fields for each gain factor separately. To be counted as a cell with two fields it was sufficient if the cell had two fields at one gain.
In case two peaks could not be determined from the double Gaussian fit, the cell was also counted as having only one field.

For cells that have multiple fields in one running direction, the identity of the fields was defined according to their firing rate: the highest peak in one gain was identified as the highest peak in the other gain and likewise, the two smaller peaks were identified with each other.

2.5.7 *LFP and phase precession*

Theta oscillations were detected by zero-phase-filtering of the raw LFP signal in the theta band 6-10 Hz (reduced from 4-12 Hz, due to movement related artefacts) using a rectangular filter function in frequency space. By means of a Hilbert transform of the filtered signal, every spike was assigned an instantaneous theta phase.

To determine the strength of phase precession, LFP phases ϕ_j and corresponding x-positions on the linear track x_j of place field spikes where fitted with a circular-linear approach (Schmidt et al., 2009; Kempter et al., 2012). Places x_j at which a spike occured were normalized by the place field width such that $x_j \in [0, 1]$. Phase offset ϕ and slope a where obtained via maximization of

$$R = \left| \frac{1}{n} \sum_{j=1}^{n} e^{i(\phi_j - 2\pi a x_j)} \right| \tag{2.3}$$

with the restriction of the range of possible slopes to $a \in [-2.5, 2.5]$ cycles per field. Fits were only performed if a minimum of four spikes were present in four or more theta cycles.

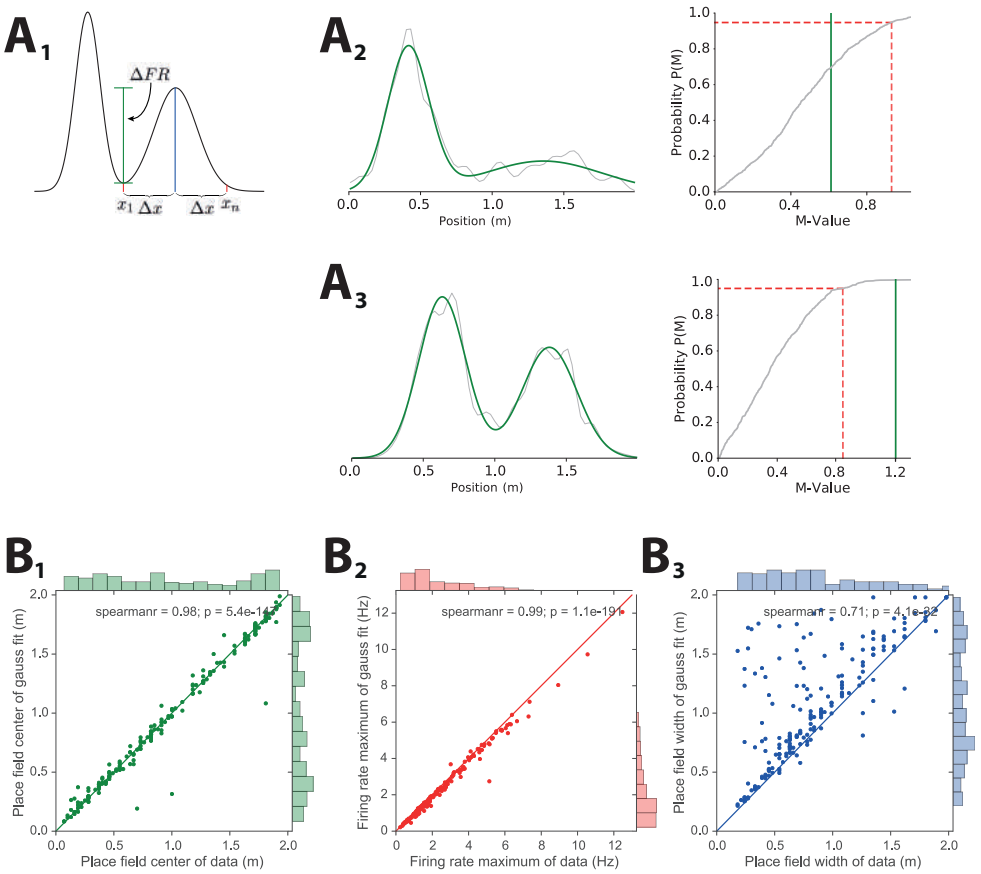

Figure 2.8: Double place field analysis. (A1) Illustration of the dip size (ΔFR) used as test statistics for classification into single or double peaked place cells. See Online Methods for details. (A2) Cell with a single place field. Left panel: Firing rate along track (gray) and fit with double Gaussian (green). Right panel: Cumulative distribution of shuffled surrogate data. Red dashed lines delimit 95% range. Green solid line marks test statistics (M-value) for the actual data, which is below the 95% boarder and identifies the cell as having a single field. (A3) Same illustration for a place cell with two fields. (B) Quality of place field fits. Correlations between place field center (B1), maximum (B2), and width (B3) with the respective fits of double gaussians.

Spike correlations

To perform theta compression analysis, crosscorrelation functions of smoothed place field spike trains were calculated. Spike train smoothing was done using a Gaussian of 10 ms width. Spike pairs were used for further analysis if a minimum of 25 pairs contributed to the crosscorrelation function, in an interval of one theta cycle around lag 0. For these pairs the lag of the peak closest to zero was extracted and transformed it to theta phase ψ. Place field distances were determined from the peak displacement of the spatial correlation function which was computed after smoothing spike locations by a Gaussian of 3 cm width.

3

RESULTS

3.1 ESTABLISHING EXTRACELLULAR PLACE CELL RECORDINGS ON A REAL LINEAR TRACK

In order to determine the response pattern of gerbil spatially-active hippocampal cells with our recording system, I initially recorded extracellularly from place cells in a real environment and compared them to published data from rats and mice (O'Keefe, 1976; O'Keefe and Recce, 1993).
Untrained, implanted gerbils where put on a real linear track (Fig. 3.1 A) and given one reward pellet when they reached either end of the track. Their position was tracked via a camera, situated above the track, which recognised coloured LEDs on the microdrive's headstage. Gerbils learned within a few sessions to shuttle back and fourth on the track, in order to collect rewards. In figure 3.1 B gerbil trajectories of one recording session are plotted in grey. The recording of one pyramidal cell shows an accumulation of spikes (Fig. 3.1 B, red dots) in one particular area, which marks the place field (more prominent in firing rate heatmap, Fig. 3.1 B, lower plot). Place cell spikes were only used in the analyses when gerbils ran at least 10 cm/s.
Whilst the animal was running, the LFP showed a strong component in the theta band (Fig. 3.1 C) at 8.2 Hz, which was determined via the fast fourier transform (FFT) of the LFP (Fig. 3.1 C, inset). When the corresponding filtered LFP hilbert phase of every place cell spike was plotted against its track position, theta phase precession was observed (Fig. 3.1 D).
With these findings, I observed place cell activity and place cell properties in the gerbil, known from rats and mice with similar peak firing rate, unidirectional activity, phase precession and LFP theta (Fig. 3.1).

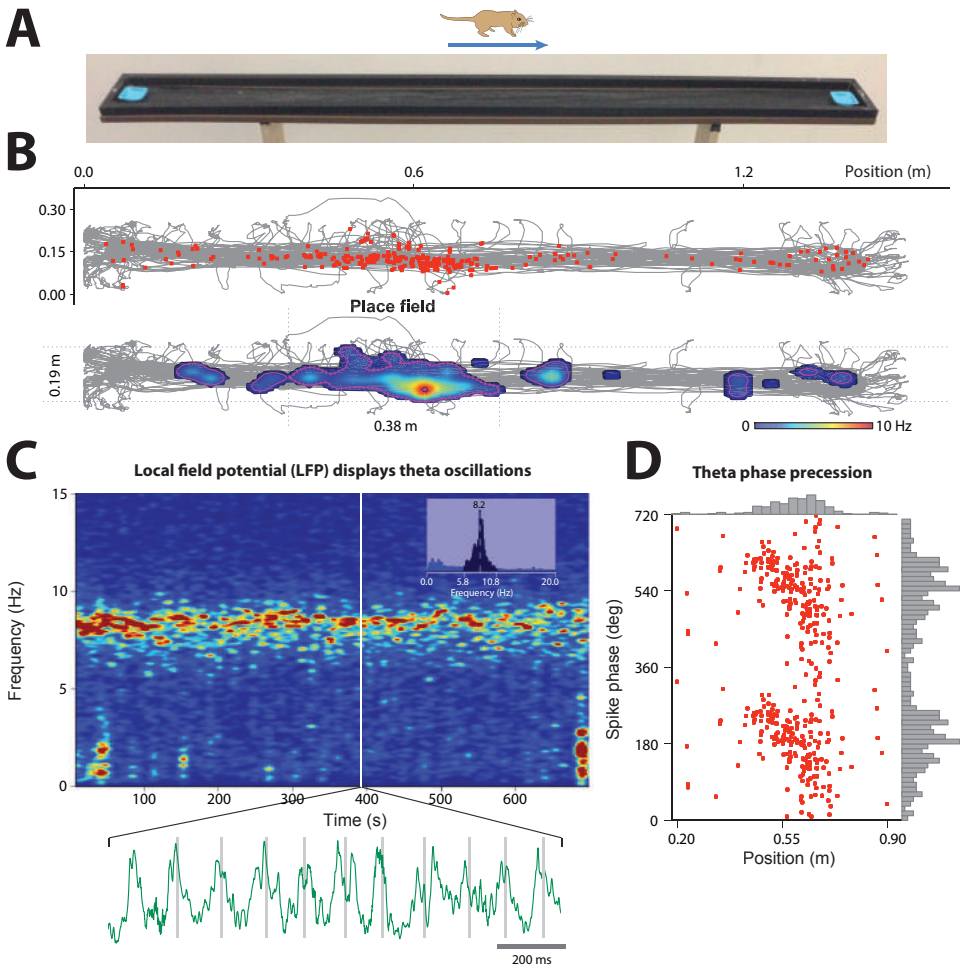

Figure 3.1: Place cell and LFP activity on a real linear track. (A) Linear track setup with blue reward bowls (see Fig. 2.1 B). (B) Example place cell activity, present only during rightward runs. Trajectory (grey) and spikes (red dots) of an example session. The associated place field is marked (dotted lines) in the firing rate heat map (bottom). (C) LFP frequency spectrum shows strongest activation in the theta band, at 8.2 Hz (inset shows FFT of the LFP). Example LFP trace is shown on the bottom. (D) Theta phase precession for cell from B.

3.2 BEHAVIOURAL TRAINING OF GERBILS ON VIRTUAL LINEAR TRACK

After having established place cell recordings on the real linear track, gerbils were trained in the VR setup. In contrast to the real environment, animals had to be acclimatised to harness, fixation in the VR and to recognise the projection as a linear track, in which they were able to earn rewards for completed single runs. In order to accelerate initial training, a gain of 1 was used between treadmill displacement and change in virtual scene. This means, that movement of the visual projection directly corresponds to the movement of the treadmill and therefore the animal.
In approximately the first two training sessions, gerbils had to learn how to navigate on the treadmill whilst being fixated via the harness. These sessions were usually shorter (5-10 min) as gerbils had difficulty understanding the task and to recognise the correlation between their limb movement and the change in virtual projection. This difficulty can be extrapolated from the movement of the animal within the virtual maze (Fig. 3.2 A). In the first session of the example animal from Fig. 3.2 A, the gerbil only traversed the entire length of the track once in 6 minutes. To allow the animal to recover from the initial stress, only one session was performed per day.
Already in session 5 the animal seemed to have learned the task. Even though it still moved occasionally along virtual walls (Fig. 3.2 B, left), in manages to perform about 44 complete single runs in 16 minutes. Figure 3.2 B (right panel) indicates that the animal performed strongly goal directed behaviour, as it was able to traverse the linear track in about 20 seconds. Even though the animal completed enough runs on day 5 (3.2 B) for recordings to be made (a minimum of 40), its behaviour was not sufficient.
Spikes are only included in the analysis when the animal had a minimum speed of 10 cm/s. This speed threshold is important as I aimed to remove place cell reactivation during immobility of the animal. Additionally this threshold allowed me to remove incidents where the animal ran into a virtual wall, where its position was reset to the entry point and therefore reduced the animal's virtual speed. At these incidents, I was not able to quantify the gain, between own movement and projection, the animal is perceiving.

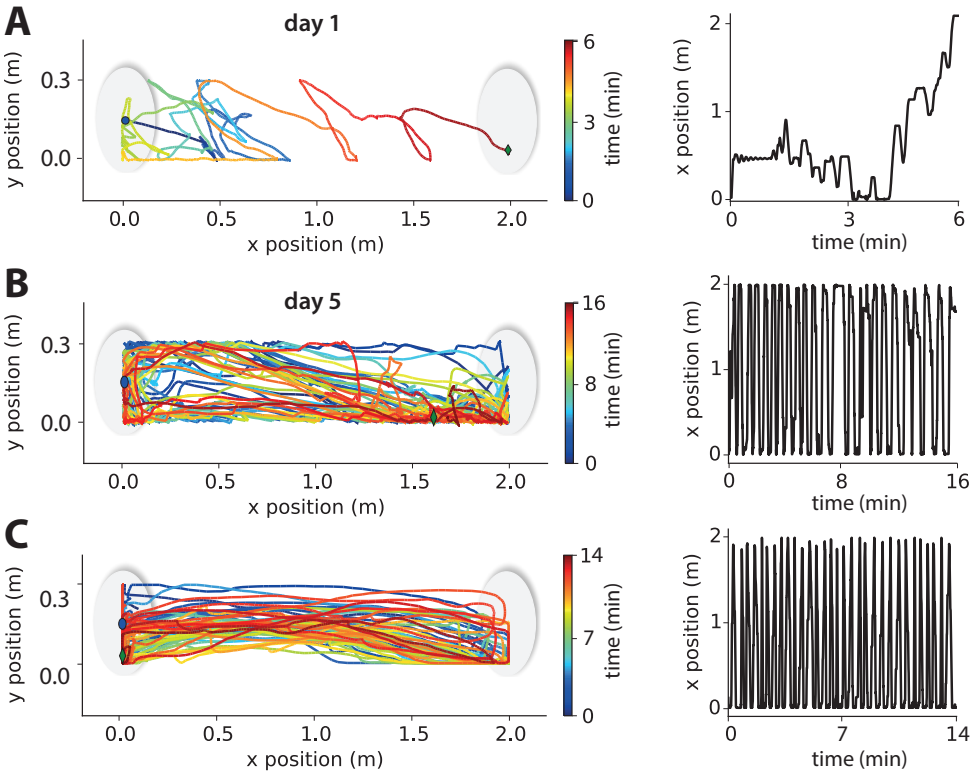

Figure 3.2: Behavioural performance in VR setup. (A) First training session of example animal. Left, the animal's trajectory on virtual track, with time color coding within the session. Oval areas show reward zones. Blue circle depicts start position and green diamond end position of the animal. Right, x-position on virtual track over time shows that only one single run is completed within 6 minutes. (B) Same as (A) only for the fifth training session of the same animal. (C) Same as (A), for a different animal and later recording session, when the animal was fully trained.

Including about 5 further training sessions and about 2 weeks of training after tetrode implantation (time to reach CA3), animals performed much better by avoiding virtual walls and therefore reaching the reward zones faster (Fig. 3.2 C). Such behaviour ensured enough place cell spikes to be included in the analysis.

In the first VR recordings, I used a gain of 1 as described for training sessions. This was done in order to ensure quality of VR recordings and similarity between VR and real environment data.
After tetrode implantation, animals were continuously trained once a day and tetrodes were lowered about 100 µm after each recording session. When a depth of about 1200 µm was reached, tetrodes were lowered more carefully (50 µm per day). Thereby new cells could be recorded every day and spike sorting was done directly after experiments. Plotting spikes of every cluster onto the animal's virtual trajectory would then determine whether hippocampal pyramidal cells had been reached. Further, LFP sharp waves during sleep sessions (5-10 minutes long) before track recordings were a strong indication that the hippocampus had been reached. If so, tetrodes were only adjusted 25 µm per day to target further principal cells.
Figure 3.3 A shows a recording of one VR place cell with gain 1. In A_1, spikes reveal that this place cell is predominantly active during rightwards runs and reliably fires around 0.5 m. When depicting the spike phase as a function of animal x-position, theta phase precession can be clearly identified and further emphasised via its circular fit (Fig. 3.3 A_2, orange line). Due to directionality, phase precession and spikes occurring reliably within the place field, VR unit activity could be classified as place cell activity.

3.3.1 *Comparison of place cell properties in real and virtual environments*

In order to compare place cells from real and virtual linear tracks, 33 place cells were recorded in the real environment and 32 place cells in the virtual environment using gain 1. Although place cell peak firing rate seemed to be reduced in virtual reality (Fig. 3.3 B), place field width and phase precession was comparable for real and virtual environments (Fig. 3.3 C and D). LFP theta frequency is known to increase with the animal's running speed in rats (Ravassard et al., 2013).

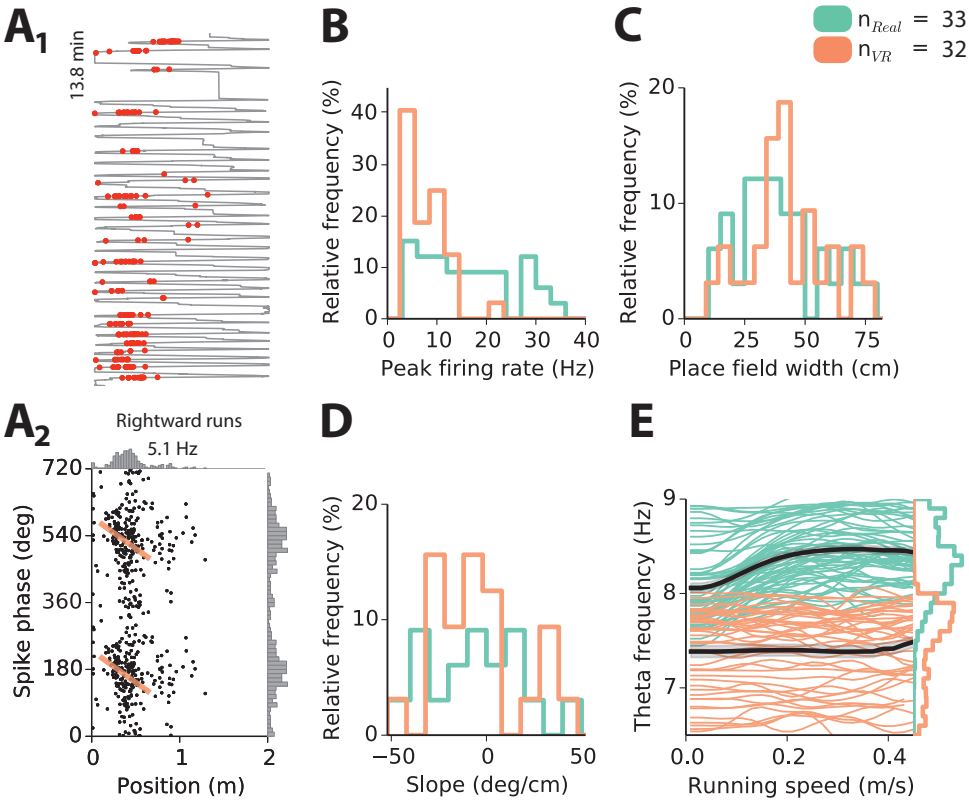

Figure 3.3: Comparison of VR gain 1 and real environment. (A) Example VR gain 1 place cell. Top, Single runs (trajectory in grey) with spikes (red dots). Bottom, phase precession with fit (orange line). (B) Peak firing rate histogram for place cells from real (green) and VR (orange) track. (C) Field width histogram for both environments. (D) VR and real histograms of phase precession slopes from fits. (E) Theta frequency as a function of running speed. Coloured lines depict single VR or real sessions. Black lines show respective mean. Data contributed by Josephine Henke and Kay Thurley.

In real linear track sessions, a similar correlation for gerbils was observed (Fig. 3.3 E, green lines with black mean). In contrast to that, VR track sessions revealed reduced theta frequency of 0.5-1 Hz (Fig. 3.3 E, orange lines with black mean) and no correlation with the animal's running speed. This difference between real and virtual tracks has been reported by Ravassard et al. (2013) with a similar virtual environment.

After having established place cell recordings in virtual reality using a gain of 1, I continued with my second thesis objective and investigated how place cells encode visual and locomotor information. To distinguish between the two sensory inputs, I altered of the relation between the animal's own movement (treadmill displacement) and visual input on a single run basis, via a gain change at reward zones of the virtual track. Gains were randomly chosen to be either 0.5 or 1.5 (Fig. 3.4 B). For both gain conditions, the projection of the virtual track was identical, whereas the distance the animal had to travel on the treadmill to reach reward zones varied with the different gains. The physical travel difference between gain 0.5 and 1.5 is a factor of three and chosen as such, to provide a clear difference in visual flow, which can be detected easily by the animal.
From all recorded place cells, 165 fulfilled chosen requirements (see subsection 2.5.2) to be considered reliable. These cells were all located in hippocampal CA3 and recorded whilst gerbils shuttled between VR reward zones (Fig. 3.4 A, B).
Out of these 165 cells, 138 were unidirectional, meaning that the majority exhibited a firing field in only one of the running directions. In contrast to this finding, Ravassard et al. (2013) reported that a large proportion of VR place fields showed bidirectional distance coding.
Additionally, I observed other response types, including cells with two firing fields, which occurred uni- or bidirectionally. Cells with two fields were also found in combination with a single field in the other running direction, indicating that both running directions are encoded separately. Further, 35% of all 165 cells where found to be only active at one gain, which can be explained by either a remapping process or a mapping, which would have its place field outside the presented track. An overview of these cell types is depicted via a pie chart in figure 3.4 C. It is important to note that the 11% of bidirectional

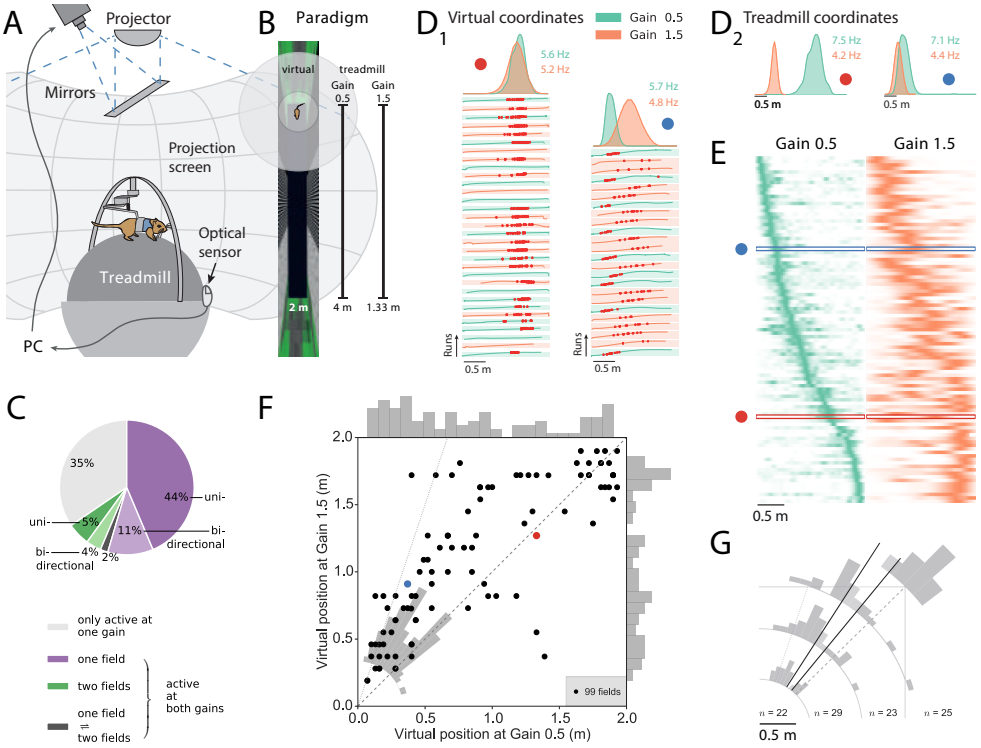

Figure 3.4: Visual and locomotor sensitivity of place cells. (A) Gerbil placed in VR setup. (B) VR track with 2.0 m virtual length and relative projection screen size (shaded area). Single run gains were chosen to be either 0.5 or 1.5. (C) Overview of place response types. (D) Two example place cells. (D_1) Consecutive rightward runs, stacked vertically with spikes (red dots) and single run trajectories (coloured lines) for two cells. 1D firing rate histograms are on top, with peak firing rates. (D_2) Example cells from D_1 replotted in treadmill coordinates. (E) Firing heatmaps of single field cells (93). Fields were normalised to their peak firing rate and ordered according to peak position at gain 0.5 (left). This order was kept for gain 1.5 (right). Red and blue dots mark cells in D and F. (F) Place field center positions depicted for both gains show visual or locomotor tuning. Both response types are conveyed via two peaks of the angular histogram. Fields encoding visual information lie close to the bisecting line (dashed). Fields driven only by locomotor information lie on the dotted line with slope 3. (G) Angular histograms for fields from (F) at different distances from the origin reveal locomotion-sensitive cells predominantly in the first part of the track. A confidence area separating both populations was removed for further analysis (black lines).

cells with one field include 12 cells which have one field in only one gain in one of the two running directions and are therefore a combination of the grey and dark purple group in figure 3.4 C.
To uncover the meaning of all these different firing behaviours, I focussed first on the simplest pattern, which included all 93 cells with a single place field at both gains, that could be either uni- or bidirectional.

3.4.1 *Distinct subclasses of place fields exhibit visual and locomotor tuning*

For each place cell, corresponding spikes and single run trajectories were divided into belonging either to gain 0.5 or 1.5. Spikes associated with one gain can therefore be treated as a separate place cell. Its own firing field and peak firing rate can be computed and compared to the field of the other gain.
I found that individual place cells exhibit a stable firing field for each gain. When fields for both gains are compared, they shift their center position according to the visual reference frame of the projected track or rather depending on the treadmill coordinates (Fig. 3.4 D, E). Figure 3.4 D_1 shows that such gain dependent place field shifts occur instantaneously and on a single run basis, already for the first gain changes (3.4 D_1, bottom single runs). Shifts do therefore not depend on paradigm adaptation and don't drift within one session.
Place field center shifts that I observed can be classified into two categories. First, 'vision-induced' place fields which fix their place field center onto one specific visual stimulus and therefore a virtual position. Such place fields overlap when plotted in virtual coordinates and are separated when plotted in treadmill coordinates (Fig. 3.4 D, red dot). This means, that in gain 0.5 the animal has to run 3 times as far to reach the specific visual stimulus than in gain 1.5, which leads to the observed place field separation in figure 3.4 D_2 (left example).
The second category of place field shifts can be referred to as 'locomotion-sensitive', as place fields for both gains overlap in treadmill coordinates but not in virtual coordinates (Fig. 3.4 D, blue dot). Such tuning is likely to be driven by non-visual cues, as fields do not over-

lap in virtual coordinates. Due to field overlap in treadmill coordinates, fields seem to rather encode self-motion cues such as motor efference copies, somatosensation (stepping on the treadmill), audition (rhythmic sound of the steps), and proprioception.
In figure 3.4 E the entire population of place cells with one firing field is displayed as 1D firing rate histograms. Such representation indicates that observed shifts from example cells in figure 3.4 D also occur for other cells in the population and could be rather prototypical.

In order to analyse which response type each cell belongs to, I correlated virtual place field peak positions obtained from both gains (Fig. 3.4 F). In such a correlation 'vision-induced' place fields, which have their firing field centres at similar virtual positions, should scatter around the bisecting line (Fig. 3.4 F, dashed line). On the other hand should 'locomotion-sensitive' place fields scatter around similar treadmill positions, which should be placed on a line with slope 3 (Fig. 3.4 F, dotted line) due to the difference in virtual displacement between the gains (factor of 3, see subsection 2.5.4).
Data points in figure 3.4 F scatter around both lines, indicating two distinct populations of cells which receive different amounts of visual and locomotor drive. The angular histogram within the figure shows a distribution of this drive with a dip in the middle, pointing towards a stronger drive of either visual or locomotor information.
Rather, locomotion-sensitive fields are positioned around the dotted line with slope 3, which is true for fields in the beginning of the track. Locomotion-sensitive fields positioned further down the track seem to cluster around a line with slope 2, which could be due to growing uncertainty with increased travel distance and additionally the impact of visual information (e.g. optic flow). Fields located in the middle of both ideal lines (dashed and dotted) would therefore receive a balanced input from locomotor and visual information.
To statistically investigate a clustering of the angular distribution (from Fig. 3.4 F) into two distinct populations, I used a likelihood ratio test to compare a bimodal Gaussian fit to the null-hypothesis of a unimodal gaussian distribution. This test rejects the unimodal model with $p = 7.7 \cdot 10^{-41}$ ($\chi^2 = 189.5$). Additionally I tested the robustness of this result by using a more conservative significance estimate. For that I split place fields into two populations by fitting a mixture of two gaussians to the same angular histogram. The separating angle was then

determined as the valley between both gaussians (53.6°). For this estimate a 95% confidence region was determined via bootstrapping to be between 51.1° and 57.7° (Fig. 3.4 G, black lines). Using the magnitude of the dip between the peaks as test statistics (see M-value in subsection 2.5.6), the Gaussian mixture for the angular distribution was compared to the Gaussian mixture fit for shuffled data sets (see subsection 2.5.6). Using this, significance of bimodality was calculated to be $p = 0.024$.
As both methods revealed a significant bimodal distribution, I assumed place fields to be clustered into two distinct response populations. For further analysis I excluded the $n = 12$ fields located within the confidence region.

After having separated place fields into two response types, I wanted to investigate whether such separation occurs equally in every portion of the linear track or whether there are any systematic changes to be observed. In order to do so, I split the track into four slices, in which I recalculated the angular distribution (Fig. 3.4 G).
I used Fisher's exact test to test for systematic differences among the four angular histograms and found that the first three histograms are all significantly different from the last (last quarter of the track), with a maximal p-value of all three tests of $p = 2.5 \cdot 10^{-8}$. Contrastingly, the first three histograms are not significantly different from each other (Fisher's exact test; minimal p-value of all four tests: $p = 0.091$).
This leads to the conclusion that the two response types are generated by place fields from different areas on the track. Fields from the first three quarters of the track rather comprise the locomotor or path-integration component, whereas the last quarter hosts place fields which are very strongly driven by visual information. This finding is consistent with previous findings (Gothard et al., 1996).
Finding only visually-driven fields in the last quarter of the linear track is however trivial in my experiments, as locomotion-sensitive place fields cannot be found for virtual positions larger than about 1.33 m (in gain 0.5). As a line with slope 2 in figure 3.4 F indicates, locomotion-sensitive fields occurring after 1.33 m for gain 0.5 would have its place field center outside the linear track for gain 1.5.
Despite such a bias towards visually-driven fields at the rear part of the track, there is a clear overrepresentation of locomotion-sensitive fields at the beginning of the track ($\leqslant$ 1.33 m).

Finding two response types in CA3 suggests that inputs from different modalities to the hippocampus are processed rather individually and would therefore not be integrated entirely on a single cell level.

3.4.2 *Properties of modality-dependent place maps*

Further, I investigated whether place maps for the two different response types differ in the way they process their modality-specific input, which could potentially result in distinct encoding optimisation. Such a difference in processing was tested via comparison of a wide spectrum of place cell properties.

In order to inspect locomotion-sensitive and vision-induced place fields individually, the categorisation obtained from figure 3.4 G (black lines) was used, which excluded place fields within a confident region (Fig. 3.5 A, top left inset). Via this clustering, firing rate heatmaps were created for each population, in virtual and treadmill coordinates (Fig. 3.5 A). This representation allows an overview of both field populations and gave insight into the distribution of field centres over the track and validated that positions for locomotion-sensitive fields (blue) overlap much better for both gains when represented in treadmill coordinates as well as vision-induced fields do so in virtual coordinates (red).
Place field center distributions revealed, that in virtual coordinates the entire track is covered with fields of either population. This finding indicates that both modalities form a complete representation of the animal's environment in an independent and simultaneous manner.
This does not hold true however for locomotion-sensitive fields, when examined in their respective coordinate system. As noted above, this field type can not be detected in gain 1.5 after 1.33 m (tack length) in treadmill coordinates (Fig. 3.5 A, vertical black line in lower plots).

Having noted that vision-induced fields are dominant in the rear region of the track, this effect was quantified by plotting field density over the respective virtual track location for both field populations and both gains per field (Fig. 3.5 B). Two findings presented them-

selves. First, vision-induced fields increase in density towards the rear part of the track, whereas locomotion-sensitive fields decrease. This decrease is present even before 1.33 m, as no fields from gain 0.5 can contribute to the presented density after. However, the dominance of locomotion-sensitive fields was prominent in the first quarter of the track (χ^2-test, $p = 0.0016$, $n = 29$ cells).
Second, vision-induced fields are not uniformly distributed over the track, but rather cluster around locations of visual texture change (Fig. 3.5 B_1). Distances between place field centres and the closest respective texture transition clustered at zero for vision-induced fields (χ^2-test, $p = 6.0 \cdot 10^{-4}$, $\chi^2 = 25.59$, $n = 78$, 39 cells for 2 gains; Fig. 3.5 B_2), meaning that all such fields lock to salient visual features on the track (texture transitions). In contrast to that were distances of locomotion-sensitive fields to texture changes consistent with a uniform distribution (χ^2-test, $p = 0.35$; $\chi^2 = 7.83$; $n = 96$, 48 cells for 2 gains).

As another place cell property, the dependence of place field size on track location was tested, as the path integration process would assume error accumulation with increasing travel distance.
Indeed I found that locomotion-sensitive place fields more than doubled their width throughout the track traversal (Fig. 3.5 C_1, blue example). In the beginning of the track, field widths were about 0.5 m, whereas they reached a width of almost 1.5 m towards the rear part of the track.
In order to ensure that narrow field width at the track beginning do not arise from the artefact of fields being cut off by the track edge, I compared widths with a surrogate data set (Fig. 3.5 C_2, grey lines). For that, place fields from the track center were randomly positioned across the entire track. The width distribution of these surrogate fields did not show the extend of field broadening at the rear part of the track, as locomotion-sensitive place fields did (Kolmogorov-Smirnov test $p = 5.1 \cdot 10^{-5}$, $n = 8$). Additionally, locomotion-sensitive fields proved to be slightly narrower at the track beginning (Kolmogorov-Smirnov test $p = 0.041$, $n = 34$).

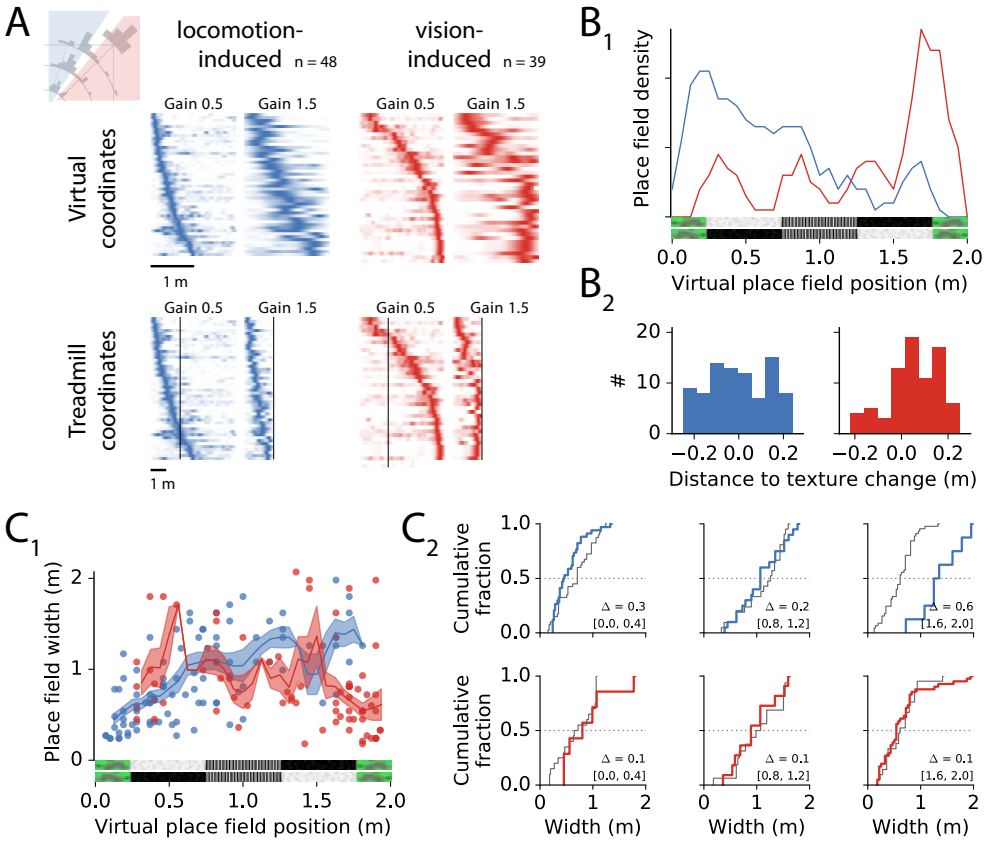

Figure 3.5: Modality-dependent place maps. (A) Place field heatmaps (as in Fig. 3.4 E) for both gains and response types (see inset and Fig. 3.4 F, G). Response profiles are more alike for both gains of each type in the respective coordinates. (B) Vision-induced fields cluster around texture changes and increase in density towards track end, whereas locomotion-sensitive field density decreases (B_1). Fields from both gains, left- and rightward runs are individual data points. (B_2) Histograms show distance of field centres to closest texture change. (C) Widths increase significantly for locomotor fields towards track end. (C_1) Width vs. position (markers: single fields; line, shading: mean $\pm$ sem). (C_2) Field width surrogate test, for which track center fields were randomly placed across the track. Surrogate width distributions (gray) significantly differ from locomotion-sensitive widths (blue) in first and last $1/5$ th of the track (left and right plot). Kolmogorov-Smirnov tests: locomotor (blue): $p = 0.04$, $d = 0.31$, $n = 34$; $p = 0.65$, $d = 0.22$, $n = 20$; $p = 5 \cdot 10^{-5}$, $d = 0.83$, $n = 8$; visual (red): $p = 0.85$, $d = 0.25$, $n = 6$, $p = 0.90$, $d = 0.21$, $n = 11$, $p = 0.56$, $d = 0.20$, $n = 41$.

In contrast to these findings did I not observe any significant difference of visually-induced field widths to the surrogate field widths (Kolmogorov-Smirnov test $p > 0.56$, 3.5 C_2 red example).
Both, increase in place field width of locomotion-sensitive cells as well as the accumulation of vision-induced place fields at positions with salient optical cues, further substantiate the hypothesis of parallel processing of distinct hippocampal input streams. At the population level this results in different coexisting representations of the spatial environment.

Additionally to place field location and field width, I investigated whether any differences in other place cell properties can be found when comparing locomotion-sensitive and vision-induced place fields. As figure 3.5 A depicts normalised firing rates, I compared peak firing rates of both response types and both gains (Fig. 3.6 A). The first two rows of figure 3.6 A reveal, that in treadmill as well as visual coordinates, locomotion-sensitive fields (blue) show an almost identical peak firing rate to vision-induced fields (red). Slight differences of peak firing rates in both coordinate systems are due to spike binning, which was fixed to 3 cm in both frameworks. The only noticeable difference in peak firing rate between both gains can be seen in visually driven fields in treadmill coordinates (Fig. 3.6 A, first row, bottom). Gain 0.5 fields seem to have an increased peak firing rate (Fig. 3.6 A, first and third row, bottom), which is however abolished when plotted in its respective visual coordinate system (Fig. 3.6 A, second and fourth row, bottom) and is therefore only a representation artifact.
Spatial information (see subsection 2.5.3) is encoded equally well in both response types (Fig. 3.6 B), as gain difference of spatial information clusters around zero for treadmill and visual coordinates (Fig. 3.6 B, bottom two rows). A slight shift towards positive values for vision-induced fields in treadmill coordinates is due to the representation artefact (as in peak firing rates).
To further corroborate findings, that peak firing rates and spatial information do not differ for both response types, I went into more detail and analysed whether mean single run spike count was stable within place fields when comparing locomotion-sensitive and vision-induced fields. This level of detail confirmed previous findings and did not uncover any differences between response types (Fig. 3.6 C, row 3 and 4 cluster around zero).

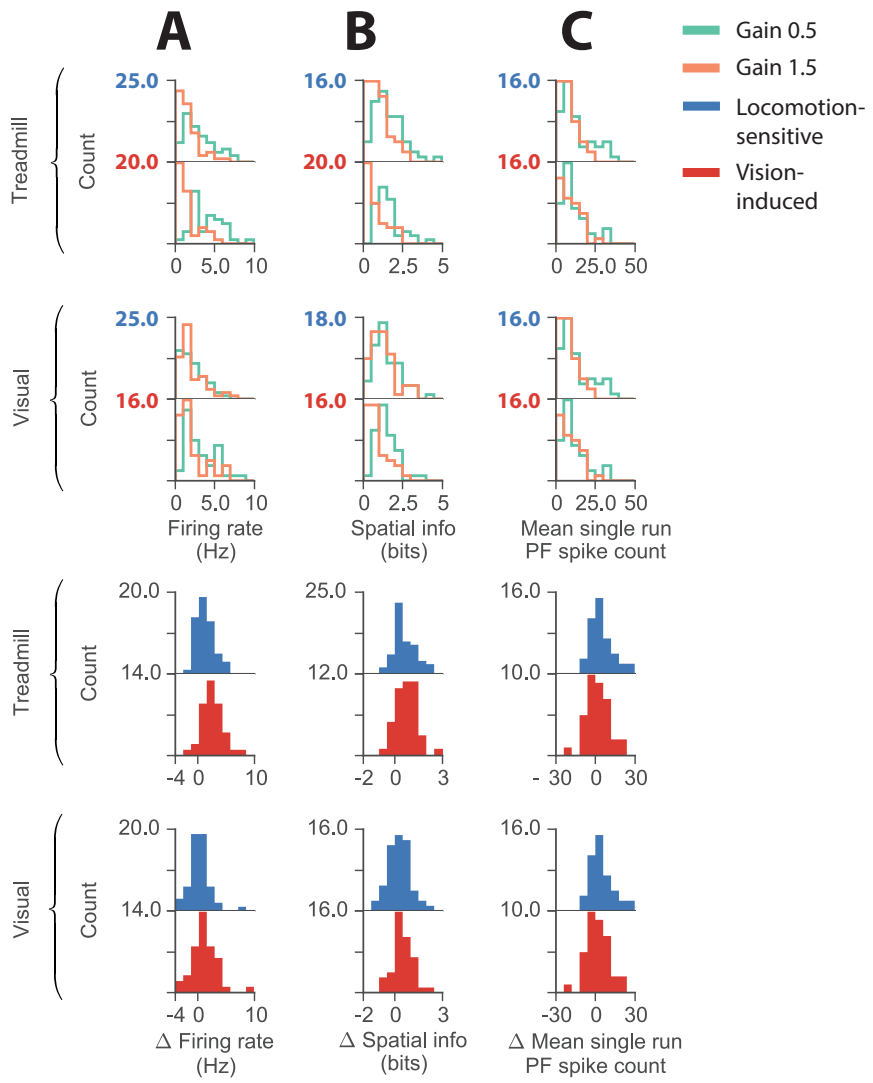

Figure 3.6: Analysis of place cell properties. Data is displayed across both gains for five different parameters (in columns from left to right): peak firing rate (A), spatial information (B) and average in-field spike count (C). Each row contains a group of two axes with data for locomotion-sensitive place fields (top) and vision-induced fields (bottom). The first two rows show histograms of the respective parameter for both gains separately (green: gain 0.5, orange: gain 1.5) in treadmill (top) and visual (bottom) coordinates. The bottom two rows depict values for gain differences (value at gain 1.5 subtracted from value at gain 0.5).

3.4.3 *Bidirectional and double-field cells*

Finding two distinct place field response types in hippocampal area CA3, which differ in place field width and position properties, indicate that CA3 processing might occur via two functionally distinct subcircuits. This begs the question, whether such differential processing is clustered also in an anatomical fashion.
As extracellular recordings were conducted using the same stereotactic coordinates across animals, one can argue that this is the case on a macroscopic scale. As gerbil brains differ in size and implantation accuracy may very, tetrode position can however not be compared on a microscopic level. Anyhow, as I succeeded to record place cells of both response types from the same tetrode and the same session (n = 17 tetrodes), even a microscopic response type clustering appears unlikely.
This hypothesis was proven to be true by the fact that I recorded from 18 bidirectional place cells (examples in 3.7 A) with one field in each direction, out of which 2 cells showed visual tuning in one running direction and locomotor tuning in the other (Fig. 3.8 A and 3.10 A). The presence of both response types within one place cell makes complete anatomical segregation impossible.

The same conclusion can be drawn from place cells with two firing fields present in one running direction (Maurer et al., 2006; examples in Fig. 3.7 B), as 19 out of such 21 spatial response profiles were found to have one field being driven by visual and the other by locomotor information (3.10 B). Such response pattern was usually conveyed in a certain order, where the first firing field was locomotion-sensitive whereas the second was vision-induced. This order goes hand in hand with the response-type-specific bias of place field centres observed in single field units (Fig. 3.4 F, G).
The 21 unidirectional response profiles with two fields are comprised of 18 single units, including 9 bidirectional units (Tab. 3.1 and Fig. 3.8 B, C). Only 3 of these bidirectional units showed two fields in both directions and at both gains (Fig. 3.8 B; examples in Fig. 3.7 B_3), leading to a total of 21 unidirectional (18 + 3) response types with two fields (42 place fields in total, see Fig. 3.10 B).
The separation into two firing fields became usually apparent at gain

0.5 (see examples in Fig. 3.7 B), as locomotion-sensitive fields appear narrower and therefore do not overlap with the second firing field. The converse argument holds true, that at gain 1.5 fields mostly overlap and therefore appear skewed (Figs. 3.9 A).
As single units with two firing fields can be categorised for each field to belong to either, the visual or locomotion-sensitive response type, these fields can be added to the single field population from figure 3.4 F. The combined data set (Fig. 3.9 C) illustrates that fields from double-field cells (Fig. 3.9 C, unfilled markers) follow the same distribution as single-field cells (slopes 1 and 2, Fig. 3.9 C, D, $p = 0.014$, dip test on Gaussian mixture model). This is corroborated by the fact that the separating angle of the angular histogram for double-field cells is 53.1°, which is consistent with the confidence region obtained from single-field cells. Figure 3.10 B illustrates which of the double fields from figure 3.9 C originate from the same cell (black lines) and shows that fields from one cell mostly belong to different response categories (blue and red area).
As single- and double-field cells follow the same clustering structure, it is plausible that both cell types receive similar inputs to drive place field formation. This is corroborated by the fact that bidirectional cells have not been found only for cells with a single field (Fig. 3.10 A) but also for cells with double fields and most importantly a mixture of the two, with one running direction displaying one firing field and the other two (Tab. 3.1 and Fig. 3.8 C).

The finding of place cells with two firing fields in one running direction driven by different modalities, rejects strict anatomical clustering of visual and locomotor response types. The additional finding of double-field centres following the distribution found for single-field cells strengthens the hypothesis that hippocampal CA3 pyramidal cells sample inputs from distinct processing streams to provide locomotor and visual information for modality-specific space representations displayed as place fields.

Figure 3.7: Place cell examples with fields shown in both, virtual (left panel) and treadmill coordinates (right panel). Scale bar corresponds to 0.5 m. (A) Bidirectional cells. (B) Two-field cell types. (C) One gain active cells, with place field in the rear 2/3 of the track (putative-locomotor, C_1, C_3) and activity in the first 1/3 (C_2, C_4).

	one field -directional		two fields -directional		one field ⇌ two fields	only active
cell type	uni	bi	uni	bi	bidirectional	at one gain
animal 1	45	9	8	5	2	28
animal 2	5	2	0	0	0	1
animal 3	16	3	1	0	1	25
animal 4	6	4	0	1	0	3
sum	72	18	9	6	3	57
percent	$43.\overline{63}$	$10.\overline{90}$	$5.\overline{45}$	$3.\overline{63}$	$1.\overline{81}$	$34.\overline{54}$

Table 3.1: Cell numbers for place field types from figure 3.4 C (identical color code). One and two field bidirectional cells include cells, active at only one gain in one direction (one field: n = 12, two fields: n = 3). Further bidirectional cells (~ 2%) show two fields in one direction and one in the other.

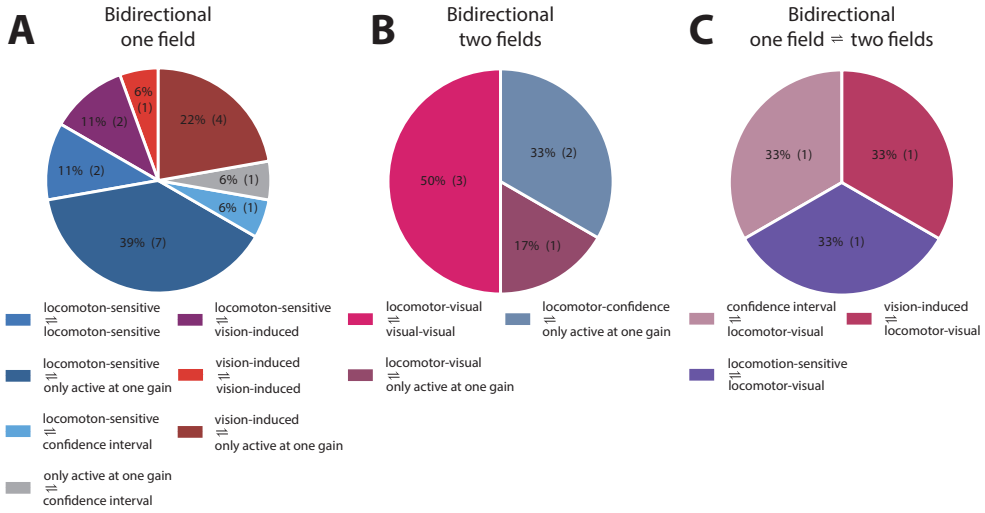

Figure 3.8: Bidirectional cells (cell numbers in brackets). Each field has a response type: locomotion-sensitive, vision-induced, confidence interval (Fig. 3.9 C, white area) or one gain active. (A) One-field cells can have any response type per direction. (B) Cells with at least two fields per direction. (C) Cells with one field in one direction and two fields in the other.

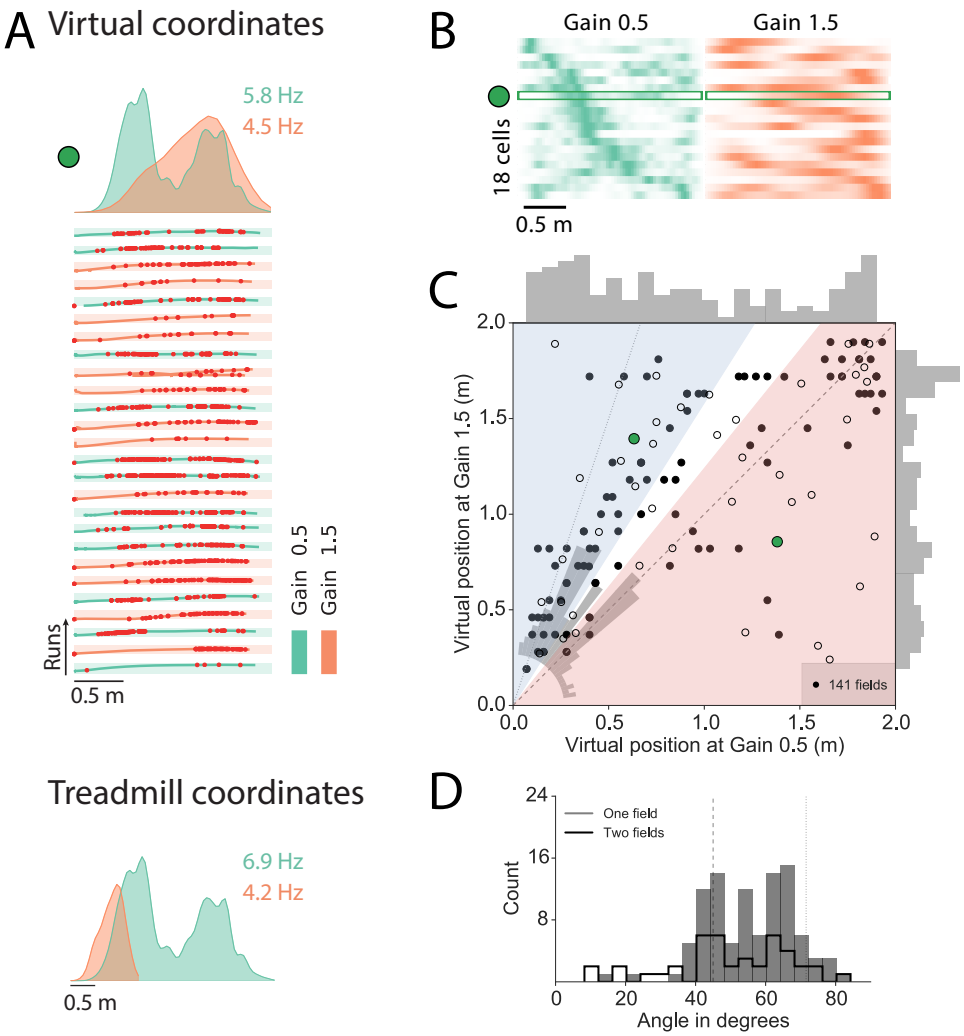

Figure 3.9: Place cells with two firing fields. (A) Unidirectional double field cell with field separation only at gain 0.5. Coordinate system comparison reveal the first field to be locomotion-sensitive and the second vision-induced. (B) Normalised firing rate heatmaps for double cells, sorted by maximal firing rate position at gain 0.5. Green circles mark example from A. (C) Virtual peak position for both gains (see Fig. 3.4 E) with double cell fields (unfilled markers). Green circles display example fields from A. (D) Angular histograms for single (grey) and double (black lines) fields. Distributions do not significantly differ from each other ($p = 0.20$, χ^2-test, $\chi^2 = 22.65$, $n = 99, 42$), but differ themselves significantly from uniformity (double: χ^2-test, $p = 0.021$, $\chi^2 = 102.32$, $n = 99$; single: $p < 0.001$, $\chi^2 = 32.19$, $n = 42$).

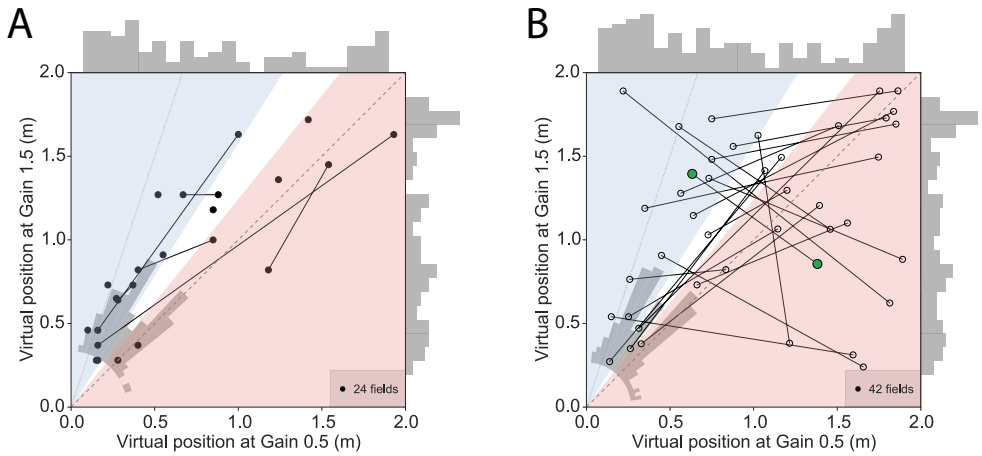

Figure 3.10: Field type classification and field-to-cell assignment for bidirectional and double-field cells. Virtual position of firing field centres for both gains (markers) for each bidirectional cell (A) and each double-field cell (unidirectional, B). Fields from the same cell are connected via a black solid line. Not connected dots in (A) are only active at one gain in the other running direction. Area for rather vision-induced fields is shaded in red, locomotion-sensitive area is shaded in blue. Dashed and dotted lines indicate positions of pure visual and pure locomotor drive, respectively. Green circle in (B) marks the two fields of example cell in figure 3.9 A.

3.4.4 *Putative locomotion-sensitive cells*

So far I have described two possible response types per place field for cells with one or two place fields. These fields account for 65% (108/165) of all recorded place cells (see Fig. 3.4 C and Tab. 3.1). The remaining 35% of cells also show spatially restricted firing fields, but only display above threshold activity in one of the two gain conditions (Fig. 3.11 A).
This observation begs the question whether these cells belong to a third category or if they can be understood according to the two described response types.

As explained in subsection 3.4.1 and 3.4.2, locomotion-sensitive fields could not be detected after 1.33 m (treadmill coordinates) at gain 1.5, as the linear track ends at this location. On the other hand does the track have a length of 4 m (treadmill coordinates) at gain 0.5. If locomotor driven fields ought to overlap in treadmill coordinates, fields after 1.33 m at gain 0.5 would not have a field at gain 1.5 as the animal cannot reach it. This interpretation of fields displaying activity only at one gain holds only true if activity can be observed at gain 0.5 and after 1.33 m (treadmill coordinates). In all other cases, locomotion-sensitive fields should be active at both gains. If not, they could be interpreted as performing remapping due to e.g. the difference in visual flow in the other gain.

Out of 72 cells which display a firing field only at one gain (57 units and one direction of 15 bidirectional units, see Tab. 3.1 and Fig. 3.8 A, B), I found only 9 cells which were active at gain 0.5 before 1.33 m (treadmill coordinates; examples in Fig. 3.7 C_2 and C_4). These 9 cells should display a firing field at gain 1.5 if they would be consistent with locomotion-sensitive fields and could therefore perform remapping at gain 1.5.
All remaining 99 cells with a field only at one gain were found to be active only at gain 0.5, after 1.33 m (treadmill coordinates) and would therefore fit into the requirements for locomotion-sensitive fields (Fig. 3.11 B, black fields; examples in Fig. 3.7 C_1 and C_3). The fact that about 92% of all cells with one gain activity are only detectable after 1.33 m at gain 0.5 argues that this field type is in fact locomotion-sensitive. This finding shaped the term 'putative locomotion-sensitive' fields for cells with fields at only one gain.

When these cells are treated as locomotion-sensitive, they can be incorporated into the overview map of spatial response profiles for cells with single fields (Fig. 3.11 B, C). Figure 3.11 C shows a complete coverage of the whole linear track for both response types, locomotion-sensitive (blue and black) as well as vision-induced (red). Also clustering of vision-induced fields at certain positions of the track (texture changes, see 3.6) becomes apparent.

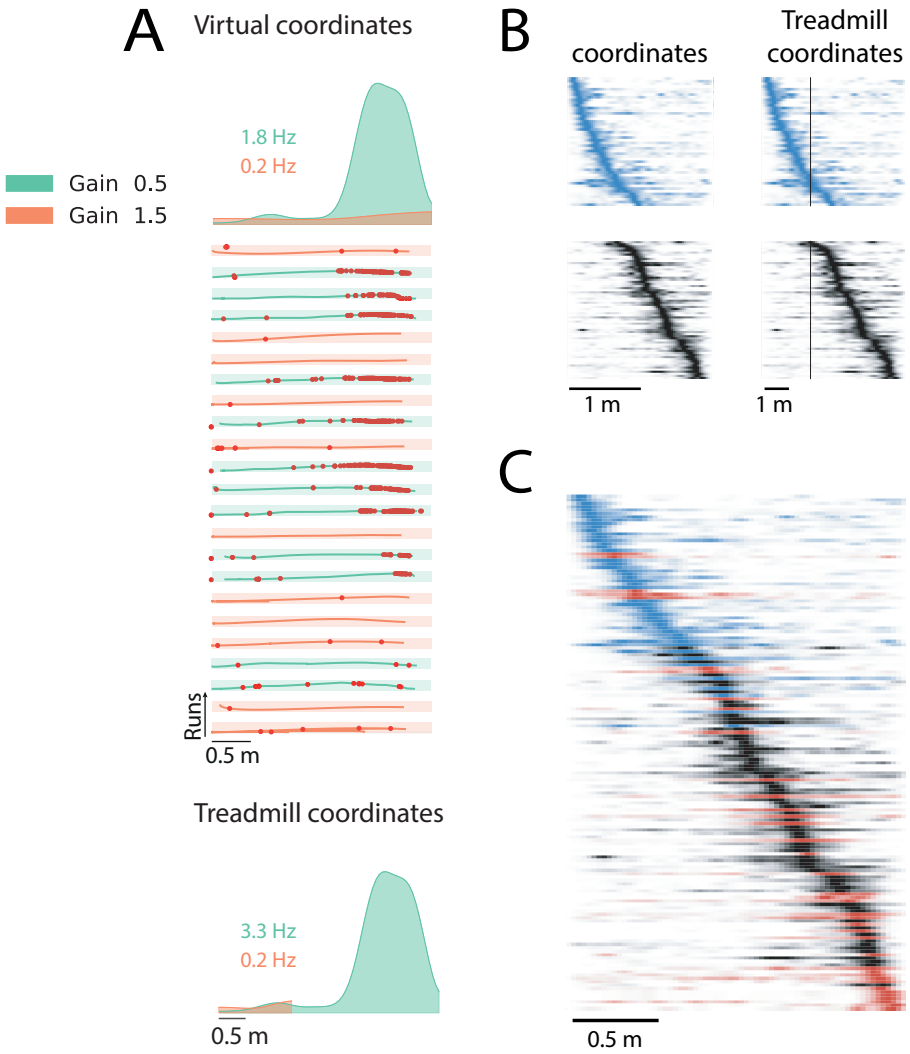

Figure 3.11: Cells active only at gain 0.5. (A) Example cell displaying its firing field only at gain 0.5. (B) Spatial response profiles for locomotion-sensitive fields (blue) from Fig. 3.5 A and fields that are only active at gain 0.5 (black). (C) Spatial response profiles for all recorded cells with single fields (visually-driven fields in red).

3.4.5 *Place cell activation in darkness*

When categorising place fields into locomotion-sensitive or vision-induced, the question arises whether locomotor or visual information alone is sufficient to drive place field response types as observed so far.
In order to provide the animal with only locomotor information for place field formation, one would have to remove all other sensory inputs to the animal. As this is impossible to do without performing additional surgery, I reduced available non-locomotor information by turning off the projection in the VR setup. As the setup is located in a sound proof chamber without any windows or additional lights, this guarantees complete darkness in the VR. As the animal would loose orientation within the virtual corridor, the light was only switched off for random single runs, as soon as the animal left the reward zone. The light was switched on again when the animal reached the next reward zone. Everything else in the gain change task was unperturbed, such that dark trials could be of gain 0.5 or 1.5.

Out of all 165 recorded place cells, 43 were recorded in this group of experiments (including 5 bidirectional cells, yielding 48 response types). For analysis described in earlier sections I removed single runs were the light was switched off. When however including these single runs, I observed two types of place cell response during dark trials. First, locomotion-sensitive place fields remained in the same position during dark runs (Fig. 3.12 A, left; n = 6 out of 48). This was also true for 'putative locomotor' fields (n = 11 out of 48), which showed activity only at gain 0.5 (see subsection 3.4.4; example in Fig. 3.12 A, right). The latter confirms the assumption that the field, active only at gain 0.5 after 1.33 m (treadmill coordinates) is indeed locomotion-sensitive, as it is active in the same location without any visual information provided. Even though activity at gain 1.5 is not possible, as the virtual track ends before the field can be reached, locomotion-sensitivity can be verified via single runs in darkness.
The second type of place cell activation in the dark can be roughly summarised as remapping. This can be observed on one hand by place cell activity reducing dramatically to disappearing completely during dark trails (example in Fig. 3.12 B; n = 26 out of 48). In contrast

to that do other place cells only show significant activity in darkness (Fig. 3.12 C; n = 3 out of 48). Such activity however, always corresponded to locomotion-sensitivity as shown in figure 3.12 C.

Cells which normally show vision-induced place fields do not show reliable activity in the dark at locations where the field should be, but instead do not fire at all in dark trials or rather activate when the animal reaches the reward zone, where the light is switched back on (n = 2 out of 48).

3.4.6 *Place cell activation in open loop experiments*

To test whether visually driven place fields respond solely to visual input, I perturbed the closed loop coupling between the movement of the animal and therefore the treadmill and the displacement of the virtual scene. Such open loop environment was created by taking the animals virtual running speed and running direction at the point where it left the reward zone and keeping these parameters constant until the animal would reach the opposite reward zone. The movement of the projection is thus independent of the animals behaviour for that single run. I introduced open loop single runs randomly within the gain change paradigm such that the animal's initial virtual speed would depend additionally on the gain of that particular run. It is important to note that when the animal moves with constant speed, open loop runs do not have any perceivable effect to the animal. This might also hold true for small speed changes as the animal might not notice small changes in visual flow.

From all 165 recorded place cells, 16 were recorded in an open loop condition (including 3 bidirectional cells, yielding 19 response types). For previous analysis open loop runs were removed. Open loop trials were more difficult to interpret as the animals behaviour (e.g. running speed) was not taken into account.
However, firing fields can be classified into three categories. First, vision-induced place fields which have their place field at a similar

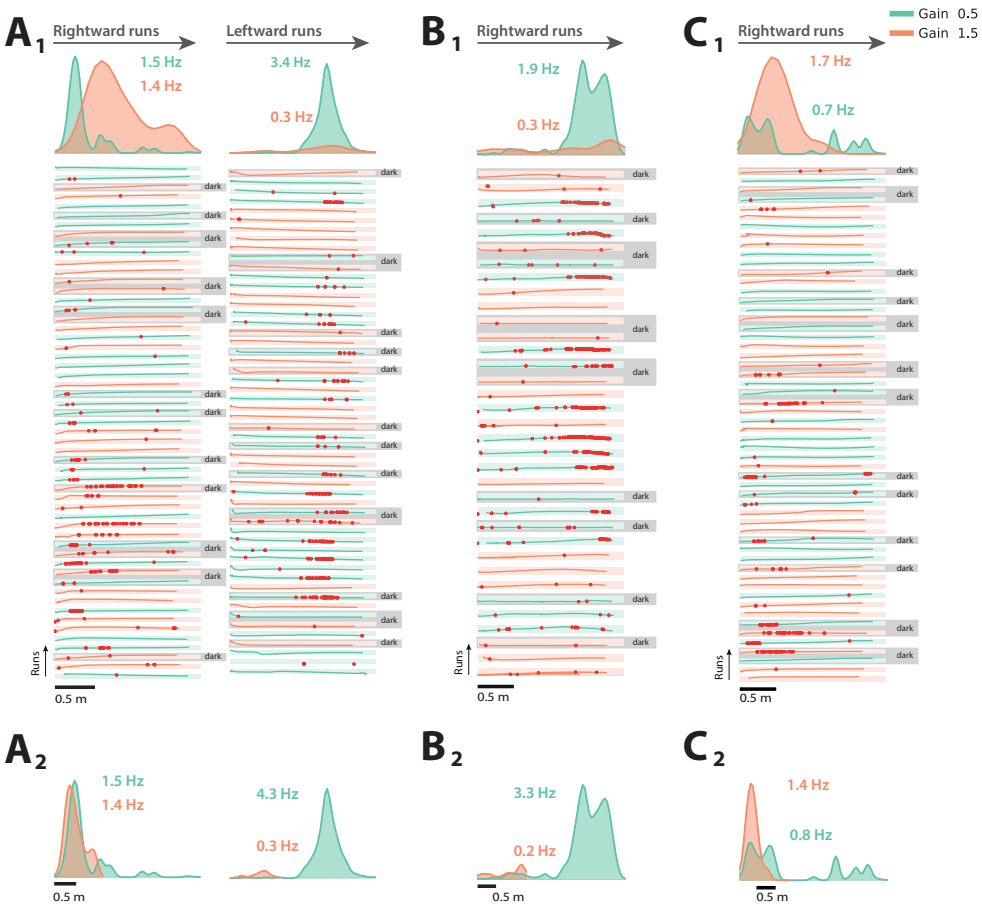

Figure 3.12: Place cell activation in darkness (dark single runs marked in grey). Single runs of one session are stacked vertically (solid line: trajectory, red dots: spikes) with the colour indicating the gain (green: 0.5, orange: 1.5). (A) Bidirectional cell with locomotion-sensitive place field for rightwards runs and 'putative locomotor' field for leftwards runs. (A_1) Both, locomotion-sensitivity and putative locomotor property is confirmed by dark runs, where activity is at the same location as in runs with the light on. (A_2) Firing rate histograms in treadmill coordinates show locomotion-sensitivity for rightwards runs with field overlap at both gains (left). (B) Putative locomotor cell, active only at gain 0.5 after 1.33 m. Dark trials show place field activity in only one run. (C) Locomotion-sensitive cell, only active in dark runs.

virtual position in open loop runs, independent of visual flow speed (n = 3 out of 19; example in Fig. 3.13 A).
Second, a locomotion-sensitive place field which was disturbed by the open loop condition, such that the place field moves to a different virtual location, depending on the visual flow (n = 1 out of 19, Fig. 3.13 B). The displacement of the place field in virtual coordinates can be solely due the difference in visual flow speed, as this corresponds to a gain manipulation. This field can therefore still code for locomotor information and is only located at a different virtual location. The same holds true for putative locomotor fields, of which I have found 2 cells to move their field in virtual coordinates during open loop runs. One locomotion-sensitive place field was found to have the same virtual location in open loop trials, which could be due to relatively constant running speed of the animal and therefore a neglectable effect of the open loop condition.
Double cells with one visual and one locomotion-sensitive field can therefore show a combination of these two response categories (see Fig. 3.13 C), where the locomotor field moves either into the visual field or disappears completely whereas the visual field stays intact and at a similar virtual location (Fig. 3.13 C, right place field).

The third category of place fields in the open loop condition includes cells which reduce or completely loose their firing field during open loop runs. These cells can be of either locomotion-sensitive (n = 3 out of 19), putative locomotor (n = 8 out of 19; example in Fig. 3.13 D) or visual (n = 1 out of 19) tuning.
This phenomenon could be explained by a remapping process during trials where the animal's locomotion and its virtual displacement do not match.

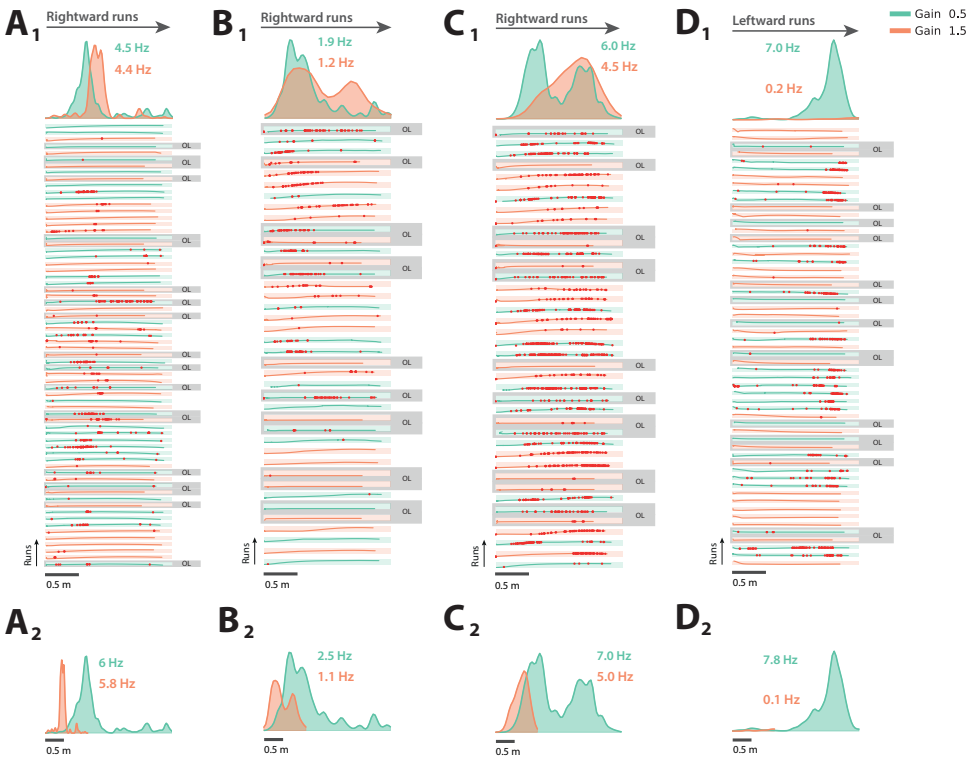

Figure 3.13: Categories of open loop experiments. Single runs belonging to one session are stacked vertically (solid line: trajectory, red dots: spikes) with the colour depicting the gain (green: 0.5, orange: 1.5). Open loop (OL) runs are marked in grey. Firing rate histogram in virtual coordinates is on top of single runs and corresponding histogram in treadmill coordinates underneath (A_2, B_2, C_2, D_2) with numbers showing peak firing rates. (A) Visually driven place field with open loop field locations at similar virtual position. (B) Locomotion-sensitive place field with open loop trials showing place field shifts in virtual coordinates. (C) Place cell with two firing fields, the first one being locomotion-sensitive and the second vision-induced. In open loop runs the locomotion-sensitive field moves into the visual one or disappears, whereas the vision-induced field remains. (D) Putative locomotor field which is not active in open loop trials.

3.4.7 *Distance versus time coding*

When an animal estimates its location via its own locomotion, it can use passed time (t) and covered distance (d) as reference frames to determine place field location. Both are connected through the animals running speed (v) via the formula $d = v \cdot t$. Thus, in order to detect a difference between time and distance for single runs, the animal has to run with different speeds. The average running speed across all gain conditions and animals was 38.89 cm/s, which means that the average animal would cover 38.89 cm in 1 second. Using this mapping, I compared a time window of 8 seconds after the animal left the reward zone and started its run, to the first 310 cm covered, after reward zone exit.

Using the described calibration, I compared time versus distance coding for all 48 locomotion-sensitive place fields from cells with a single place field and found only few fields (n = 7) which seemed to be rather tuned to a certain time after reward zone exit (example in Fig. 3.14 A). In most cases, animals are therefore not estimating time after reward zone exit, but rather tune field location based on their running speed or covered distance.
Indeed, when aligning single runs to reward zone exit and comparing spike location based on covered distance, single run place fields are at a similar location for most place fields (n = 41). An example for such a distance coding cell is shown in figure 3.14 B, where single run fields align much better for distance (right plot) than for time (left plot).

Visually driven fields were not compared for time and distance coding, as they were shown to form their firing field at similar visual coordinates. These coordinates can be met by either integrating visual flow or encoding certain landmarks in the virtual linear track. Due to different gain conditions, one specific landmark would therefore appear next to the animal at very different times or distances, measured from reward zone exit.

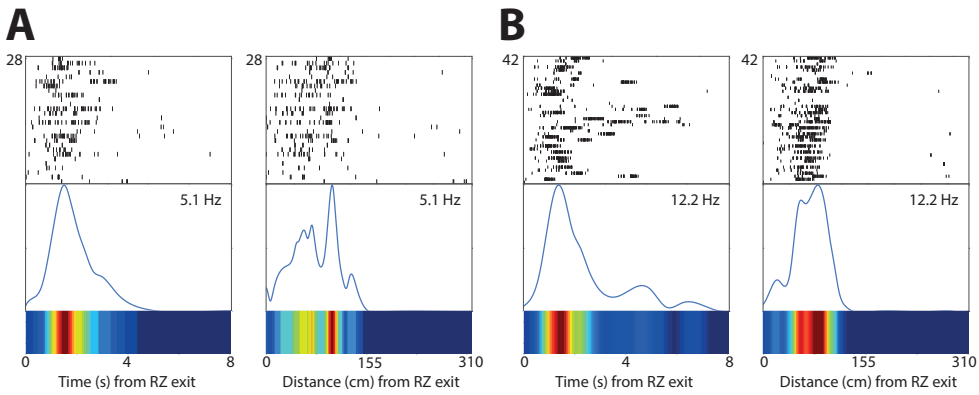

Figure 3.14: Time versus distance coding of locomotion-sensitive fields. The bottom heatmap shows the 1D firing rate and indicates the place field center and its accuracy. Above, the 1D firing rate is plotted as a smoothed histogram with its maximum shown in the top right corner. In the top box, single runs are stacked vertically (single run number shown by top left number) and spikes are plotted as vertical black lines. (A) Rather time coding locomotion-sensitive place field, with a smoother spike distribution across the firing field in the time domain (left, middle and bottom plot). (B) Locomotion-sensitive place field encoding rather distance from reward zone than time, best noticeable in single runs (top plots)

As already reported in subsection 3.3.1, theta frequency in real and virtual environments differ in about 0.5 Hz with theta oscillations on the virtual linear track having the lower frequency of about 7.5 Hz for low running speeds of the animal. Additionally, theta oscillations in virtual reality were found to not increase their frequency with running speeds up to 40 cm/s.
Further I investigated whether theta frequency speed dependence differs for different gain conditions in the virtual reality setup and whether results differ for higher running speeds.

3.5.1 *Theta frequency speed dependence for different gains*

To investigate LFP frequency and virtual running speed separately for both gains, the fitted filtered signal (red line in 3.15 A) was used and the time interval and distance between two maxima was determined. The reciprocal time was used as the instantaneous LFP frequency and the fraction of distance and time was used as instantaneous speed. This analysis method allowed to analyse information for each gain separately.
Via multiplication of obtained speeds with the respective gain, virtual speeds were calculated. This allowed to compare LFP frequency at both gains under virtual or treadmill speeds (Fig. 3.15 B and C). Such comparison revealed that at both gains LFP frequency increased by about 1 Hz, starting at treadmill running speeds of about 1 m/s (see solid lines showing medians of respective gains in Fig. 3.15 C). This frequency increase however plateaus for gain 0.5 around 1.5 m/s. For gain 1.5 not enough data points are available in the higher speed range to observe such an effect. This is due to the fact, that at gain 1.5 the animal reaches the track end much faster which leads to the animal slowing down much earlier and therefore not allowing the gerbil to reach high running speeds.

The raise in LFP frequency of about 1 Hz is also observable for virtual speeds, starts however at different virtual speeds for both gains (Fig. 3.15 B). This result shows that animals seem to adjust LFP frequency based on locomotor speed rather than on visual flow speed.

When comparing my findings of LFP frequency increase with running speed of the gerbil to findings from Ravassard et al. (2013) in the rat, my results confirm no LFP frequency increase up to running speeds of 80 cm/s in virtual reality whereas frequency increase on real world tracks is present as soon as the animal starts running (min 10 cm/s; Fig. 3.3 E and Ravassard et al., 2013). Virtual reality data was however not present for running speeds above 80 cm/s in Ravassard et al. (2013).
For treadmill running speeds larger than 80 cm/s, I find a correlation of LFP frequency with running speed, indicating that in virtual reality theta oscillations require a stronger drive to increase their frequency than in the real environment.

3.5.2 *Phase precession comparison for high and low gain*

In order to compare phase precession for both gains, I conducted both, phase precession analysis of spikes pooled over all runs and single runs using circular-linear fits (see Methods, subsection 2.5.7). These fits provide estimates for phase precession rate, displayed via the slope of the circular linear fit (in units of cycles per field) where negative slopes indicate phase precession.
Pooled phase precession is as expected slightly shifted towards negative values (Fig. 3.16 A, first two rows; Tab. 3.2, first row; more detailed analysis in subsection 3.5.3 and Fig. 3.17 F-I) and does not reveal any differences between response types or gains (between response types: $p = 0.19$, t-statistic $t = -1.32$; gains: $p = 0.94$, t-statistic $t = 0.07$, see Tab. 3.2, first row and similar distribution in Fig. 3.16 A, last two rows). A similar effect can be observed for field-averaged single run phase precession (see Tab. 3.2, second row; Fig. 3.16 B), although gain differences from figure 3.16 B could not be calculated due to the fact,

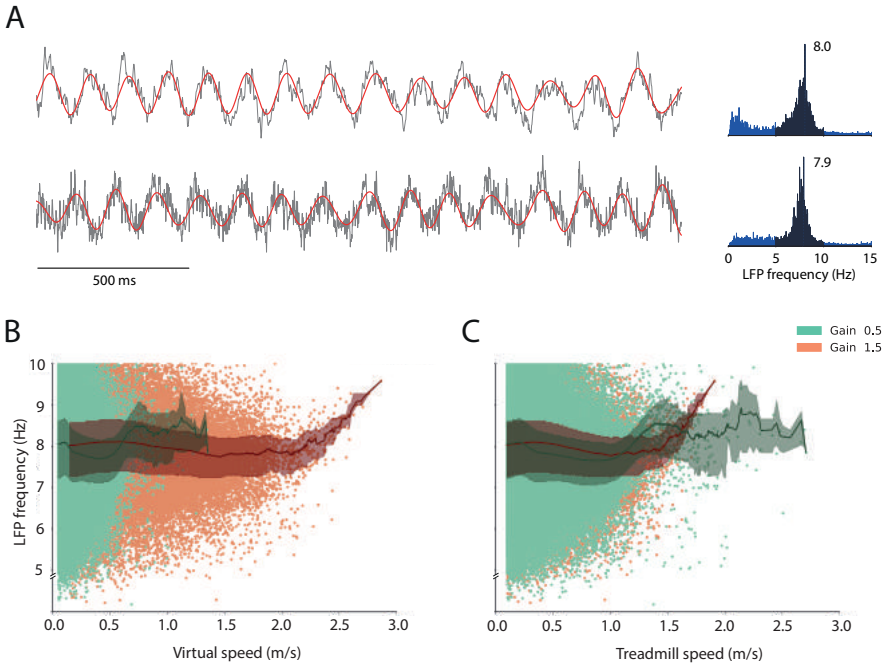

Figure 3.15: Theta frequency speed dependence for both gains. (A) Example LFP recordings (left) for two animals and corresponding frequency spectra (right). Raw traces are displayed in gray and theta band filtered signals in red. (B-C) Instantaneous theta frequency vs. instantaneous speed. Dots indicate single cycle data, population medians are depicted by solid lines, 25% to 75% inter quantile range is shown as shaded areas. Different gains are indicated by green (0.5) and orange (1.5) colors. Plots are similar for virtual (B) and treadmill coordinates (C).

that individual sessions did not always yield values for average single run phase precession. Single run values were not available if spike and theta cycle threshold (min. 4 spikes in min. 4 cycles, see subsection 2.5.7) was not reached for the phase precession fit.
Even when only single runs with significant phase precession slope fit were compared, no significant difference was found (Tab. 3.2, last row, fit p-value calculated according to p = 1 - erf($|z|/\sqrt{2}$), Kempter et al., 2012, p. 122).

	mean slope, n				mean slope, n			
data type	visual	locomoto	p	t	gain 0.5	gain 1.5	p	t
pooled over all runs	-0.22, 62	-0.27, 85	0.19	-1.32	-0.22, 83	-0.22, 84	0.94	0.071
field-averaged single runs	-0.25, 60	-0.26, 81	0.27	-1.12	-0.28, 83	-0.21, 77	0.26	-1.13
significant single runs	-0.39, 37	-0.32, 47	0.91	-0.11	-0.38, 55	-0.31, 39	0.22	-1.22

Table 3.2: Phase precession comparison analysis. Phase precession slopes are not significantly different between response types or gain conditions, shown via p-values (p) and t-test statistic (t). Slopes are in units of cycles per field from circular linear fits with respective number of values (n).

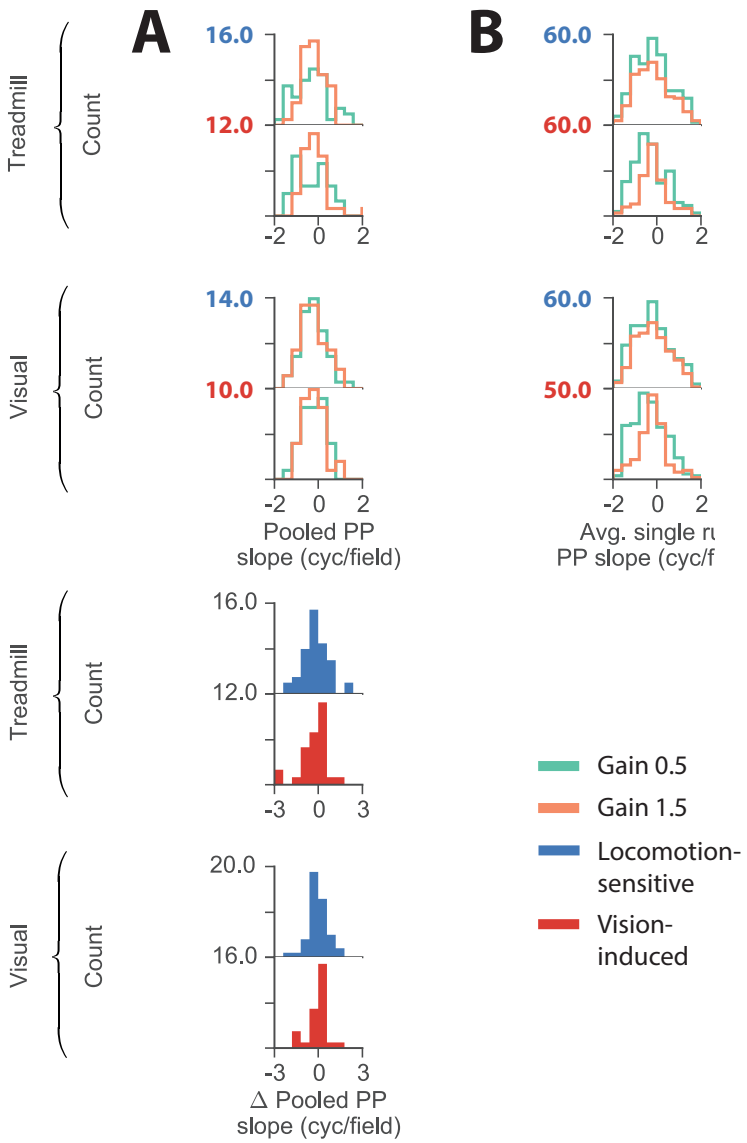

Figure 3.16: Analysis of phase precession for two gains. (A) pooled and (B) average single run phase precession slope. Each row has data for locomotion-sensitive place fields on the top axis and data from vision-induced fields on the bottom axis. Top two rows show individual histograms for both gains (green: gain 0.5, orange: gain 1.5) in treadmill (top) and visual (bottom) coordinates. Two lower rows illustrate histograms for gain differences (value at gain 1.5 subtracted from value at gain 0.5).

3.5.3 *Multimodal integration in time*

So far, my findings indicate that each of the two response types (vision-induced and locomotion-sensitive) reflects a largely independent input stream property and is encoded separately for each place field. It is however not clear whether place fields operate completely independently or whether place field activities are integrated into a common processing frame. In order to address this question, a well-established approach was used to assess the temporal coordination of action potentials from overlapping hippocampal place fields with respect to the local population activity. This approach is feasible, as integration of visual and locomotor information of both fields could occur in a compressed manner within one theta cycle by encoding their relation to each other via ordered spike-timing. Phase precession is generally thought to reflect temporal compression of behavioural sequences to the theta time scale, i.e., the spatial difference of the place field centres of a pair of neurons correlates linearly with their phase differences in a theta cycle.

Before analysing overlapping fields, I confirmed theta oscillations and phase precession to be identical under both gains. For that, the phase relation between place field spikes and the local field potential was quantified and strong theta oscillations (Fig. 3.15) as well as stereotypical hippocampal theta phase precession was found for both gains (examples in Fig. 3.17 A-E).
As described in subsection 3.5.2, both pooled and single trial analysis indicated to be similar for both response types and revealed significantly negative slopes (Fig. 3.17 F-I; t-tests, vision-induced: pooled, $p = 0.0012$, $t = -3.34$; field averaged single runs, $p = 2.5 \cdot 10^{-5}$, $t = -4.47$; field averaged significant single runs, $p = 0.0047$, $t = -2.97$; locomotion-sensitive: pooled, $p = 7.0 \cdot 10^{-5}$, $t = -4.18$; field averaged single runs, $p = 1.5 \cdot 10^{-5}$, $t = -4.61$; field averaged significant single runs, $p = 0.0042$, $t = -3.01$; for n numbers see Table 3.2).

I simultaneously recorded from 9 pairs of overlapping place cells with sufficient spiking in the place field overlap (see Methods 2.5.7). For each cell pair, cross-correlation functions were used to estimate theta phase shift and spatial offset between cells (Fig. 3.18 A, B for an ex-

ample). Spatial correlation of the example cell pairs in figure 3.18 B reveal that there is a difference in place field peaks for gain 0.5 and none for gain 1.5 in virtual coordinates. This observation indicates that one of the cells could be visually driven and the other rather locomotion-sensitive, similar to the two different examples in figure 3.17 A_1 and A_2. This order is kept when performing spike-correlation (Fig. 3.18 A), even for small correlation lags τ (Fig. 3.18 A, inset).

When pooling over all cell pairs and both gains, spatial difference of place field centers correlate linearly with the theta cycle difference, which can be observed via significant theta phase compression (circular-linear test with $p = 0.036$, $\rho = 0.48$, $n = 18$, Fig. 3.18 C). This finding shows that spike correlations at the theta scale reflect place field shifts in the behavioural paradigm.
After a gain change, locomotion-sensitive fields shift relative to vision-induced fields which begs the question whether this shift is also observable in the theta phase. As suggested by pooling over different gains, the circular-linear correlation of theta phase shift difference between the two gains and gain-induced place field shift was significant (circular linear correlation, $p = 0.040$, $\rho = 0.77$, $n = 9$; Fig. 3.18 D). Theta-scale timing therefore changes with place field rearrangement.

These findings indicate that hippocampal place fields integrate inputs from distinct streams into consistent timing relations on the theta time scale. This suggests that multimodal integration in the hippocampus occurs on the level of the spike timing correlations across the population of CA3 pyramidal cells, and is therefore accessible to downstream centers.

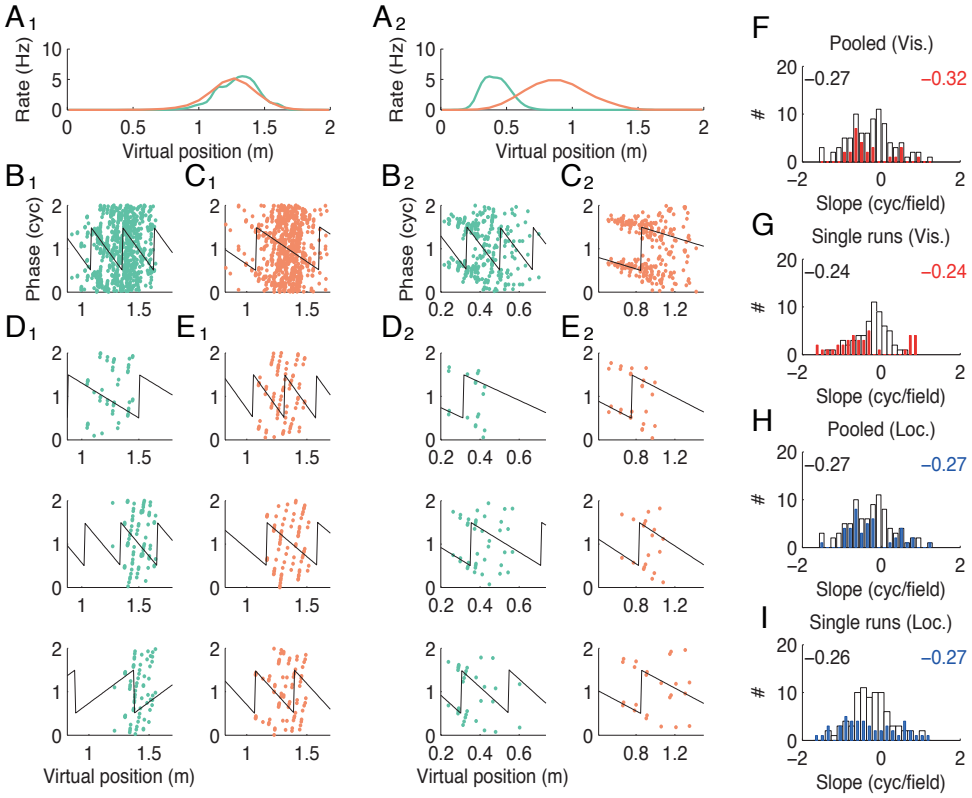

Figure 3.17: Phase precession slopes for both response types. Place field activity of the vision-induced place field $(A\text{-}D)_1$ and the locomotion-sensitive field $(A\text{-}D)_2$ from figure 3.4 D. (A) Firing rate as a function of position for gain 0.5 (green) and 1.5 (orange). (B,C) Theta-phase of all spikes as a function of position. Black line indicates best circular-linear slope. (D,E) Spike phases from 3 example single runs for each condition. (F) Fitted circular-linear slope to all pooled phase-position plots (as in B,C) from vision-induced place field (both gain conditions). Red bars indicate slopes for which the fit was significantly different from 0. Numbers on top show means. (G) Fitted single trial slopes averaged per vision-induced field. Red bars display histogram where only significant single-trial slopes were averaged. (H,I) As F,G for locomotion-sensitive fields.

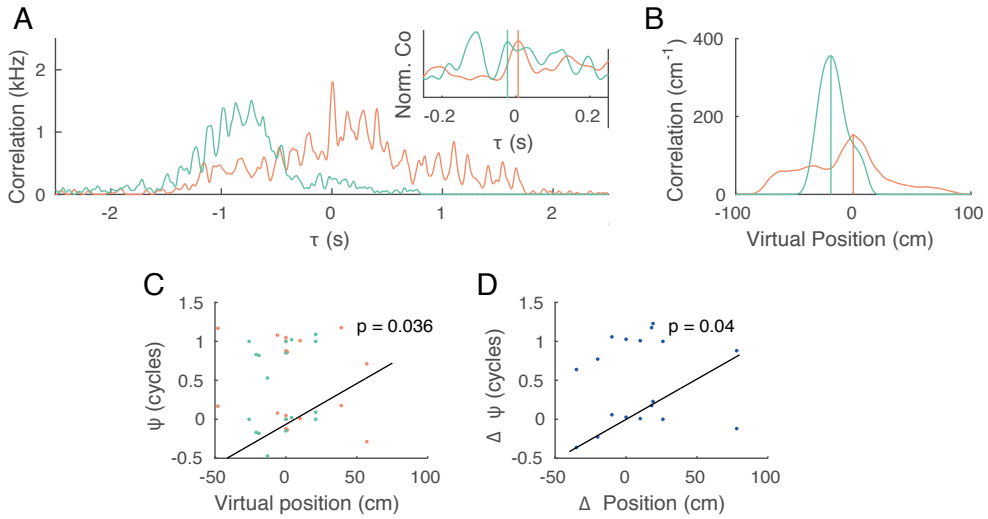

Figure 3.18: Theta-scale spike timing. (A) Spike-crosscorrelation for a pair of simultaneously recorded cells. Green indicates gain 0.5 and orange gain 1.5. Inset: Same as A expanded for small correlation lags τ and normalised to equal peak amplitudes. (B) Spatial correlation of the same cell pair. (C) Theta phase shift ψ of peaks from A as a function of place field distance from B indicates significant circular-linear correlation (black line, n=9 pairs, 2 gain conditions, for which more than 25 spike pairs occurred in a theta cycle around lag 0 at both gains). (D) Theta phase shift difference between two gains vs. difference of place field distance taken from C.

4

DISCUSSION

4.1 SUMMARY OF RESULTS

I used a virtual reality environment and extracellular electrophysiological recordings in hippocampal area CA3 to demonstrate that locomotor and visual information are processed differentially and in parallel to provide two sensory place field maps. These maps are integrated into distinct timing relations within single theta cycles.
Previous recordings in the rodent hippocampus in virtual reality tasks have highlighted the importance of unperturbed interplay of different sensory modalities in order to achieve normal place cell firing (Ravassard et al., 2013; Aghajan et al., 2015; Aronov and Tank, 2014; Acharya et al., 2016). In order to investigate the impact of different sensory modalities to place field formation, I perturbed the closed loop linkage between own movement of the animal and visual movement within the virtual linear track by displaying a visual movement which equals the animal's own movement multiplied by a gain factor. This allowed me to decouple vision-induced information, such as landmarks and optic flow from locomotion-sensitive-information which may stem from path integration, motor efference copies or sensory feedback of self-motion e.g. via steps on the treadmill.
I found that such gain changes elicited instantaneous changes in the hippocampal place code, by shifting the location of place field centres. These shifts clustered into two classes, by either linking to visual features of the projected linear track or by being influenced strongly by the distance the animal had travelled from the beginning of a single run. The latter locomotion-sensitive fields showed to dominate in the beginning of the linear track and broaden their field width towards the rear of the track. Visually driven fields on the other hand did not show significant field broadening but clustered around visual texture

changes in the virtual track. Locomotor and visual response types have been observed in dark or open loop trials respectively, confirming field tuning to internal or external sensory information. Additionally, locomotion-sensitive fields revealed to be rather encoding distance covered than time passed since the animal left the previous reward zone.
Furthermore, I have identified about 10% of recorded place cells which exhibited two place fields driven by visual and locomotor information, providing strong evidence against anatomical segregation of response types.

4.2 MULTIMODAL POPULATION REPRESENTATION OF SPACE

Anatomical sensory convergence in the hippocampus has been reported to result in different sensory modalities influencing the rodent's spatial representation of its environment. Electrophysiological evidence for the hippocampus to act as a sensory integrator has been indicated by Wiebe and Stäubli (1999), who found that hippocampal principal cells seem to encode a variety of sensory inputs. One of the described encoding modes was odour-selective activity, often predictive of behavioural performance. Other cells displayed e.g. activity at visually salient maze positions, such as at the entry point of a test arm.
Odour selective place fields would allow to rather rely on olfactory cues in e.g. darkness (Save et al., 1998; Save et al., 2000), when other sensory information is not as informative. Providing an animal with visual information on the other hand showed that limited changes in the visual environment result in rate modulations of place fields (Muller and Kubie, 1987; Leutgeb et al., 2004), which therefore indicates the dependence of place field formation on visual information. Such findings beg the question whether different sensory inputs drive different place cell populations, as well as how and where sensory inputs are integrated to form an unconflicting representation of the animal's environment.

The hypothesis that spatial information is computed separately for different sensory modalities via specific subcircuits which project to an overlapping population of hippocampal pyramidal neurons was strengthened by several aspects.
Moser et al. (2014) described that a range of anatomical pathways project to the hippocampus, carrying a rich diversity of spatial cues stemming from different sensory modalities. My results have demonstrated that each place field in hippocampal area CA3 is sensitive to locomotor or visual information. These findings contribute to the ongoing debate on mechanisms of place field generation (Barry et al., 2006; Brandon et al., 2011; Koenig et al., 2011; Wills et al., 2012; Hales et al., 2014; Kammerer and Leibold, 2014; Schlesiger et al., 2015) and suggest fields to be driven by distinct sensory information, resulting in multiple parallel maps of space.
The hypothesis that such maps are formed by overlapping sensory pathways and are therefore not anatomically segregated is corroborated by place cells with multiple firing fields (Maurer et al., 2005) which I found to be mostly driven by different input streams.

The fact that I found overlapping spatial maps simultaneously for different sensory inputs is supported by the finding of Geva-Sagiv et al. (2016), which showed place field tuning to bat echolocation in darkness and to visual information in light in hippocampal CA1. The hippocampus does therefore not act as an abstract spatial map but rather hosts coexisting maps for different sensory modalities. It can however associate coexisting information, which can be of spatial and non-spatial nature to generate a multimodal population representation of space. The hippocampus could thereby link e.g. a spatial location to other sensory experiences, such as food reward or electric shock, which would provide the animal with important information for e.g. relocating a food source in order to secure survival.
I found that such integration of information, occurs via the precise timing relations of populations of place fields during theta oscillations (Dragoi and Buzsáki, 2006).

4.2.1 *Visual flow versus landmarks and reward zone expectation*

As discussed above, rodents can use different types of sensory stimuli to form spatial maps and navigate through a virtual environment. Youngstrom and Strowbridge (2012) suggest that mice are able to navigate to goal location using only visual cues and therefore only one of the coexisting spatial maps. It is however not clear whether rodents integrate visual flow, update their position estimation based on certain visual landmarks or rather estimate the distance to the goal location. In gain change experiments this difference is not trivial to resolve as visual flow increases with a higher gain, which correlates with landmarks appearing earlier as well as with the reward zone being reached faster. As visual textures are provided all over the linear track in my experiments, place fields integrating visual flow should be distributed equally over the track. I found however an increased density of place fields at visual texture changes in the virtual maze, indicating the importance of salient visual landmarks in addition to visual flow.
Additionally I observed an increase of visually driven place fields towards the end of the track, suggesting that visual information increases in importance. This could be the case due to locomotor information decreasing in accuracy and the approaching reward zone providing a better estimate of the animals location.

According to Aghajan et al. (2015) distal visual cues such as the reward zone are alone not sufficient to generate a robust spatial rate code. Reward zone expectation is however crucial for place cell activity as firing does not only depend on local sensory cues but also on planned behaviour (Ferbinteanu and Shapiro, 2003). Thus, when an animal is placed in a t-shaped maze, a place field in the trunk of the maze will only activate significantly when the animal plans to run into e.g. the left arm of the maze (Ferbinteanu and Shapiro, 2003). Place field activation in that case depends on a visual location as well as on the planned behaviour or the context the animal is in. Similarly did place fields in rats link to the expected start box of a linear track run, even when the visually different finish box was used instead (Skaggs and McNaughton, 1998).

In contrast to firing fields which depend on an expected location, the primary visual cortex (V1) also carries information regarding visual speed to the hippocampus. As visual speed is normally identical to the running speed of the animal, the finding that most V1 neurons predict a linear combination of visual and run speeds (Saleem et al., 2013) seems suitable. In my results I revealed place fields, mostly in the middle of the track, to lie in between ideal visual and locomotor tuning. Such fields could therefore be driven by these inputs from V1 and thus represent visual and running speed information equally.

4.2.2 *Significance of the visual spatial map*

When analysing different components important for visual spatial map formation, the question arises whether a visual spatial map provides equal contribution to navigation and orientation as spatial maps from other senses.
Evidence has been provided from the barn owl that spatial information provided by vision is used to calibrate other sensory maps such as the neural representation of auditory space (Knudsen and Knudsen, 1985; Knudsen and Knudsen, 1989; Brainard and Knudsen, 1993). When the barn owl was raised wearing visual field shifting prismatic spectacles, the developing auditory map was found to be shifted by an equivalent amount and therefore leading to the preservation of the alignment of the visual and auditory map of space. This discovery implies an innate dominance in barn owls of the visual map over the development of the auditory spatial map, used e.g. for sound localisation. The same conclusion can be drawn from barn owls raised with one ear plug. Using their visual map, sound localisation errors due to the ear plug can be corrected when the plug is removed. This is however not the case when visual information is not provided (Knudsen and Knudsen, 1985).

Blind humans were found to be able to calibrate their auditory spatial map using sensory-motor feedback instead of visual feedback (Ashmead et al., 1998; Lessard et al., 1998; Voss et al., 2004). Individuals even demonstrated supra-normal auditory performance without re-

lying on a visual map of space, demonstrating that vision is not essential to develop spatial concepts and that compensation can occur via remaining senses, e.g. via self motion (turning the head or locomotion). This was shown also for late-onset blind subjects, indicating that significant compensation for the lack of visual information can also occur in the adult brain (Voss et al., 2004). The formation of sensory maps seems therefore to be a plastic mechanism, which can vary in accuracy depending on the pressure from other e.g. faulty maps.

The contribution of visual information to normal spatial map calibration is however crucial for proprioceptive and vestibular systems (Prechtl et al., 2001), important for locomotor-sensitive maps found in my recordings. During preterm and term periods, blind infants showed no significant impact of lacking visual information on motor activity. Starting at about two month postterm, infants developed a handicap observable via delay in head control and abnormal movements (Prechtl et al., 2001). Other sensory maps, such as the auditory map were intact but not sufficient to restore movement and posture dependent maps. It would therefore be interesting to investigate whether locomotor-sensitive spatial maps found in my recordings would be altered in blind gerbils and therefore confirm findings from blind infants.

4.2.3 *The importance of locomotion to navigation*

Without any external information, provided e.g. by the visual system, spatiotemporal information was shown to be provided by self-motion cues (Villette et al., 2015). In darkness, these were able to contribute to the emergence of recurring sequences of neuronal activation in the hippocampus (CA1) of awake mice. These sparse and stereotyped chains of activity were shown to integrate spatiotemporal behavioural components, such as travelled distance and are therefore crucial for path integration. Villette et al. (2015) described such periods of activity as 'distance unit', which is suppose to provide a population metric for distance as travelled distance of the animal can be estimated via integer multiples of sequence spans. This finding suggests that intern-

ally prewired networks provide a distance representation of space, but does not confirm that such a representation provides sufficient input to a locomotor-sensitive map.

Brain activation during navigation in humans is often analysed using fMRI, which prohibits individuals to move freely. Results from such studies have shown that humans rely strongly on locomotor information or active movement of the participant, which depends e.g. on motor efference copies and proprioceptive feedback (Taube et al., 2013). This dependence is indicated by the finding that active exploration of an environment usually correlates with greater spatial knowledge than when the environment is explored only passively (Simons and Wang, 1998; Wang and Simons, 1999). The difference in spatial performance was observed via underestimated distance in virtual environments compared to real ones (Witmer and Kline, 1998) as well as via differences in heading judgement between active locomotion and passive transport, e.g. the experience of optic flow in simulated locomotion (Klatzky et al., 1998).

In rodents passive movement have also been studied, which allowed the animal access to vestibular and somatosensory information. Terrazas et al. (2005) found that under such conditions less place cells were active, which displayed larger fields and revealed a lower information content. However, as soon as limb movement correlates with experienced optic flow, robust place cell activity can be observed (Chen et al., 2013). Even though vestibular information in these head-restrained mice was not available to them, visual and locomotor information seemed sufficient for normal place cell activity. For 75% of these cells, movement of the mouse was reported to be required to allow normal firing.

Although humans perform virtual navigational tasks in an immobile and unnatural position within an fMRI scanner, whereas rodent virtual realities allow for active movement, locomotion was found in both species to be a crucial component for accurate navigation and estimation of the environment's dimensions.

4.2.4 *Are visual and locomotor inputs processed in a weighted fashion?*

In my recordings I found place cells displaying two fields in one running direction. Most of these cells had one locomotor-sensitive field and one visually driven field. This observation requires information from different senses to arrive at the same cell. It is therefore plausible, that not only visual and locomotor information reaches one place cell, but that information from other senses also converge on the same cell. Field-specific sensory information could thus stem from one of these inputs, whereas the peak firing frequency within a place field could be due to a weight factor attached to its specific input. Figure 4.1 shows this hypothesis for visual (left) and locomotor (right) inputs, which arrive at the apical dendrite of one pyramidal cell. Inputs arrive at the synapse with a certain intensity (I_1 and I_2) which is regulated by its weight factor (w_1 and w_2). Depending on the amplitude of the evoked EPSP, sense-specific spatial information could induce a sense-specific place field and modulate the peak firing rate of the resulting place field.
Different weights for each sensory input to the place cell would allow for all combinations of firing rate peak amplitudes in coexisting place fields. In my data I found place fields in one running direction and of different sensory drive to have non-discrete peak amplitudes and to display any combination of amplitudes. Fields showed therefore e.g. equal drive for both inputs when fields had similar peak firing rates (for an example see Fig. 3.7 C_4) and different drive when one field had a higher amplitude then the other (for an example see Fig. 3.9 A).

According to this hypothesis, place cells with a single field could also receive inputs from all senses but with one dominant input due to a high weighting factor, whereas all other weights would be either too low to elicit a place field or display a place field, which does not rise above noise level.
The weight for each sensory input would thus define the specification of each place cell and therefore to which sensory input it responds to. Weight distributions across the hippocampal place cell population would thus allow to e.g. randomly distribute sensory

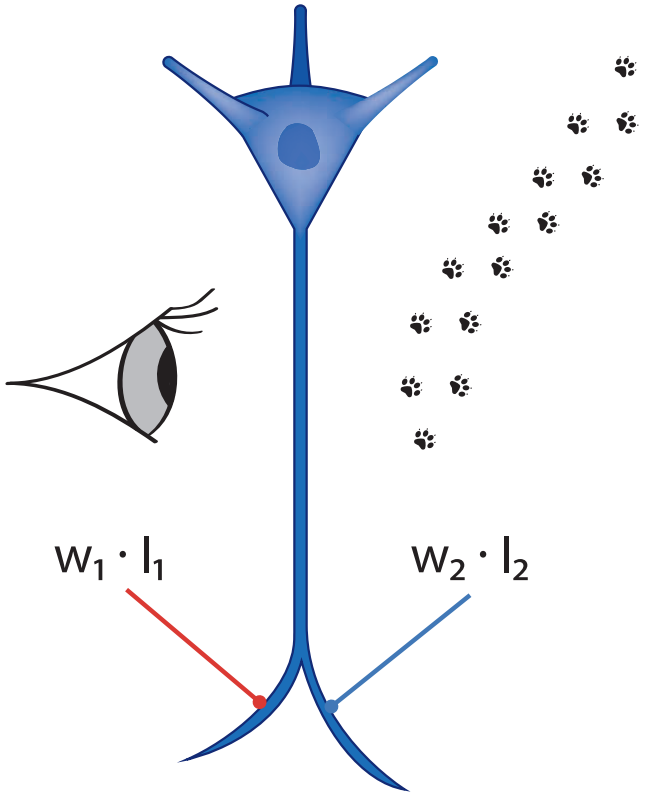

Figure 4.1: Weighted visual (red) and locomotor (blue) inputs to a pyramidal neuron. I_1 and I_2 symbolise the sensory specific input arriving at a synapse of the apical dendrite of the pyramidal cell. Inputs are weighed by a factor (w_1 and w_2) allowing for a modulation of sensory specific place field peak frequency.

specificity, form clusters or drive sensory specific representation stronger for specific inputs when others become more unreliable. If for example an animal could not rely as much on its visual information due to e.g. visual disabilities, weights could shift towards suppressing visual information and rather enhancing place field formation for other sensory information.

Overlapping place fields of different sensory drive have shown to swap their place field sequence for different gains (see 3.5.3). This shift was reflected by spike correlations of both field types at the theta scale. As it takes the animal a few seconds and therefore several theta cycles to cross one place field, constant spike phase difference in either gain condition is repeated several times. Such temporal coordination thus repeatedly mirrors the behavioural sequence of place cells in a particular gain within a short time window (about 100-150 ms), which allows for episodic memory formation via LTP.
Gain induced place field swap would therefore evoke two coexistent episodic memories which would be available to downstream areas to assess.

Phase precession (see Fig. 1.2) was revealed to be a crucial factor to allow for temporal compression of place field sequences and therefore episodic memory formation (Levy and Steward, 1983; Bi and Poo, 1998). This fact begs the question how hippocampal phase precession can occur and whether underlying mechanisms rely on other brain structures than the hippocampus.

As existing models for phase precession overlap in many aspects, it is reasonable to categorise models into two main classes. First, phase precession based on synaptic interaction on a systems or network-level and second, phase precession generation via the interference of two inputs in one pyramidal cell.

4.3.1 *Network-based models for phase precession*

Similar to Hebb's phase sequence concept (Hebb, 1949), phase precession could be a generated via recurrently interconnected pyramidal neurons in the hippocampus (Tsodyks et al., 1996). If cells would be repeatedly activated in a fixed order, recurrent connections would

form different synaptic strengths in both directions. Such asymmetric connections of cell assemblies would lead to neurons in the beginning activating the later assembly. Thus, when an animal enters a place field, the respective place cell would receive excitatory input (e.g. from EC layer II) and fire in the early theta cycle. Due to asymmetric connections, this activity would trigger cells according to the stored sequence, which would fire in the later theta cycle. This asymmetric spread of activation would form phase precession and recall the learned sequence of passed place cells.
The activity wave propagation over pyramidal neurons could only appear after the animal learned the layout of the environment and therefore altered its synaptic strengths, such that sequence learning must have already taken place. However, experimental findings show that phase precession can be observed in environments novel to the animal (Rosenzweig et al., 2000).

4.3.2 *Models based on intrinsic dynamics*

Two detuned oscillators were proposed by O'Keefe and Recce (1993) to result in phase precession via the interaction of one slow and one fast oscillation in one pyramidal cell. Such oscillations could arise from LFP theta oscillation and entorhinal cell activity respectively.
When the animal is not situated in a place field, oscillators are assumed to be 180° out of phase, such that oscillations with identical amplitude and frequency would cancel each other and no place field activity would be generated. In contrast to that, natural frequency increase from the entorhinal input occurs when the animal enters the place field. The coupling of LFP theta oscillation with such an entorhinal input oscillation would result in detuned oscillators of different frequency as described by O'Keefe and Recce (1993). The oscillation elicited by their interaction would move its peaks to progressively earlier phases, when compared to the LFP theta oscillation and would therefore elicit phase precession. When the animal exits the place field, oscillators would be out of phase again as described for before place field entry.

Similar to the two detuned oscillator approach, the soma-dendritic interference model utilises the interplay of two oscillatory inputs to one hippocampal pyramidal cell (Harvey et al., 2009). One being the LFP theta modulated inhibitory input and the other the dendritic excitation (Kamondi et al., 1998), which as mentioned above could arise from the EC. Dendritic currents were assumed to have the same frequency and to be 180° out of phase with oscillations at the soma.
As the animal enters a place field, the distal, excitatory drive is suppose to increase which results in a ramp like depolarisation as well as in an amplitude increase of excitatory oscillations. As the depolarisation is increased, the inhibition at the soma can be overcome at earlier phases, which therefore results in spikes occurring at earlier theta phases (phase precession).
The location of excitatory dendritic input was shown to determine the exact pattern of phase precession (Magee, 2001), such that a more gradual shift in spike initiation can be achieved by a more distal located excitatory input.

According to these models, phase precession could be either due to replay of prior learned place field sequences or rather due to the sum of theta oscillation and an external oscillation, which could be provided by the EC.
This external input could therefore also carry either locomotor or visual information, arising from other cortical areas. The observed spike timing relations in overlapping fields seem to speak against a network model, as spike timing relations switch depending on the presented gain, which appears randomly and cannot be due to a previously learned layout of the environment or task.

4.4 IMPACT OF VESTIBULAR INFORMATION ON THETA OSCILLATIONS AND PLACE CELL ACTIVITY

In my extracellular hippocampal recordings I observed LFP frequency to increase with the animal's running speed only for speeds above 80 cm/s (see subsection 3.5.1). Additionally I found theta frequency to be reduced in VR experiments by 0.5-1 Hz, when compared to the real environment (see subsection 3.3.1).
Other research groups (e.g. Ravassard et al., 2013) also report theta frequency reduction and no correlation of LFP frequency and running speed in the rat below 80 cm/s.

This observation begs the question where differences to real environments arise from, where LFP frequency increases with running speed as soon as the animal starts moving and what potential consequences of such a disruption may be.

The primary candidate for the disruption of normal theta and running speed correlation in the rodent brain was shown to be the vestibular system, which could also impact on robust place cell activity.

4.4.1 *Theta oscillations in virtual reality*

That movement-related LFP frequency depends strongly on vestibular signals was shown by Russell et al. (2006) via lesions of the vestibular system, which reduces theta amplitude during locomotion. Vestibular information is thus important for the LFP but proved to be also sufficient to drive continuous theta by passive whole-rotation of rats (Tai et al., 2012) but showed to be reduced in magnitude when compared to active locomotion of the animal (Terrazas et al., 2005). When animals perform active locomotion in VR but do not receive rotatory vestibular information, as for body fixed rats (Ravassard et al., 2013) or head fixed mice (Chen et al., 2013), theta frequency and power seem to be altered.
In humans EEG frequencies were detected during VR spatial tasks

(Caplan et al., 2003; Ekstrom et al., 2005), it is however unclear whether theta amplitude and other characteristics are different to the real environment, which involve active locomotion and complete vestibular information.

The VR setup used for my experiments provides the animal with rotational vestibular information, as the animal is able to rotate around its own vertical body axis (see section 2.3) and can move its head freely. The animal therefore receives information from the horizontal semicircular canal, located in the inner ear (Day and Fitzpatrick, 2005). Due to movement in the horizontal plane, inertia causes the endolymph fluid in the canal to lag behind and therefore stimulate sensory receptors (hair cells) in the canal. Movements of the animals head additionally provide information from the superior and posterior semicircular canals via the same mechanism.
Additionally to rotational movements carried out by the head and body of the animal, can the vestibular organs sense linear acceleration via two otolith organs (Day and Fitzpatrick, 2005). Located between cochlear and semicircular canals are the utricle and saccule, which are oriented perpendicular to each other and host a membrane of dense calcium crystals (otoliths). Gravitational or inertial forces move this membrane in the direction of linear acceleration and thus initiate action potentials in the afferent nerve fibres (Day and Fitzpatrick, 2005). Linear acceleration therefore stimulates one of the two described functional units of the vestibular organs. In VR setups where the animal is fixed such that it can not change its location within the setup, information from linear acceleration is not provided by the vestibular system. Even though, the setup used for my project allowed for rotational vestibular information, it cannot provide the animal with linear acceleration information consistent with its virtual movement.

The fact that therefore otolith organs are not stimulated in my virtual environment tasks might explain the missing correlation between theta frequency and running speed, observed in VR for running speeds below 80 cm/s.

4.4.2 *The impact of vestibular information on place field formation*

When an animal is body fixed in a VR setup such that it cannot turn its body around its vertical axis, the animal does not receive rotational information other that via its head movements. According to experiments conducted by Aghajan et al. (2015), such a restriction in vestibular information could in some cases lead to abnormal place cell activity, in this study referred to as 'hippocampal-motifs'. On the other hand was robust place cell firing behaviour observed in similar two-dimensional virtual environments as soon as rotational information was provided (Aronov and Tank, 2014). In contrast to findings from Aghajan et al. (2015), robust spatial selectivity was also found in body fixed rats on a virtual linear track (Ravassard et al., 2013). Their findings suggested that VR bidirectional place cells preferentially encoded distance along the virtual track, whilst real environment place cells coded for absolute position. My findings however showed, that running directions were encoded differentially by one place cell and were therefore not comparable. Place cells in head fixated mice were also found to have robust spatial coding and were shown to receive a variety of relative influence of visual and own movement related information (Chen et al., 2013), such that place field location remained hard to interpret based on sensory information.

Nonetheless, it was demonstrated that an intact vestibular system and its natural activation is crucial for the generation of normal place cell activity (Stackman et al., 2002; Russell et al., 2003), with vestibular dysfunction leading to impaired performance in spatial tasks (Ossenkopp and Hargreaves, 1993; Wallace et al., 2002). These findings suggest that accurate navigation and normal spatial encoding depends besides other sensory systems heavily on intact vestibular information. On a behavioural level this has been demonstrated for hippocampal-dependent spatial tasks, in which performance was disrupted after vestibular lesions (Smith et al., 2005).
Importantly, active locomotion resulting in the activation of the vestibular system as well as providing proprioceptive information, has been shown to be a key factor for place field encoding in rodents (Terrazas et al., 2005).
Supporting this evidence, experiments revealed that the direct activ-

ation of the medial vestibular nucleus via electrical stimulation was sufficient to increase the activity of CA1 complex spike cells and therefore possibly also place cells (Horii et al., 2004).

The dependence of normal hippocampal function on the vestibular system has also been confirmed in humans, where vestibular loss revealed to cause spatial memory impairments and navigation deficits (Brandt, 2005).

5

CONCLUSION

The execution of behaviour requires that animals interact with and respond to changes in their environment. This implies that the nervous system must be able to represent both the internal state and the external world in the form of neuronal activity. The spatial and temporal precision of these representations underpins many behaviours crucial to survival. It is now one of the central goals of neuroscience to understand the extent to which different sensory modalities contribute to integrated representations and how this is implemented.
A crucial underlying concept for the understanding of an external environment is the neuronal representation of space. In the 1970s the hippocampus was identified as a key player for the encoding of space via place cells, which activate at certain locations (place fields) (O'Keefe and Dostrovsky, 1971).

It remained unclear, however, how information from different sensory modalities is used to form a crossmodal representation of space. Due to the hippocampus' position at the apex of the cortical hierarchy, its neuronal firing patterns are strongly dependent on intrinsic cortical computations, which makes it challenging to analyse the impact of a specific sensory input to place field formation.

During my PhD I approached this problem and found that the convergence of different sensory input pathways in the hippocampus resulted in the formation of coexisting spatial maps where each input produced an independent map conveyed through place fields.
A current hypothesis in the field suggests that hippocampal place fields are fixed to an animal's allocentric environment and therefore comprise one spatial map. Contrastingly, I found that the input from different sensory modalities led to multiple maps, each of which was observed to be sensitive to one specific input. This allows the animal

to dynamically employ the most relevant map and therefore adapt to changes in its environment. Further investigation would reveal whether an unreliable sensory signal causes other spatial maps to adapt and play a more dominant role in the neuronal representation of space.

The coexistence of spatial maps tuned to different sensory modalities could also be crucial for the strengthening of unambiguous memories. My data revealed that spike timing relations between overlapping fields that belong to two coexisting maps switch upon gain change. This indicates that sequence compression within single theta cycles may not allow for stable episodic memory formation via STDP, as input-specific place fields would reverse their order when a gain change occurs. Memory formation could thus rely predominantly on unambiguous relations between input-specific maps. It would therefore be interesting to compare spatial memory formation in ambiguous gain change environments to memory formation in an unambiguous control experiment.

Research on the hippocampus has already revealed substantial insights into its anatomy and functional significance. After the discovery that place cell activity encodes a spatial map researchers focussed heavily on the hippocampus as a neural substrate for navigation. Moving forward it will be increasingly important to look beyond the hippocampus' role in representing space and to consider its broader functions in relation to learning and memory. Critically, we need to understand how a singular neural mechanism underpins spatial representation, navigation, and memory formation across all sensory modalities. A complete understanding of hippocampal function should necessarily include descriptions of how it represents and integrates all sensory modalities, not just those (vision, proprioception, etc.) that provide the most intuitive framework for understanding the hippocampal representation of multisensory space.

6

REFERENCES

Acharya, Lavanya, Zahra M Aghajan, Cliff Vuong, Jason J Moore and Mayank R Mehta (2016). 'Causal Influence of Visual Cues on Hippocampal Directional Selectivity.' *Cell* 164.1-2, pp. 197–207.

Acsády, L, A Kamondi, A Sik, T Freund and G Buzsaki (1998). 'GABAergic cells are the major postsynaptic targets of mossy fibers in the rat hippocampus.' *Journal of Neuroscience* 18.9, pp. 3386–3403.

Aghajan, Zahra M, Lavanya Acharya, Jason J Moore, Jesse D Cushman, Cliff Vuong and Mayank R Mehta (2015). 'Impaired spatial selectivity and intact phase precession in two-dimensional virtual reality.' *Nature Neuroscience* 18.1, pp. 121–128.

Amaral, D. G. (1978). 'A Golgi study of cell types in the hilar region of the hippocampus in the rat.' *Journal of Comparative Neurology* 182, pp. 851–914.

Amaral, D G, C Dolorfo and P Alvarez-Royo (1991). 'Organization of CA1 projections to the subiculum: a PHA-L analysis in the rat.' *Hippocampus* 1.4, pp. 415–435.

Andersen, P, T W Blackstad and T Lömo (1966a). 'Location and identification of excitatory synapses on hippoeampal pyramidal cells'. *Exp Brain Res*, pp. 236–248.

Andersen, P, T. V. Bliss and K. K. Skrede (1971). 'Lamellar organization of hippocampal excitatory pathways'. *Experimental Brain Research* 13, pp. 222–238.

Andersen, P, B Holmqvist and P E Voorhoeve (1966b). 'Excitatory synapses on hippocampal apical dendrites activated by entorhinal stimulation.' *Acta physiologica Scandinavica* 66.4, pp. 461–472.

Andersen, Per (1975). *Organization of Hippocampal Neurons and Their Interconnections*. Vol. 1. The Hippocampus. New York, Plenum Press, pp. 155–175.

Andersen, Per, Richard Morris, David Amaral, Tim Bliss and John O'Keefe (2007). *The Hippocampus Book*. Oxford University Press.

Arnolds, D E, F H Lopes da Silva, J W Aitink, A Kamp and P Boeijinga (1980). 'The spectral properties of hippocampal EEG related to behaviour in man.' *Electroencephalography and clinical neurophysiology* 50.3-4, pp. 324–328.

Aronov, Dmitriy and David W Tank (2014). 'Engagement of neural circuits underlying 2D spatial navigation in a rodent virtual reality system.' *Neuron* 84.2, pp. 442–456.

Ashmead, D H, R S Wall, K A Ebinger, S B Eaton, M M Snook-Hill and X Yang (1998). 'Spatial hearing in children with visual disabilities.' *Perception* 27.1, pp. 105–122.

Barlow, J S (1964). 'Inertial navigation as a basis for animal navigation.' *Journal of theoretical biology* 6.1, pp. 76–117.

Barry, Caswell, Colin Lever, Robin Hayman, Tom Hartley, Stephen Burton, John O'Keefe, Kate Jeffery and Neil Burgess (2006). 'The boundary vector cell model of place cell firing and spatial memory.' *Reviews in the neurosciences* 17.1-2, pp. 71–97.

Battaglia, Francesco P, Gary R Sutherland and Bruce L McNaughton (2004). 'Local sensory cues and place cell directionality: additional evidence of prospective coding in the hippocampus.' *The Journal of neuroscience : the official journal of the Society for Neuroscience* 24.19, pp. 4541–4550.

Bechterew, W. von (1900). 'Demonstration eines Gehirns mit Zerstörung der vorderen und inneren Theile der Hirnrinde beider Schläfenlappen.' *Neurologisches Zentralblatt* 19, pp. 990–991.

Best, P J and J Orr (1973). 'Effects of hippocampal lesions on passive avoidance and taste aversion conditioning.' *Physiology & behavior* 10.2, pp. 193–196.

Bi, G Q and M M Poo (1998). 'Synaptic modifications in cultured hippocampal neurons: dependence on spike timing, synaptic strength,

and postsynaptic cell type.' *Journal of Neuroscience* 18.24, pp. 10464–10472.

Bird, Chris M and Neil Burgess (2008). 'The hippocampus and memory: insights from spatial processing.' *Nature reviews. Neuroscience* 9.3, pp. 182–194.

Bliss, T V and T Lømo (1973). 'Long-lasting potentiation of synaptic trans- mission in the dentate area of the aneasthetized rabbit following stim- ulation of the perforant path. ' *J. Physiol.* 232, pp. 331–356.

Boccara, Charlotte N, Francesca Sargolini, Veslemøy Hult Thoresen, Trygve Solstad, Menno P Witter, Edvard I Moser and May-Britt Moser (2010). 'Grid cells in pre- and parasubiculum.' *Nature Neuroscience* 13.8, pp. 987–994.

Bódizs, R, S Kántor, G Szabó, A Szûcs, L Erõss and P Halász (2001). 'Rhythmic hippocampal slow oscillation characterizes REM sleep in humans.' *Hippocampus* 11.6, pp. 747–753.

Bragin, A, G Jandó, Z Nádasdy, J Hetke, K Wise and G Buzsaki (1995). 'Gamma (40-100 Hz) oscillation in the hippocampus of the behaving rat.' *Journal of Neuroscience* 15.1 Pt 1, pp. 47–60.

Brainard, M S and E I Knudsen (1993). 'Experience-dependent plasticity in the inferior colliculus: a site for visual calibration of the neural representation of auditory space in the barn owl.' *Journal of Neuroscience* 13.11, pp. 4589–4608.

Brandon, Mark P, Andrew R Bogaard, Christopher P Libby, Michael A Connerney, Kishan Gupta and Michael E Hasselmo (2011). 'Reduction of theta rhythm dissociates grid cell spatial periodicity from directional tuning.' *Science* 332.6029, pp. 595–599.

Brandon, Mark P, Julie Koenig, Jill K Leutgeb and Stefan Leutgeb (2014). 'New and distinct hippocampal place codes are generated in a new environment during septal inactivation.' *Neuron* 82.4, pp. 789–796.

Brandt, T (2005). 'Vestibular loss causes hippocampal atrophy and impaired spatial memory in humans'. *Brain* 128.11, pp. 2732–2741.

Brodal, Alf (1947). 'The hippocampus and the sense of smell.' *Brain* 70, pp. 179–222.

Brodmann, K (1909). 'Vergleichende Lokalisationslehre der Grosshirnrinde in ihren Prinzipien dargestellt auf Grund des Zellenbaues'. *Leipzig: Barth*.

Brun, Vegard Heimly, Trygve Solstad, Kirsten Brun Kjelstrup, Marianne Fyhn, Menno P Witter, Edvard I Moser and May-Britt Moser (2008). 'Progressive increase in grid scale from dorsal to ventral medial entorhinal cortex.' *Hippocampus* 18.12, pp. 1200–1212.

Bullock, T H, G Buzsaki and M C McClune (1990). 'Coherence of compound field potentials reveals discontinuities in the CA1-subiculum of the hippocampus in freely-moving rats.' *Neuroscience* 38.3, pp. 609–619.

Burwell, R D and D M Hafeman (2003). 'Positional firing properties of postrhinal cortex neurons.' *Neuroscience* 119.2, pp. 577–588.

Buzsaki, G (1986). 'Hippocampal sharp waves: their origin and significance.' *Brain research* 398.2, pp. 242–252.

Buzsaki, G (1989). 'Two-stage model of memory trace formation: a role for "noisy" brain states.' *Neuroscience* 31.3, pp. 551–570.

Buzsaki, G, J Czopf, I Kondákor and L Kellényi (1986). 'Laminar distribution of hippocampal rhythmic slow activity (RSA) in the behaving rat: current-source density analysis, effects of urethane and atropine.' *Brain research* 365.1, pp. 125–137.

Buzsaki, G, Z Horváth, R Urioste, J Hetke and K Wise (1992). 'High-frequency network oscillation in the hippocampus.' *Science* 256.5059, pp. 1025–1027.

Buzsáki, György (2002). 'Theta oscillations in the hippocampus.' *Neuron* 33.3, pp. 325–340.

Buzsáki, György (2005). 'Theta rhythm of navigation: link between path integration and landmark navigation, episodic and semantic memory.' *Hippocampus* 15.7, pp. 827–840.

Buzsáki, György, Costas A Anastassiou and Christof Koch (2012). 'The origin of extracellular fields and currents — EEG, ECoG, LFP and spikes', pp. 1–14.

Canto, Cathrin B and Menno P Witter (2012). 'Cellular properties of principal neurons in the rat entorhinal cortex. I. The lateral entorhinal cortex.' *Hippocampus* 22.6, pp. 1256–1276.

Caplan, Jeremy B, Joseph R Madsen, Andreas Schulze-Bonhage, Richard Aschenbrenner-Scheibe, Ehren L Newman and Michael J Kahana (2003). 'Human theta oscillations related to sensorimotor integration and spatial learning.' *The Journal of neuroscience : the official journal of the Society for Neuroscience* 23.11, pp. 4726–4736.

Cappaert, Natalie L M, Niels M Van Strien and Menno P Witter (2015). 'Hippocampal Formation'. *The Rat Nervous System*. Elsevier, pp. 511–573.

Chahl, J S and M V Srinivasan (1997). 'Reflective surfaces for panoramic imaging.' *Applied optics* 36.31, pp. 8275–8285.

Chen, Guifen, John A King, Neil Burgess and John O'Keefe (2013). 'How vision and movement combine in the hippocampal place code.' *Proceedings of the National Academy of Sciences of the United States of America* 110.1, pp. 378–383.

Chevaleyre, Vivien and Steven A Siegelbaum (2010). 'Strong CA2 pyramidal neuron synapses define a powerful disynaptic cortico-hippocampal loop.' *Neuron* 66.4, pp. 560–572.

Coan, E J and G L Collingridge (1987). 'Characterization of an N-methyl-D-aspartate receptor component of synaptic transmission in rat hippocampal slices.' *Neuroscience* 22, pp. 1–8.

Collingridge, Graham L, Stephane Peineau, John G Howland and Yu Tian Wang (2010). 'Long-term depression in the CNS'. *Nature Reviews Neuroscience* 11.7, pp. 459–473.

Csicsvari, J, H Hirase, A Czurkó, A Mamiya and G Buzsaki (1999). 'Oscillatory coupling of hippocampal pyramidal cells and interneurons in the behaving Rat.' *Journal of Neuroscience* 19.1, pp. 274–287.

Csicsvari, J, H Hirase, A Mamiya and G Buzsaki (2000). 'Ensemble patterns of hippocampal CA3-CA1 neurons during sharp wave-associated population events.' *Neuron* 28.2, pp. 585–594.

Cushman, Jesse D, Daniel B Aharoni, Bernard Willers, Pascal Ravassard, Ashley Kees, Cliff Vuong, Briana Popeney, Katsushi Arisaka and Mayank R Mehta (2013). 'Multisensory control of multimodal behavior: do the legs know what the tongue is doing?' *PloS one* 8.11, e80465.

Dan, Yang and Mu-ming Poo (2004). 'Spike timing-dependent plasticity of neural circuits.' *Neuron* 44.1, pp. 23–30.

Davis, S., S. P. Butcher and R. G. M. Morris (1992). 'The NMDA receptor antagonist D-2-amino-5-phosphonopentanoate (D-AP5) impairs spatial learning and LTP in vivo at intracerebral concentrations comparable to those that block LT P in vitro.' *J. Neurosci.* 12, pp. 21–34.

Day, Brian L and Richard C Fitzpatrick (2005). 'The vestibular system.' *CURBIO* 15.15, R583–6.

Deshmukh, Sachin S, Jeremy L Johnson and James J Knierim (2012). 'Perirhinal cortex represents nonspatial, but not spatial, information in rats foraging in the presence of objects: comparison with lateral entorhinal cortex.' *Hippocampus* 22.10, pp. 2045–2058.

Dragoi, George and György Buzsáki (2006). 'Temporal Encoding of Place Sequences by Hippocampal Cell Assemblies'. *Neuron* 50.1, pp. 145–157.

Dugladze, T, U Heinemann and T Gloveli (2001). 'Entorhinal cortex projection cells to the hippocampal formation in vitro.' *Brain research* 905.1-2, pp. 224–231.

Eacott, M. J. and E. A. Gaffan (2005). 'The roles of perirhinal cortex, postrhinal cortex, and the fornix in memory for objects, contexts, and events in the rat'. *The Quarterly Journal of Experimental Psychology Section B* 58.3-4, pp. 202–217.

Eichenbaum, Howard, Magdalena Sauvage, Norbert Fortin, Robert Komorowski and Paul Lipton (2012). 'Towards a functional organ-

ization of episodic memory in the medial temporal lobe.' *Neuroscience and biobehavioral reviews* 36.7, pp. 1597–1608.

Ekstrom, Arne D, Jeremy B Caplan, Emily Ho, Kirk Shattuck, Itzhak Fried and Michael J Kahana (2005). 'Human hippocampal theta activity during virtual navigation.' *Hippocampus* 15.7, pp. 881–889.

Ferbinteanu, Janina and Matthew L Shapiro (2003). 'Prospective and retrospective memory coding in the hippocampus.' *Neuron* 40.6, pp. 1227–1239.

Frisch, K von (1967). 'The Dance Language and Orientation of Bees.' *Harvard University Press*.

Fyhn, Marianne, Torkel Hafting, Alessandro Treves, May-Britt Moser and Edvard I Moser (2007). 'Hippocampal remapping and grid realignment in entorhinal cortex.' *Nature* 446.7132, pp. 190–194.

Fyhn, Marianne, Sturla Molden, Menno P Witter, Edvard I Moser and May-Britt Moser (2004). 'Spatial representation in the entorhinal cortex.' *Science* 305.5688, pp. 1258–1264.

Gaarskjaer, F. B. (1978). 'Organization of the mossy fiber system of the rat studied in extended hippocampi.' *Journal of Comparative Neurology* 178, pp. 49–88.

Garbers, Christian, Josephine Henke, Christian Leibold, Thomas Wachtler and Kay Thurley (2015). 'Contextual processing of brightness and color in Mongolian gerbils.' *Journal of vision* 15.1, p. 15.1.13.

Geva-Sagiv, Maya, Sandro Romani, Liora Las and Nachum Ulanovsky (2016). 'Hippocampal global remapping for different sensory modalities in flying bats.' *Nature Neuroscience* 19.7, pp. 952–958.

Gibson, J J (1954). 'The visual perception of objective motion and subjective movement.' *Psychological review* 61.5, pp. 304–314.

Giocomo, Lisa M, Syed A Hussaini, Fan Zheng, Eric R Kandel, May-Britt Moser and Edvard I Moser (2011). 'Grid cells use HCN1 channels for spatial scaling.' *Cell* 147.5, pp. 1159–1170.

Girardeau, Gabrielle and Michaël Zugaro (2011). 'Hippocampal ripples and memory consolidation'. *Current Opinion in Neurobiology* 21.3, pp. 452–459.

Gloveli, T, T Dugladze, D Schmitz and U Heinemann (2001). 'Properties of entorhinal cortex deep layer neurons projecting to the rat dentate gyrus.' *The European journal of neuroscience* 13.2, pp. 413–420.

Gothard, K M, W E Skaggs and B L McNaughton (1996). 'Dynamics of mismatch correction in the hippocampal ensemble code for space: interaction between path integration and environmental cues.' *Journal of Neuroscience* 16.24, pp. 8027–8040.

Govardovskii, V I, P Röhlich, A Szél and T V Khokhlova (1992). 'Cones in the retina of the Mongolian gerbil, Meriones unguiculatus: an immunocytochemical and electrophysiological study.' *Vision research* 32.1, pp. 19–27.

Grothe, Benedikt and Michael Pecka (2014). 'The natural history of sound localization in mammals–a story of neuronal inhibition.' *Frontiers in neural circuits* 8, p. 116.

Haeften, Theo van, Luciënne Baks-te-Bulte, Peter H Goede, Floris G Wouterlood and Menno P Witter (2003). 'Morphological and numerical analysis of synaptic interactions between neurons in deep and superficial layers of the entorhinal cortex of the rat.' *Hippocampus* 13.8, pp. 943–952.

Hafting, Torkel, Marianne Fyhn, Sturla Molden, May-Britt Moser and Edvard I Moser (2005). 'Microstructure of a spatial map in the entorhinal cortex.' *Nature* 436.7052, pp. 801–806.

Haggerty, Daniel Christopher and Daoyun Ji (2015). 'Activities of visual cortical and hippocampal neurons co-fluctuate in freely moving rats during spatial behavior.' *eLife* 4.

Hales, Jena B, Magdalene I Schlesiger, Jill K Leutgeb, Larry R Squire, Stefan Leutgeb and Robert E Clark (2014). 'Medial entorhinal cortex lesions only partially disrupt hippocampal place cells and hippocampus-dependent place memory.' *Cell reports* 9.3, pp. 893–901.

Hamam, B N, T E Kennedy, A Alonso and D G Amaral (2000). 'Morphological and electrophysiological characteristics of layer V neurons of the rat medial entorhinal cortex.' *The Journal of comparative neurology* 418.4, pp. 457–472.

Hangya, Balázs, Zsolt Borhegyi, Nóra Szilágyi, Tamás F Freund and Viktor Varga (2009). 'GABAergic neurons of the medial septum lead the hippocampal network during theta activity.' *The Journal of neuroscience : the official journal of the Society for Neuroscience* 29.25, pp. 8094–8102.

Harvey, Christopher D, Forrest Collman, Daniel A Dombeck and David W Tank (2009). 'Intracellular dynamics of hippocampal place cells during virtual navigation'. *Nature* 461.7266, pp. 941–946.

Hasselmo, ME (1999). 'Neuromodulation: acetylcholine and memory consolidation.' *Trends in cognitive sciences* 3.9, pp. 351–359.

Hawkins, Robert D, Gregory A Clark and Eric R Kandel (2006). 'Operant conditioning of gill withdrawal in Aplysia.' *The Journal of neuroscience : the official journal of the Society for Neuroscience* 26.9, pp. 2443–2448.

Hebb, D O (1949). *The Organization of Behavior*. Wiley:New York.

Hjorth-Simonsen, A (1973). 'Some intrinsic connections of the hippocampus in the rat: an experimental analysis.' *The Journal of comparative neurology* 147.2, pp. 145–161.

Hollup, S A, S Molden, J G Donnett, M B Moser and E I Moser (2001). 'Accumulation of hippocampal place fields at the goal location in an annular watermaze task.' *The Journal of neuroscience : the official journal of the Society for Neuroscience* 21.5, pp. 1635–1644.

Holscher, C, A Schnee, H Dahmen, L Setia and H A Mallot (2005). 'Rats are able to navigate in virtual environments.' *The Journal of experimental biology* 208.Pt 3, pp. 561–569.

Hopfield, J J (1995). 'Pattern recognition computation using action potential timing for stimulus representation.' *Nature* 376.6535, pp. 33–36.

Horii, Arata, Noah A. Russell, Paul F. Smith, Cynthia L. Darlington and David K. Bilkey (2004). 'Vestibular influences on CA1 neurons in the rat hippocampus: an electrophysiological study in vivo'. *Experimental Brain Research* 155.2, pp. 245–250.

Ingle, D J (1981). 'New methods for analysis of vision in the gerbil.' *Behavioural brain research* 3.2, pp. 151–173.

Ishizuka, N, W M Cowan and D G Amaral (1995). 'A quantitative analysis of the dendritic organization of pyramidal cells in the rat hippocampus.' *The Journal of comparative neurology* 362.1, pp. 17–45.

Jeffery, Kathryn J and Michael I Anderson (2003). 'Dissociation of the geometric and contextual influences on place cells.' *Hippocampus* 13.7, pp. 868–872.

Jensen, O and J E Lisman (1996). 'Hippocampal CA3 region predicts memory sequences: accounting for the phase precession of place cells.' *Learning & memory (Cold Spring Harbor, N.Y.)* 3.2-3, pp. 279–287.

Jones, Matthew W and Thomas J McHugh (2011). 'Updating hippocampal representations: CA2 joins the circuit.' *Trends in neurosciences* 34.10, pp. 526–535.

Jouvet, M (1969). 'Biogenic amines and the states of sleep.' *Science* 163.3862, pp. 32–41.

Jouvet, M., F Michel and J. L. Courjon (1959). 'L'activite electrique du rhinencephale au cours du sommeil chez le chat.' *C. R. Soc. Biol. (Paris)* 153, pp. 101–105.

Jung, M W, S I Wiener and B L McNaughton (1994). 'Comparison of spatial firing characteristics of units in dorsal and ventral hippocampus of the rat.' *Journal of Neuroscience* 14.12, pp. 7347–7356.

Kahana, M J, R Sekuler, J B Caplan, M Kirschen and J R Madsen (1999). 'Human theta oscillations exhibit task dependence during virtual maze navigation.' *Nature* 399.6738, pp. 781–784.

Kammerer, Axel and Christian Leibold (2014). 'Hippocampal remapping is constrained by sparseness rather than capacity.' *PLoS computational biology* 10.12, e1003986.

Kamondi, A, L Acsády, X J Wang and G Buzsaki (1998). 'Theta oscillations in somata and dendrites of hippocampal pyramidal cells in vivo: activity-dependent phase-precession of action potentials.' *Hippocampus* 8.3, pp. 244–261.

Kandel, Eric R, James H Schwartz, Thomas M Jessell, Steven A Siegelbaum and A J Hudspeth (2013). *PRINCIPLES OF NEURAL SCIENCE*. Fifth.

Kant, Immanuel (1781). *Critik der reinen Vernunft*. Vol. 1. Johann Friedrich Hartknoch.

Kaplan, H. and C. Miezejeski (1972). 'Development of seizures in the mongolian gerbil (Meriones unguiculatus).' *J.Inst.Anim.Tech.* 19, pp. 56–60.

Kautzky, Magdalena and Kay Thurley (2016). 'Estimation of self-motion duration and distance in rodents.' *Royal Society open science* 3.5, p. 160118.

Kempter, Richard, Christian Leibold, György Buzsáki, Kamran Diba and Robert Schmidt (2012). 'Quantifying circular–linear associations: Hippocampal phase precession'. *Journal of Neuroscience Methods* 207.1, pp. 113–124.

Kim, Soyun, Maya Sapiurka, Robert E Clark and Larry R Squire (2013). 'Contrasting effects on path integration after hippocampal damage in humans and rats.' *Proceedings of the National Academy of Sciences of the United States of America* 110.12, pp. 4732–4737.

Kim, Yujin and Nelson Spruston (2012). 'Target-specific output patterns are predicted by the distribution of regular-spiking and bursting pyramidal neurons in the subiculum.' *Hippocampus* 22.4, pp. 693–706.

Klatzky, Roberta L, Jack M Loomis, Andrew C Beall, Sarah S Chance and Reginald G Golledge (1998). 'Spatial Updating of Self-Position and Orientation During Real, Imagined, and Virtual Locomotion'. *Psychological Science* 9.4, pp. 293–298.

Klausberger, Thomas and Peter Somogyi (2008). 'Neuronal diversity and temporal dynamics: the unity of hippocampal circuit operations.' *Science* 321.5885, pp. 53–57.

Klink, R and A Alonso (1997). 'Morphological characteristics of layer II projection neurons in the rat medial entorhinal cortex.' *Hippocampus* 7.5, pp. 571–583.

Kloosterman, Fabian, Theo van Haeften, Menno P Witter and Fernando H Lopes Da Silva (2003). 'Electrophysiological characterization of interlaminar entorhinal connections'. *The European journal of neuroscience* 18.11, pp. 3037–3052.

Knudsen, E I and P F Knudsen (1985). 'Vision guides the adjustment of auditory localization in young barn owls.' *Science* 230.4725, pp. 545–548.

Knudsen, E I and P F Knudsen (1989). 'Vision calibrates sound localization in developing barn owls.' *Journal of Neuroscience* 9.9, pp. 3306–3313.

Koenig, Julie, Ashley N Linder, Jill K Leutgeb and Stefan Leutgeb (2011). 'The spatial periodicity of grid cells is not sustained during reduced theta oscillations.' *Science* 332.6029, pp. 592–595.

Kramis, R, C H Vanderwolf and B H Bland (1975). 'Two types of hippocampal rhythmical slow activity in both the rabbit and the rat: relations to behavior and effects of atropine, diethyl ether, urethane, and pentobarbital.' *Experimental neurology* 49.1 Pt 1, pp. 58–85.

Kraus, N, D I Smith, T McGee, L Stein and C Cartee (1987). 'Development of the middle latency response in an animal model and its relation to the human response.' *Hearing research* 27.2, pp. 165–176.

Lee, Hsiao-Yu, Ming-Dar Kuo, Teng-Ching Chang, Yi-Shiang Ou-Yang and Jia-Jin Jason Chen (2007). 'Development of Virtual Reality Environment for Tracking Rat Behavior'. *journal of Medical and Biological Engineering* 27, pp. 71–78.

Lessard, N, M Paré, F Lepore and M Lassonde (1998). 'Early-blind human subjects localize sound sources better than sighted subjects.' *Nature* 395.6699, pp. 278–280.

Leutgeb, Jill K, Stefan Leutgeb, Alessandro Treves, Retsina Meyer, Carol A Barnes, Bruce L McNaughton, May-Britt Moser and Edvard I Moser (2005a). 'Progressive transformation of hippocampal neuronal representations in "morphed" environments.' *Neuron* 48.2, pp. 345–358.

Leutgeb, Stefan, Jill K Leutgeb, May-Britt Moser and Edvard I Moser (2005b). 'Place cells, spatial maps and the population code for memory.' *Current Opinion in Neurobiology* 15.6, pp. 738–746.

Leutgeb, Stefan, Jill K Leutgeb, Alessandro Treves, May-Britt Moser and Edvard I Moser (2004). 'Distinct ensemble codes in hippocampal areas CA3 and CA1.' *Science* 305.5688, pp. 1295–1298.

Levy, W B and O Steward (1983). 'Temporal contiguity requirements for long-term associative potentiation/depression in the hippocampus.' *Neuroscience* 8.4, pp. 791–797.

Li, X G, P Somogyi, A Ylinen and G Buzsaki (1994). 'The hippocampal CA3 network: an in vivo intracellular labeling study.' *The Journal of comparative neurology* 339.2, pp. 181–208.

Lorente de Nó, R. (1933). 'studies of the structure of the cerebral cortex.' *Journal of Physiology and Neurology* 45.

Lorente de Nó, R. (1934). 'studies of the structure of the cerebral cortex II Continuation of the study of the amminic system.' *Journal of Physiology and Neurology* 46, pp. 113–177.

Löwel, S and W Singer (1992). 'Selection of intrinsic horizontal connections in the visual cortex by correlated neuronal activity.' *Science* 255.5041, pp. 209–212.

Lubenov, Evgueniy V and Athanassios G Siapas (2009). 'Hippocampal theta oscillations are travelling waves.' *Nature* 459.7246, pp. 534–539.

Lynch, M A (2004). 'Long-term potentiation and memory.' *Physiological reviews* 84.1, pp. 87–136.

Magee, J C (2001). 'Dendritic mechanisms of phase precession in hippocampal CA1 pyramidal neurons.' *Journal of neurophysiology* 86.1, pp. 528–532.

Maia, Tiago V (2009). 'Reinforcement learning, conditioning, and the brain: Successes and challenges.' *Cognitive, affective & behavioral neuroscience* 9.4, pp. 343–364.

Maier, Joost X and Jennifer M Groh (2009). 'Multisensory guidance of orienting behavior.' *Hearing research* 258.1-2, pp. 106–112.

Malenka, Robert C. (2003). 'The long-term potential of LTP.' *Nature Reviews Neuroscience* 4.11, pp. 923–926.

Markus, E J, Y L Qin, B Leonard, W E Skaggs, B L McNaughton and C A Barnes (1995). 'Interactions between location and task affect the spatial and directional firing of hippocampal neurons.' *Journal of Neuroscience* 15.11, pp. 7079–7094.

Maurer, Andrew P, Stephen L Cowen, Sara N Burke, Carol A Barnes and Bruce L McNaughton (2006). 'Organization of hippocampal cell assemblies based on theta phase precession.' *Hippocampus* 16.9, pp. 785–794.

Maurer, Andrew P, Shea R VanRhoads, Gary R Sutherland, Peter Lipa and Bruce L McNaughton (2005). 'Self-motion and the origin of differential spatial scaling along the septo-temporal axis of the hippocampus.' *Hippocampus* 15.7, pp. 841–852.

McNaughton, B L, C A Barnes and J O'Keefe (1983). 'The contributions of position, direction, and velocity to single unit activity in the hippocampus of freely-moving rats.' *Exp Brain Res* 52.1, pp. 41–49.

Mehta, M R, A K Lee and M A Wilson (2002). 'Role of experience and oscillations in transforming a rate code into a temporal code.' *Nature* 417.6890, pp. 741–746.

Mittelstaedt, H and M L Mittelstaedt (1980). 'Homing by path integration in a mammal'. *Naturwissenschaften* 67, pp. 566–567.

Mittelstaedt, M L and S Glasauer (1991). 'Idiothetic navigation in gerbils and humans.' *Zool. Jb. Physiol.* 95, pp. 427–435.

Moller, P and P Görner (1994). 'Homing by path integration in the spider Agelena labyrinthica Clerk.' *J. Comp. Physiol.* 174, pp. 221–229.

Morris, R. G. M. (1981). 'Spatial localization does not require the presence of local cues.' *Learn. Motiv.* 12, pp. 239–260.

Morris, R. G. M. (1989). 'Synaptic plasticity and learning: selective impairment of learning in rats and blockade of long-term potentiation in vivo by the N-methyl-D-aspartate receptor antagonist AP5.' *J. Neurosci.* 9, pp. 3040–3057.

Morris, R. G. M., P. Garrud, J. N. P. Rawlins and J. O'Keefe (1982). 'Place navigation impaired in rats with hippocampal lesions.' *Nature* 297, pp. 681–683.

Moser, Edvard I and May-Britt Moser (2013). 'Grid cells and neural coding in high-end cortices.' *Neuron* 80.3, pp. 765–774.

Moser, Edvard I, Yasser Roudi, Menno P Witter, Clifford Kentros, Tobias Bonhoeffer and May-Britt Moser (2014). 'Grid cells and cortical representation.' *Nature reviews. Neuroscience* 15.7, pp. 466–481.

Müller, M and Rüdiger Wehner (1988). 'Path integration in desert ants, Cataglyphis fortis.' *Proc. Natl. Acad. Sci.* 85, pp. 5287–5290.

Muller, R U, E Bostock, J S Taube and J L Kubie (1994). 'On the directional firing properties of hippocampal place cells.' *Journal of Neuroscience* 14.12, pp. 7235–7251.

Muller, R U and J L Kubie (1987). 'The effects of changes in the environment on the spatial firing of hippocampal complex-spike cells.' *Journal of Neuroscience* 7.7, pp. 1951–1968.

Naber, P A, F H Lopes da Silva and M P Witter (2001). 'Reciprocal connections between the entorhinal cortex and hippocampal fields CA1 and the subiculum are in register with the projections from CA1 to the subiculum.' *Hippocampus* 11.2, pp. 99–104.

Nakazawa, Kazu, Thomas J McHugh, Matthew A Wilson and Susumu Tonegawa (2004). 'NMDA receptors, place cells and hippocampal spatial memory.' *Nature reviews. Neuroscience* 5.5, pp. 361–372.

Neves, Guilherme, Sam F Cooke and Tim V P Bliss (2008). 'Synaptic plasticity, memory and the hippocampus: a neural network approach to causality.' *Nature reviews. Neuroscience* 9.1, pp. 65–75.

Ohl, F W, W Wetzel, T Wagner, A Rech and H Scheich (1999). 'Bilateral ablation of auditory cortex in Mongolian gerbil affects discrimination of frequency modulated tones but not of pure tones.' *Learning & memory (Cold Spring Harbor, N.Y.)* 6.4, pp. 347–362.

O'Keefe, J (1976). 'Place units in the hippocampus of the freely moving rat.' *Experimental neurology* 51.1, pp. 78–109.

O'Keefe, J (1978). *The Hippocampus as a Cognitive Map*. Clarendon, Oxford.

O'Keefe, J and N Burgess (1996). 'Geometric determinants of the place.' *Nature* 381.6581, pp. 425–428.

O'Keefe, J, N Burgess, J G Donnett, K J Jeffery and E A Maguire (1998). 'Place cells, navigational accuracy, and the human hippocampus.' *Philosophical transactions of the Royal Society of London. Series B, Biological sciences* 353.1373, pp. 1333–1340.

O'Keefe, J and D H Conway (1978). 'Hippocampal place units in the freely moving rat: why they fire where they fire.' *Exp Brain Res* 31.4, pp. 573–590.

O'Keefe, J and J Dostrovsky (1971). 'The hippocampus as a spatial map. Preliminary evidence from unit activity in the freely-moving rat.' *Brain research* 34.1, pp. 171–175.

O'Keefe, John and Lynn Nadel (1978). 'The Hippocampus as a Cognitive Map'. *Oxford University Press*.

O'Keefe, John and Michael Recce (1993). 'Phase Relationship Between Hippocampal Place Units andthe EEG Theta Rhythm'. *Hippocampus* 3.3, pp. 317–330.

Olton, D S, M Branch and P J Best (1978). 'Spatial correlates of hippocampal unit activity.' *Experimental neurology* 58.3, pp. 387–409.

Ossenkopp, Klaus-Peter and Eric L Hargreaves (1993). 'Spatial learning in an enclosed eight-arm radial maze in rats with sodium arsanilate-induced labyrinthectomies'. *Behavioral and Neural Biology* 59.3, pp. 253–257.

Papez, J W (1937). *A proposed mechanism of emotion.* Vol. 7.

Paré, D and D R Collins (2000). 'Neuronal correlates of fear in the lateral amygdala: multiple extracellular recordings in conscious cats.' *The Journal of neuroscience : the official journal of the Society for Neuroscience* 20.7, pp. 2701–2710.

Parron, Carole and Etienne Save (2004). 'Evidence for entorhinal and parietal cortices involvement in path integration in the rat.' *Exp Brain Res* 159.3, pp. 349–359.

Patel, Jagdish, Shigeyoshi Fujisawa, Antal Berényi, Sebastien Royer and György Buzsáki (2012). 'Traveling theta waves along the entire septotemporal axis of the hippocampus.' *Neuron* 75.3, pp. 410–417.

Pavlov, I P (1927). 'CONDITIONED REFLEXES'. *Oxford University Press*.

Petsche, H, C Stumpf and G Gogolak (1962). '[The significance of the rabbit's septum as a relay station between the midbrain and the hippocampus. I. The control of hippocampus arousal activity by the septum cells].' *Electroencephalography and clinical neurophysiology* 14, pp. 202–211.

Pietrewicz, A T, M P Hoff and S A Higgins (1982). 'Activity rhythms in the Mongolian gerbil under natural light conditions.' *Physiology & behavior* 29.2, pp. 377–380.

Piskorowski, Rebecca A. and Vivien Chevaleyre (2012). 'Synaptic integration by different dendritic compartments of hippocampal CA1 and CA2 pyramidal neurons'. *Cellular and Molecular Life Sciences* 69.1, pp. 75–88.

Prechtl, H F, G Cioni, C Einspieler, A F Bos and F Ferrari (2001). 'Role of vision on early motor development: lessons from the blind.' *Developmental medicine and child neurology* 43.3, pp. 198–201.

Raghavachari, S, M J Kahana, D S Rizzuto, J B Caplan, M P Kirschen, B Bourgeois, J R Madsen and J E Lisman (2001). 'Gating of human theta oscillations by a working memory task.' *The Journal of neuroscience : the official journal of the Society for Neuroscience* 21.9, pp. 3175–3183.

Ramón y Cajal, S. (1909). 'Histologie du Systeme Nerveux de l'Homme et des Vertebres.' *Paris: Maloine*.

Ranganath, Charan and Maureen Ritchey (2012). 'Two cortical systems for memory-guided behaviour.' *Nature reviews. Neuroscience* 13.10, pp. 713–726.

Ravassard, Pascal, Ashley Kees, Bernard Willers, David Ho, Daniel Aharoni, Jesse Cushman, Zahra M Aghajan and Mayank R Mehta (2013). 'Multisensory control of hippocampal spatiotemporal selectivity.' *Science* 340.6138, pp. 1342–1346.

Ribak, C E, J E Vaughn and K Saito (1978). 'Immunocytochemical localization of glutamic acid decarboxylase in neuronal somata following colchicine inhibition of axonal transport.' *Brain research* 140.2, pp. 315–332.

Riedel, G. (1999). 'Reversible neural inactivation reveals hippocampal participation in several memory processes.' *Nature Neurosci.* 2, pp. 898–905.

Ros, Tomas, Bernard J Baars, Ruth A Lanius and Patrik Vuilleumier (2014). 'Tuning pathological brain oscillations with neurofeedback: a systems neuroscience framework.' *Frontiers in human neuroscience* 8, p. 1008.

Rosenzweig, E.S., A.D. Ekstrom, A.D. Redish, B.L. McNaughton and C.A. Barnes (2000). 'Phase precession as an experience-independent process: hippocampal pyramidal cell phase precession in a novel environment and under NMDA-receptor blockade.' Soc. Neurosci. Abstr.

Russell, Noah A, Arata Horii, Paul F Smith, Cynthia L Darlington and David K Bilkey (2003). 'Long-term effects of permanent vestibular lesions on hippocampal spatial firing.' *The Journal of neuroscience : the official journal of the Society for Neuroscience* 23.16, pp. 6490–6498.

Russell, Noah A, Arata Horii, Paul F Smith, Cynthia L Darlington and David K Bilkey (2006). 'Lesions of the vestibular system disrupt hippocampal theta rhythm in the rat.' *Journal of neurophysiology* 96.1, pp. 4–14.

Sainsbury, R S, A Heynen and C P Montoya (1987). 'Behavioral correlates of hippocampal type 2 theta in the rat.' *Physiology & behavior* 39.4, pp. 513–519.

Saint Paul, U von (1982). 'Do geese use path integration for walking home?' *Avian Navigation*, pp. 298–307.

Saleem, Aman B, Aslı Ayaz, Kathryn J Jeffery, Kenneth D Harris and Matteo Carandini (2013). 'Integration of visual motion and locomotion in mouse visual cortex.' *Nature Neuroscience* 16.12, pp. 1864–1869.

Save, E, A Cressant, C Thinus-Blanc and B Poucet (1998). 'Spatial firing of hippocampal place cells in blind rats.' *Journal of Neuroscience* 18.5, pp. 1818–1826.

Save, E, L Nerad and B Poucet (2000). 'Contribution of multiple sensory information to place field stability in hippocampal place cells.' *Hippocampus* 10.1, pp. 64–76.

Schlesiger, Magdalene I, Christopher C Cannova, Brittney L Boublil, Jena B Hales, Emily A Mankin, Mark P Brandon, Jill K Leutgeb, Christian Leibold and Stefan Leutgeb (2015). 'The medial entorhinal cortex is necessary for temporal organization of hippocampal neuronal activity.' *Nature Neuroscience* 18.8, pp. 1123–1132.

Schmidt, R, K Diba, C Leibold, D Schmitz, G Buzsaki and R Kempter (2009). 'Single-Trial Phase Precession in the Hippocampus'. *Journal of Neuroscience* 29.42, pp. 13232–13241.

Schmitzer-Torbert, N, J Jackson, D Henze, K Harris and A D Redish (2005). 'Quantitative measures of cluster quality for use in extracellular recordings.' *Neuroscience* 131.1, pp. 1–11.

Scoville, W. B. and B. Milner (1957). 'Loss of recent memory after bilateral hippocampal lesions.' *J. Neurol. Neurosurg. Psychiatry* 20, pp. 11–21.

Scoville, W B and B Milner (2000). *Loss of recent memory after bilateral hippocampal lesions. 1957.* Vol. 12. Patient H. M.

Simons, D J and R F Wang (1998). 'Perceiving real-world viewpoint changes'. *Psychological Science* 9, pp. 315–320.

Singer, W (1993). 'Synchronization of cortical activity and its putative role in information processing and learning.' *Annual review of physiology* 55.1, pp. 349–374.

Skaggs, W E and B L McNaughton (1998). 'Spatial firing properties of hippocampal CA1 populations in an environment containing two visually identical regions.' *Journal of Neuroscience* 18.20, pp. 8455–8466.

Skaggs, W E, B L McNaughton, M A Wilson and C A Barnes (1996). 'Theta phase precession in hippocampal neuronal populations and

the compression of temporal sequences.' *Hippocampus* 6.2, pp. 149–172.

Skaggs, William E., Bruce L. McNaughton, Katalin M. Gothard and Etan J. Markus (1993). 'An Information-Theoretic Approach to Deciphering the Hippocampal Code'. *Advances in Neural Information Processing Systems 5, [NIPS Conference]*. San Francisco, CA, USA: Morgan Kaufmann Publishers Inc., pp. 1030–1037. ISBN: 1-55860-274-7. URL: http://dl.acm.org/citation.cfm?id=645753.668057.

Smith, Paul F., Arata Horii, Noah Russell, David K. Bilkey, Yiwen Zheng, Ping Liu, D. Steve Kerr and Cynthia L. Darlington (2005). 'The effects of vestibular lesions on hippocampal function in rats'. *Progress in Neurobiology* 75.6, pp. 391–405.

Somogyi, Peter (2010). 'Hippocampus: Intrinsic organization.' *Handbook of Brain Microcircuits*. Ed. by G. Shepherd and S. Grillner. Progress in Brain Research. New York: Oxford Univeristy Press, pp. 148–164.

Squire, L R (1987). 'The organization and neural substrates of human memory.' *Int J Neurol.* pp. 218–222.

Squire, L R, P C Slater and P M Chace (1975). 'Retrograde amnesia: temporal gradient in very long term memory following electroconvulsive therapy.' *Science* 187.4171, pp. 77–79.

Squire, Larry R (1986). 'Mechanisms of memory'. *Science*, pp. 1–9.

Stackman, Robert W, Ann S Clark and Jeffrey S Taube (2002). 'Hippocampal spatial representations require vestibular input.' *Hippocampus* 12.3, pp. 291–303.

Stensola, Hanne, Tor Stensola, Trygve Solstad, Kristian Frøland, May-Britt Moser and Edvard I Moser (2012). 'The entorhinal grid map is discretized.' *Nature* 492.7427, pp. 72–78.

Steriade, M (2000). 'Corticothalamic resonance, states of vigilance and mentation.' *Neuroscience* 101.2, pp. 243–276.

Storm-Mathisen, J. and F. Fonnum (1972). 'Localization of Transmitter Candidates in the Hippocampal Region'. *Biochemical and Pharmacological Mechanisms Underlying Behaviour*. Ed. by P.B. Bradley and

R.W. Brimblecombe. Vol. 36. Progress in Brain Research. Elsevier, pp. 41–58.

Stuermer, I W and H Scheich (2000). 'Early unilateral auditory deprivation increases 2-deoxyglucose uptake in contralateral auditory cortex of juvenile Mongolian gerbils.' *Hearing research* 146.1-2, pp. 185–199.

Stuermer, Ingo W (2003). *Haus- und Versuchstiepflege - Mongolische Wüstenrennmaus (Gerbil)*. Enke Verlag, Stuttgart.

Stuermer, Ingo W, Karsten Plotz, Axel Leybold, Olaf Zinke, Otto Kalberlah, Ravchikh Samjaa and Henning Scheich (2003). 'Intraspecific Allometric comparison of Laboratory gerbils with Mongolian Gerbils Trapped in the Wild Indicates Domestication in Meriones unguiculatus (Milne-Edwards, 1867) (Rodentia: Gerbillinae)'. *Zoologischer Anzeiger - A Journal of Comparative Zoology* 242.3, pp. 249–266.

Sullivan, David, Jozsef Csicsvari, Kenji Mizuseki, Sean Montgomery, Kamran Diba and György Buzsáki (2011). 'Relationships between hippocampal sharp waves, ripples, and fast gamma oscillation: influence of dentate and entorhinal cortical activity.' *The Journal of neuroscience : the official journal of the Society for Neuroscience* 31.23, pp. 8605–8616.

Surjosukotjo, D., S. Steinlechner and I. W. Stuermer (1999). 'INfluence of light and temperature cycles on the activity rhythm of laboratory strain and wild type Mongolian gerbils (Meriones unguiculatus).' *Zoology* 102, p. 73.

Tai, Siew Kian, Jingyi Ma, Klaus-Peter Ossenkopp and L Stan Leung (2012). 'Activation of immobility-related hippocampal theta by cholinergic septohippocampal neurons during vestibular stimulation.' *Hippocampus* 22.4, pp. 914–925.

Tamamaki, N, K Abe and Y Nojyo (1987). 'Columnar organization in the subiculum formed by axon branches originating from single CA1 pyramidal neurons in the rat hippocampus.' *Brain research* 412.1, pp. 156–160.

Tamamaki, N and Y Nojyo (1995). 'Preservation of topography in the connections between the subiculum, field CA1, and the entorhinal

cortex in rats.' *The Journal of comparative neurology* 353.3, pp. 379–390.

Taube, J S, R U Muller and J B Ranck (1990). 'Head-direction cells recorded from the postsubiculum in freely moving rats. I. Description and quantitative analysis.' *Journal of Neuroscience* 10.2, pp. 420–435.

Taube, Jeffrey S (2007). 'The head direction signal: origins and sensory-motor integration.' *Annual Review of Neuroscience* 30, pp. 181–207.

Taube, Jeffrey S, Stephane Valerio and Ryan M Yoder (2013). 'Is navigation in virtual reality with FMRI really navigation?' *Journal of cognitive neuroscience* 25.7, pp. 1008–1019.

Taylor, M M (1973). 'The Problem of Stimulus Structure in the Behavioural Theory of Perception'. *South African Journal of Psychology* 3, pp. 23–45.

Terrazas, Alejandro, Michael Krause, Peter Lipa, Katalin M Gothard, Carol A Barnes and Bruce L McNaughton (2005). 'Self-motion and the hippocampal spatial metric.' *The Journal of neuroscience : the official journal of the Society for Neuroscience* 25.35, pp. 8085–8096.

Tesche, C D and J Karhu (2000). 'Theta oscillations index human hippocampal activation during a working memory task.' *Proceedings of the National Academy of Sciences* 97.2, pp. 919–924.

Thorndike, E.L. (1901). 'Animal intelligence: An experimental study of the associative processes in animals.' *Psychological Review Monograph Supplement* 2, pp. 1–109.

Thurley, Kay and Aslı Ayaz (2017). 'Virtual reality systems for rodents'. *Current Zoology*, zow070–11.

Thurley, Kay, Josephine Henke, Joachim Hermann, Benedikt Ludwig, Christian Tatarau, Aline Wätzig, Andreas V M Herz, Benedikt Grothe and Christian Leibold (2014). 'Mongolian gerbils learn to navigate in complex virtual spaces.' *Behavioural brain research* 266, pp. 161–168.

Tolman, E C (1948). 'Cognitive maps in rats and men.' *Psychological review* 55.4, pp. 189–208.

Tsodyks, M V, W E Skaggs, T J Sejnowski and B L McNaughton (1996). 'Population dynamics and theta rhythm phase precession of hippocampal place cell firing: a spiking neuron model.' *Hippocampus* 6.3, pp. 271–280.

Vanderwolf, C H (1969). 'Hippocampal electrical activity and voluntary movement in the rat.' *Electroencephalography and clinical neurophysiology* 26.4, pp. 407–418.

Vickerstaff, Robert J and Allen Cheung (2010). 'Which coordinate system for modelling path integration?' *Journal of theoretical biology* 263.2, pp. 242–261.

Villette, Vincent, Arnaud Malvache, Thomas Tressard, Nathalie Dupuy and Rosa Cossart (2015). 'Internally Recurring Hippocampal Sequences as a Population Template of Spatiotemporal Information'. *Neuron* 88.2, pp. 357–366.

Voss, Patrice, Maryse Lassonde, Frederic Gougoux, Madeleine Fortin, Jean-Paul Guillemot and Franco Lepore (2004). 'Early- and late-onset blind individuals show supra-normal auditory abilities in far-space.' *CURBIO* 14.19, pp. 1734–1738.

Wallace, Douglas G, Dustin J Hines, Sergio M Pellis and Ian Q Whishaw (2002). 'Vestibular information is required for dead reckoning in the rat.' *The Journal of neuroscience : the official journal of the Society for Neuroscience* 22.22, pp. 10009–10017.

Wang, R F and D J Simons (1999). 'Active and passive scene recognition across views.' *Cognition* 70.2, pp. 191–210.

Weiskrantz, Lawrence (1956). 'Behavioral changes associated with ablation of the amygdaloid complex in monkeys.' *Journal of Comparative and Physiological Psychology* 49, pp. 381–391.

Wiebe, S P and U V Stäubli (1999). 'Dynamic filtering of recognition memory codes in the hippocampus.' *Journal of Neuroscience* 19.23, pp. 10562–10574.

Wills, Thomas J, Caswell Barry and Francesca Cacucci (2012). 'The abrupt development of adult-like grid cell firing in the medial entorhinal cortex.' *Frontiers in neural circuits* 6, p. 21.

Wilson, M A and B L McNaughton (1993). 'Dynamics of the hippocampal ensemble code for space.' *Science* 261.5124, pp. 1055–1058.

Winckler, Jürgen (1973). 'Vital Staining of Lysosomes and Other Cell Organelles of the Rat with Neutral Red'. *Progress in Histochemistry and Cytochemistry* 6.3, pp. 1–89.

Winters, Boyer D and Timothy J Bussey (2005). 'Transient inactivation of perirhinal cortex disrupts encoding, retrieval, and consolidation of object recognition memory.' *The Journal of neuroscience : the official journal of the Society for Neuroscience* 25.1, pp. 52–61.

Witmer, Bob G. and Paul B. Kline (1998). 'Judging Perceived and Traversed Distance in Virtual Environments.' *Presence: Teleoperators and virtual environments* 7, pp. 144–167.

Witter, M P, P A Naber, T van Haeften, W C Machielsen, S A Rombouts, F Barkhof, P Scheltens and F H Lopes da Silva (2000). 'Cortico-hippocampal communication by way of parallel parahippocampal-subicular pathways.' *Hippocampus* 10.4, pp. 398–410.

Wittlinger, Matthias, Rüdiger Wehner and Harald Wolf (2006). 'The ant odometer: stepping on stilts and stumps.' *Science* 312.5782, pp. 1965–1967.

Ylinen, A, A Bragin, Z Nádasdy, G Jandó, I Szabó, A Sik and G Buzsaki (1995). 'Sharp wave-associated high-frequency oscillation (200 Hz) in the intact hippocampus: network and intracellular mechanisms.' *Journal of Neuroscience* 15.1 Pt 1, pp. 30–46.

Youngstrom, Isaac A and Ben W Strowbridge (2012). 'Visual landmarks facilitate rodent spatial navigation in virtual reality environments.' *Learning & memory (Cold Spring Harbor, N.Y.)* 19.3, pp. 84–90.

Zeil, J (1988). 'Himing in fiddler crabs (Uca lactea annulipes and Uca vomeris: Ocypodidae)'. *J. Comp. Physiol.* 183, pp. 367–377.

Zola-Morgan, S, L R Squire and D G Amaral (1986). 'Human amnesia and the medial temporal region: enduring memory impairment following a bilateral lesion limited to field CA1 of the hippocampus.' *Journal of Neuroscience* 6.10, pp. 2950–2967.

7

APPENDIX

Chemical substance	Bath duration
Neutral red	~ 8 min
Distilled water	rinse until colorless
70% EtOH	~2.5 min
96% EtOH	~2.5 min
96% EtOH	~2.5 min
100% Isopropanol	~2.5 min
100% Isopropanol	~2.5 min
Xylol	~2.5 min
Xylol	~2.5 min
Xylol	~2.5 min

Table 7.1: Neutral red staining protocol (adapted from Winckler, 1973).

ACKNOWLEDGEMENTS

I would like to thank my supervisors Prof. Dr. Christian Leibold and Dr. Kay Thurley for hosting me in the lab and for providing me with wide ranging scientific and technical support throughout my PhD.
With their help and encouragement I was able to participate in several scientific conferences and learned to present complex ideas and concepts via posters or talks. Additionally, they gave me the freedom to pursue passions such as being the student representative of my graduate school (GSN).

I very much enjoyed the atmosphere in the Leibold lab and want to thank all members of the lab for all their support over the years and the many inspiring coffee break discussions.

Also, I want to thank my thesis advisory committee, Prof. Dr. Christian Leibold, Prof. Dr. Mark Hübener, Dr. Conny Kopp-Scheinpflug and Dr. Kay Thurley who were very helpful in discussing my work, problems and future possible steps of my project.
I am also very thankful to the Graduate School of Systemic Neurosciences and particularly Prof. Dr. Benedikt Grothe for providing not only a fruitful academic framework but also great opportunities for connecting with other scientists through excursions and social activities.
Financially, I was supported by the "Graduiertenkolleg 1091 - Orientierung und Bewegung im Raum" (GRK) and the "Bernstein Center for Computational Neuroscience" (BCCN).

Last but not least I want to thank Laurence Lewis, my family and friends (especially Christan Kellner and Delwen Franzen) for their emotional and professional support in good and in bad times. They made my PhD to a valuable, formative chapter in my life that I would not want to have missed.

PUBLICATION LIST

ARTICLES

Haas, Olivia Valerie, Josephine Henke, Christian Leibold and Kay Thurley. 'Input-specific subpopulations of place fields coexist in the hippocampus.' under review.

SELECTED CONFERENCE PRESENTATIONS

Haas, Olivia Valerie, Alireza Chenani, Stefan Leutgeb, Kay Thurley and Christian Leibold (2014). 'Characterizing gerbil hippocampal activity in virtual reality'. *Conference Abstract: Bernstein Conference*. DOI: 10.12751/nncn.bc2014.0209.

Haas, Olivia Valerie, Josephine Henke, Christian Leibold and Kay Thurley (2015). 'Differential drive of hippocampal place cells by visual and proprioceptive input'. *Conference Abstract: Bernstein Conference*. DOI: 10.12751/nncn.bc2015.0203.

Haas, Olivia Valerie, Josephine Henke, Christian Leibold and Kay Thurley (2016a). 'Hippocampal place cells differentially integrate visual and locomotor inputs'. *Conference Abstract: SFN Conference*.

Haas, Olivia Valerie, Josephine Henke, Christian Leibold and Kay Thurley (2016b). 'Visual and non-visual contributions to hippocampal place coding'. *Conference Abstract: FENS Conference*.

EIDESSTATTLICHE VERSICHERUNG / AFFIDAVIT

Hiermit versichere ich an Eides statt, dass ich die vorliegende Dissertation *Input-Dependent Neuronal Representations of Virtual Environments in the Hippocampus* selbstständig angefertigt habe, mich außer der angegebenen keiner weiteren Hilfsmittel bedient und alle Erkenntnisse, die aus dem Schrifttum ganz oder annähernd übernommen sind, als solche kenntlich gemacht und nach ihrer Herkunft unter Bezeichnung der Fundstelle einzeln nachgewiesen habe.

I hereby confirm that the dissertation *Input-Dependent Neuronal Representations of Virtual Environments in the Hippocampus* is the result of my own work and that I have only used sources or materials listed and specified in the dissertation.

München, im 11. April, 2017
Munich, 11th April, 2017

Olivia V. Haas

AUTHOR CONTRIBUTIONS

The contributions of the authors Olivia V. Haas (OVH), Josephine Henke (JH), Christian Leibold (CL) and Kay Thurley (KT) to the studies conducted during my PhD are as follows:

Olivia V. Haas, Josephine Henke, Christian Leibold, Kay Thurley (2017). **Input-specific subpopulations of place fields coexist in the hippocampus**. (in review)
CL and KT conceived the study. OVH, CL, and KT designed the experiments. KT created the virtual reality paradigm and OVH performed the experiments with help of JH. OVH analysed the data with help of CL and KT. OVH created all figures with the exception of figure 2 B and C which was created by KT and figure 5 which was created by CL. OVH, CL and KT wrote the manuscript.

We assert that aforementioned author contributions are correct and accurate:

Olivia V. Haas

Prof. Dr. Christian Leibold